

PACIFIC EARTHQUAKE ENGINEERING RESEARCH CENTER

In-Situ Monitoring of the Force Output of Fluid Dampers: Experimental Investigation

Dimitrios Konstantinidis

Department of Civil Engineering
McMaster University, Canada

James M. Kelly

Department of Civil and Environmental Engineering
University of California, Berkeley

Nicos Makris

Department of Civil Engineering
University of Patras, Greece

Disclaimer

The opinions, findings, and conclusions or recommendations expressed in this publication are those of the author(s) and do not necessarily reflect the views of the study sponsor(s) or the Pacific Earthquake Engineering Research Center.

In-Situ Monitoring of the Force Output of Fluid Dampers: Experimental Investigation

Dimitrios Konstantinidis

Assistant Professor
Department of Civil Engineering
McMaster University, Canada

James M. Kelly

Professor Emeritus
Department of Civil and Environmental Engineering
University of California, Berkeley

Nicos Makris

Professor
Department of Civil Engineering
University of Patras, Greece

PEER Report 2011/103
Pacific Earthquake Engineering Research Center
College of Engineering
University of California, Berkeley

April 2011

ABSTRACT

An alarming problem of leaking dampers has emerged in recent years in some California bridges, such as the west span of the San Francisco–Oakland Bay Bridge and the Vincent Thomas Bridge crossing the Los Angeles Harbor. This reports presents the results of an experimental testing program that was undertaken to develop and validate a simple and reliable way to monitor the force output of viscous fluid dampers in bridges.

The research includes *indoor* and *outdoor* experiments on two medium-size (250 kips at 42 in/sec piston velocity, ± 8.0 in. stroke capacity) and two large-size (450 kips at 85 in/sec piston velocity, ± 19.0 in. stroke capacity) viscous fluid dampers at the Earthquake Simulator Laboratory of the Pacific Earthquake Engineering Research (PEER) Center at the Richmond Field Station, University of California, Berkeley. The former two dampers are identical to the fluid dampers installed in the 91/5 over-crossing in Orange Country, CA, while the latter two are identical to the Type-A dampers that were installed at the west span of the San Francisco–Oakland Bay Bridge.

In Chapter 2 we discuss the concept of measuring the force output of a damper using strain gauges attached on the damper housing or on the damper extender. To prove the concept, we present the results of a series of indoor experiments that were conducted at the Earthquake Simulator Laboratory and included tests with a wide range of combinations of displacements and velocities. The damper force obtained from the strain gauges was in very good agreement with the damper force measured directly with a load cell. The force obtained from the strain gauges in-situ can be compared to the theoretical force output of a damper which is a function of velocity, $F(v) = C_d v^\alpha$, where the velocity v can be measured using a transducer. If the difference between the measured force and the theoretical force exceeds a threshold, the damper needs to be checked for damage. The tests showed that the theoretical force function (which is obtained at design velocities) is not valid at low velocities. Consequently, dampers to be health monitored on a bridge need to be tested before installation not only at design velocities, but also at the range of low velocities that the bridge is expected to experience under service conditions.

In Chapter 3 we describe a sequence of experiments that were conducted outdoors. After the concept of using strain gauges to estimate the damper force was proven in the indoor experiments, a 450-kip damper was mounted on a surplus steel test frame outside the laboratory, located

very near the San Francisco Bay (approximately 0.3 mile) and exposed to wind coming in from the bay. The purpose of this series of experiments was to investigate possible changes in the force output of the damper over time under service loading conditions, where the frequency and amplitude of the displacement cycles are very small. The damper was cycled repeatedly for an average of ten hours a day for approximately 3.5 months. In addition, the damper was again instrumented with position transducers as well as strain gauges, to examine the effect of environmental conditions on these sensors. The data was transmitted to a remote location inside the laboratory.

Finally, in Chapter 4 we describe a portable data acquisition system with very flexible capabilities that can be used to collect and transmit data from a damper on a bridge to a remote location. The system which is based on commercially available components manufactured by Opto 22 uses a wired Ethernet network interface and/or a wireless LAN interface to transmit/receive data. The device is highly scalable to accommodate a number of channels with a variety of different sensor types. There is large flexibility on sampling rates, and the device can be equipped with a buffer memory to save data before an event is triggered. The components of the system are contained within a heavy-duty plastic, hermetically sealed enclosure box. Special sealed fittings can be installed, through which cables can enter the enclosure.

ACKNOWLEDGMENTS

We would like to express our gratitude to Dr. Allaoua Kartoum and Dr. Tim Delis of Caltrans for their valuable feedback during the course of this study.

We would like to acknowledge the following laboratory staff at the Pacific Earthquake Engineering Research Center of the University of California, Berkeley: Don Clyde, Wes Neighbour, Dr. Shakhzod Takhirov, David Maclam, Jose Robles, Nate Knight and Robert Cerney. Their technical support made this experimental study possible.

Financial support for this study was provided by the California Department of Transportation (Caltrans) under grant 59A0658. The publication of this report was sponsored by the Pacific Earthquake Engineering Research Center. Any opinions, findings, and conclusions or recommendations presented in this material are those of the authors and do not necessarily reflect those of the funding agencies.

CONTENTS

ABSTRACT	iii
ACKNOWLEDGMENTS	v
CONTENTS	vii
LIST OF FIGURES	ix
LIST OF TABLES	xiii
1 INTRODUCTION	1
2 INDOOR EXPERIMENTS: PROOF OF CONCEPT	5
2.1 Problem Statement.....	5
2.2 Using the Damper as a Load Cell to Measure Force Output.....	5
2.3 Damper Specimens	8
2.3.1 250-Kip Damper.....	8
2.3.2 450-Kip Damper.....	10
2.4 Experimental Program.....	11
2.4.1 250-Kip Damper with Bondable Strain Gauges.....	11
2.4.2 250-Kip Damper with Weldable Strain Gauges.....	14
2.4.3 450-Kip Damper.....	15
2.5 Experimental Results.....	20
2.5.1 Results of Tests on the 250-Kip Damper Equipped with Bondable Strain Gauges.....	20
2.5.2 Results of Tests on the 250-Kip Damper Equipped with Weldable Strain Gauges.....	30
2.5.3 Results of Tests on the 450-Kip Damper	35
2.6 Choice of Position Transducer and Smoothing of Data	40
2.7 Force at Low Velocities.....	40
3 OUTDOOR EXPERIMENTS ON 450-KIP DAMPER	47
3.1 Experimental Program.....	47
3.2 Results of Outdoor Tests	54

3.2.1 Results of Daily First Cycle Tests with Damper Force Obtained from Load Cell	61
3.2.2 Effect of Temperature on Peak Damper Force Obtained from Load Cell	63
3.2.3 Damper Force Estimated from the Strain Gauges.....	66
3.2.4 Sampling Rate	84
3.2.5 Force at Low Velocity.....	84
3.3 Conclusions	87
3.4 Research Ideas Arising from Project.....	89
3.4.1 Prediction of Damper Temperature Rise during Wind Storms.	89
3.4.2 Health Monitoring of In-Situ Bay-Bridge Dampers	89
4 WIRELESS SYSTEM FOR MONITORING OF DAMPERS	91
REFERENCES.....	97
APPENDIX A: INSTALLATION AND PROTECTION OF WELDABLE STRAIN GAUGES.....	99

LIST OF FIGURES

Fig. 1.1	View of 250-kip damper tested at the Pacific Earthquake Engineering Research Center, U.C. Berkeley. The damper shown mounted on the testing machine is one of the fluid dampers from the 91/5 overcrossing tested during the viscous heating investigation by Black and Makris (2005, 2007).	2
Fig. 1.2	View of 450-kip damper tested in an outdoor setting at the Pacific Earthquake Engineering Research Center, U.C. Berkeley.	3
Fig. 1.3	Portable data acquisition system that can be used to collect data and transmit them via wired ethernet or wireless (Wi-Fi) communication networks.	4
Fig. 2.1	Principal strains ϵ_{xx} and $\epsilon_{\theta\theta}$	6
Fig. 2.2	<i>Example:</i> axial strain level along the damper shell of the 250-kip damper when stressed at 1/5 of its capacity = 50 kips.	7
Fig. 2.3	250-kip damper in the damper testing machine at the Pacific Earthquake Engineering Research Center laboratory, UC Berkeley.	8
Fig. 2.4	Cross section of 250-kip damper.	9
Fig. 2.5	450-kip damper in the damper testing machine at the Pacific Earthquake Engineering Research Center laboratory, UC Berkeley.	10
Fig. 2.6	Cross section of 450-kip damper.	11
Fig. 2.7	Strain-gauge rosettes on the casing of the 250-kip damper.	12
Fig. 2.8	Strain-gauge rosette on the extender of the 250-kip damper.	13
Fig. 2.9	Vishay Micro-Measurements 700 portable strain-gauge welding and soldering unit.	14
Fig. 2.10	A built-up rosette of weldable strain gauges.	15
Fig. 2.11	Location of weldable strain gauges on the 450-kip damper.	17
Fig. 2.12	Celesco PT5AV position and velocity transducer.	18
Fig. 2.13	Transtek 0127-0001 linear velocity transducer and Novotechnik TLH-1000 position transducer.	19
Fig. 2.14	Novotechnik TLH position transducer.	20
Fig. 2.15	Results of Test No. 41 on the 250-kip damper equipped with bondable strain gauges.	22

Fig. 2.16	Results of Test No. 39 on the 250-kip damper equipped with bondable strain gauges.	23
Fig. 2.17	Schematic of the cross-section of a fluid damper showing the stressing of the damper casing during (a) tension of the piston rod, and (b) compression.	25
Fig. 2.18	Displacement, velocity and force histories for Test No. 39 on the 250-kip damper. ..	27
Fig. 2.19	Results of Test No. 38 on the 250-kip damper equipped with bondable strain gauges.	28
Fig. 2.20	Results of Test No. 43 on the 250-kip damper equipped with bondable strain gauges.	29
Fig. 2.21	Results of Test No. 48 on the 250-kip damper equipped with weldable strain gauges.	31
Fig. 2.22	Results of Test No. 46 on the 250-kip damper equipped with weldable strain gauges.	32
Fig. 2.23	Results of Test No. 56 on the 250-kip damper equipped with weldable strain gauges.	33
Fig. 2.24	Results of Test No. 60 on the 250-kip damper equipped with weldable strain gauges.	34
Fig. 2.25	Results of Test No. 104 on the 450-kip damper.	36
Fig. 2.26	Results of Test No. 105 on the 450-kip damper.	37
Fig. 2.27	Results of Test No. 95 on the 450-kip damper.	38
Fig. 2.28	The thin line shows the velocity signal obtained by differentiating the displacement signal, while the bold line shows the smoothed signal obtained by after taking the simple moving average with span N of that velocity signal. v_{peak} is the peak of the smoothed signal.	41
Fig. 2.29	Force output of 450-kip damper.	44
Fig. 3.1	The outdoor test setup is approximately 1/3 mile from the San Francisco Bay. The X in the smaller photograph marks the location of the test setup outside the PEER laboratory at the Richmond Field Station, University of California, Berkeley (Images from Google Maps).	48
Fig. 3.2	Outdoor test setup.	49

Fig. 3.3	Old frame salvaged from the PEER laboratory yard for use in the outdoor testing program.	50
Fig. 3.4	ATS controller and data acquisition cart; portable hydraulic pump.	50
Fig. 3.5	Fully instrumented 450-kip damper mounted on the outdoor testing machine at the PEER laboratory, University of California, Berkeley.	51
Fig. 3.6	Built-up rosette of weldable strain gauges covered with Vishay Micro-Measurements protective M-Coat A, B and J. Below the rosette is a single weldable gauge (longitudinal strain) that is only covered with the transparent M-Coat A.	53
Fig. 3.7	Results of a slow outdoor test with low-displacement amplitude.	59
Fig. 3.8	Results of a fast outdoor test with large-displacement amplitude.	60
Fig. 3.9	Comparison of the results from the first two cycles of a fast test (0.63 in/sec). Test No. 310 (right), which was conducted 2.295 miles (cumulative travel) after Test 275 (left), shows a 15% drop in peak recorded force.	62
Fig. 3.10	Peak force and temperature rise over the course of Tests 257 and 258.	64
Fig. 3.11	Peak force and temperature rise over the course of Tests 329 and 330.	64
Fig. 3.12	Peak force and temperature rise over the course of Tests 298 and 299.	65
Fig. 3.13	Peak force and temperature rise over the course of Tests 295, 296 and 297.	65
Fig. 3.14	Damper force for Test No. 298 as obtained from the load cell and as computed from the strain gauges attached on the damper extender.	67
Fig. 3.15	Damper force for the first 500 seconds of Test No. 299 as obtained from the load cell and as computed from the strain gauges attached on the damper extender.	68
Fig. 3.16	Damper force for Test No. 242 as obtained from the load cell and as computed from the strain gauges attached on the damper extender.	69
Fig. 3.17	Results of Test 271 (conducted on March 31, 2010). LC: force obtained from the load cell; SG: force computed from the strain gauges.	71
Fig. 3.18	Results of Test 283 (conducted on April 14, 2010). LC: force obtained from the load cell; SG: force computed from the strain gauges.	72
Fig. 3.19	Results of Test 289 (conducted on April 21, 2010). LC: force obtained from the load cell; SG: force computed from the strain gauges.	73
Fig. 3.20	Results of Test 295 (conducted on May 03, 2010). LC: force obtained from the load cell; SG: force computed from the strain gauges.	74

Fig. 3.21	Results of Test 302 (conducted on May 06, 2010). LC: force obtained from the load cell; SG: force computed from the strain gauges.....	75
Fig. 3.22	Results of Test 306 (conducted on May 10, 2010). LC: force obtained from the load cell; SG: force computed from the strain gauges.....	76
Fig. 3.23	Hystereses loops of Figs. 3.17 to 3.22.	77
Fig. 3.24	Results of Test 318 (conducted on May 14, 2010). LC: force obtained from the load cell; SG: force computed from the strain gauges.....	78
Fig. 3.25	Results of Test 324 (conducted on May 17, 2010). LC: force obtained from the load cell; SG: force computed from the strain gauges.....	79
Fig. 3.26	Results of Test 333 (conducted on May 21, 2010). LC: force obtained from the load cell; SG: force computed from the strain gauges.....	80
Fig. 3.27	Results of Test 339 (conducted on May 25, 2010). LC: force obtained from the load cell; SG: force computed from the strain gauges.....	81
Fig. 3.28	Hystereses loops of Figs. 3.24 to 3.27.	82
Fig. 3.29	Comparison of the results from a test with ± 1.5 in stroke and 15 sec period conducted indoors with short cables (left) and outdoors with long cables (right).	83
Fig. 3.30	Response quantities for Test No. 318 recorded with a sampling rate of 10 Hz and for Test No. 319 recorded with a sampling rate of 2 Hz.	85
Fig. 3.31	Velocity-dependence of damper force output at low velocities. The bold black line shows the force of the manufacturer's specification at design velocity, while the heavy grey line shows a fit of the experimental data in the 0.1–0.7 in/s velocity range.....	86
Fig. 4.1	Opto22 system featuring board with central unit with wireless antenna, six channel modules (one displacement, one velocity, and four strain gauge) and two power supplies. The system is protected by a hermetically sealed plastic enclosure box.	92
Fig. 4.2	Opto 22 connected to a laptop computer with ethernet LAN line.	93
Fig. 4.3	Schematic diagram of wireless monitoring system in which each damper is configured with its own Opto22 enclosure box (as the one shown in Fig. 4.1) communicating with a remote computer.	94
Fig. 4.4	Schematic diagram of wireless monitoring system in which two dampers share an Opto22 enclosure box communicating with a remote computer.	95

LIST OF TABLES

Table 2.1	Geometrical characteristics and mechanical properties of the two dampers considered in this study.....	9
Table 2.2	Tests conducted on the 250-kip damper equipped with bondable strain gauges.	13
Table 2.3	Tests conducted on the 250-kip damper equipped with weldable strain gauges.....	16
Table 2.4	Tests conducted on the 450-kip damper.	21
Table 2.5	Velocity dependence of force and error between target and experimental force.	43
Table 3.1	Channel list for outdoor tests on 450-kip damper.	52
Table 3.2	Outdoor tests conducted on the 450-kip damper.	55
Table 3.2	Outdoor tests conducted on the 450-kip damper.	56
Table 3.2	Outdoor tests conducted on the 450-kip damper.	57
Table 3.2	Outdoor tests conducted on the 450-kip damper.	58

1 Introduction

The rapid success of fluid dampers as seismic protection devices, in association with the increasing need for safe bridges, has accelerated the implementation of large-capacity damping devices in bridges. For instance, the Vincent Thomas suspension bridge, the Coronado bridge, and the 91/5 highway over-crossing (Delis et al. 1996, Makris and Zhang 2004), all three in southern California, as well as the Rion-Antirion cable-stayed bridge (Papanikolas 2002) in western Greece, are all examples of bridges that have been equipped with fluid dampers.

The main challenge with fluid dampers is whether they will maintain their long-term integrity when placed in such large structures that are subjected to a variety of loads, appreciable dynamic displacements and long-term deformation patterns. While large displacements and velocities are expected during earthquake loading, a prolonged wind loading would increase substantially the temperature of the damper. Similarly, traffic loading that induces vibrations of small amplitude but very long duration may fatigue the damper and eventually lead to leaking. The problem of leaking dampers has emerged in recent years in some California bridges, such as the west span of the San Francisco–Oakland Bay Bridge and the Vincent Thomas Bridge crossing the Los Angeles Harbor.

In this project, a comprehensive component testing program was undertaken to develop and validate simple and reliable technologies to monitor the force output and velocity histories of fluid dampers when installed in the field.

The research included experiments on four medium-size to large-size fluid dampers at the Earthquake Simulator Laboratory of the Pacific Earthquake Engineering Research (PEER) Center at the Richmond Field Station, University of California, Berkeley. Two of the dampers were identical to the fluid dampers installed in the 91/5 over-crossing in Orange Country, CA (maximum stroke = ± 8.0 inches with maximum force output = 250 kips at 42 in/sec piston velocity). One of these two 91/5 dampers (shown in Fig. 1.1) was extensively tested during 2001–2002 while



Fig. 1.1 View of 250-kip damper tested at the Pacific Earthquake Engineering Research Center, U.C. Berkeley. The damper shown mounted on the testing machine is one of the fluid dampers from the 91/5 overcrossing tested during the viscous heating investigation by Black and Makris (2005, 2007).

studying the problem of viscous heating of fluid dampers (Black and Makris 2005, 2007). In addition to the two 91/5 dampers, two larger fluid dampers (maximum stroke = ± 19.0 inches with maximum force output = 450 kips at 85 in/sec piston velocity) were tested. These larger dampers were the same type of dampers as those installed at the west span of the San Francisco–Oakland Bay Bridge.

The first series of component tests were conducted at the Earthquake Simulator Laboratory with the damper testing machine shown in Fig. 1.1. These tests included a wide range of combinations of displacements and velocities in order to examine the fidelity and dependability of using bondable and weldable strain gauges, as well as displacement and velocity transducers, to



Fig. 1.2 View of 450-kip damper tested in an outdoor setting at the Pacific Earthquake Engineering Research Center, U.C. Berkeley.

estimate the force output of a damper. The force output computed from the strain gauges and the displacement and velocity transducers was compared with the force output from the load cell.

After the first series of component tests was completed indoors, a 450-kip damper was moved outside of the laboratory and was mounted on a surplus test frame (Fig. 1.2). Since the facility is on the edge of the San Francisco Bay, the damper was exposed to environmental conditions that might be expected in an actual field installation. The condition of the damper and the various transducers over time were remotely (using cables) assessed from inside the laboratory. The damper was cycled continually an average of ten hours per day at low displacements and frequencies typical of what would be experienced in the field. At the end of the outdoor tests, the cumulative stroke on the damper had exceeded 5.5 miles.

During the experimental effort, the issue of transmitting data wirelessly to a remote recording center was investigated (Fig. 1.3). We examined how recent advances in technology can be applied to health monitoring of fluid viscous dampers in bridges. Using commercially available electronic components manufactured by Opto 22, we built a portable data acquisition system that can be used to collect and transmit data from a damper on a bridge to a remote loca-

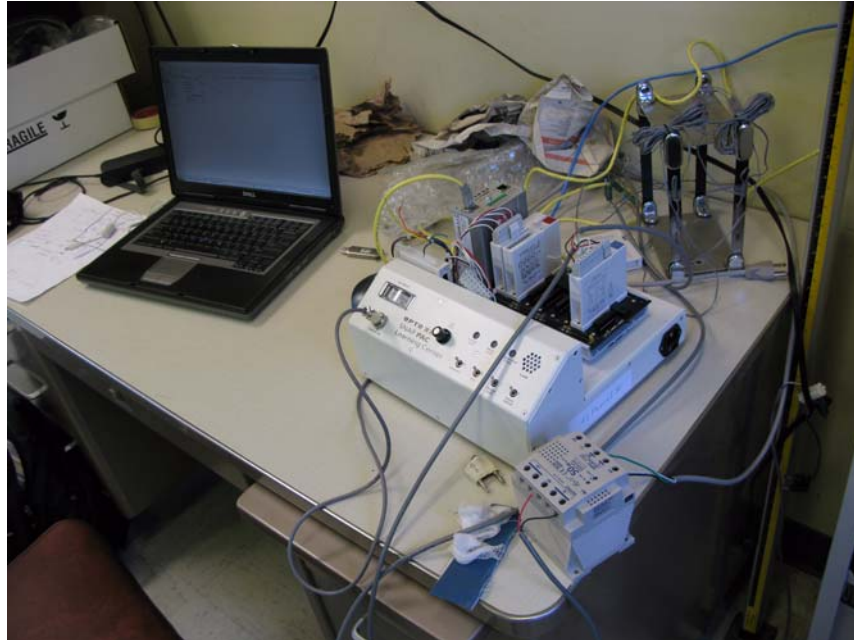


Fig. 1.3 Portable data acquisition system that can be used to collect data and transmit them via wired ethernet or wireless (Wi-Fi) communication networks.

tion using wireless communication (Wi-Fi). We hope that we will have a chance to instal and test this technology on an actual bridge in the near future.

The validation of the proposed technology together with the development of simple, inexpensive and reliable methods to transfer and record data will benefit Caltrans. The benefits include the ability to continuously monitor the forces that develop on dampers and therefore assess their condition; together with the ability to evaluate how intense is the loading of dampers that are installed in various bridges. If a substantial drop in the force output of a damper is detected, the specific damper can be replaced safely on time.

2 Indoor Experiments: Proof of Concept

2.1 PROBLEM STATEMENT

The main challenge with fluid dampers is whether they will maintain their long-term integrity when placed in such large structures, exposed to corrosive marine environment conditions and subjected to a variety of loads and movements. While large displacements and velocities are expected during earthquake loading, a prolonged wind loading would increase substantially the temperature of the damper. Similarly, traffic loading that induces vibrations of small amplitude but very long duration may be detrimental in the event that installation imperfections are present. The alarming problem of leaking dampers that has emerged in recent years in California bridges has prompted this investigation into health monitoring of fluid dampers in bridges.

There has been past experience from in-service monitoring of bridges using strain gauges. Howell and Shenton (2006) describe a small digital data acquisition system with strain transducers, battery packs and an environmental enclosure that is resistive to marine environments. In this project, we experimentally measure the force output of the damper by applying both adhesive-bonded strain gauges and weldable strain gauges on the damper housing and damper extender. The goal is to examine whether strain gauges can be used to accurately measure the force output.

2.2 USING THE DAMPER AS A LOAD CELL TO MEASURE FORCE OUTPUT

In this research, we use strain gauges to monitor the force output of fluid dampers. The damper housing is merely a steel cylinder that is intended to be loaded along its principal direction and can be easily transformed to a load cell. Assuming that the attachments of the damper are perfectly aligned, the principal directions of deformation are the longitudinal direction ($x-x$) and the tangential direction ($\theta-\theta$) of the cylindrical housing, as shown in Fig. 2.1. In this case, strain

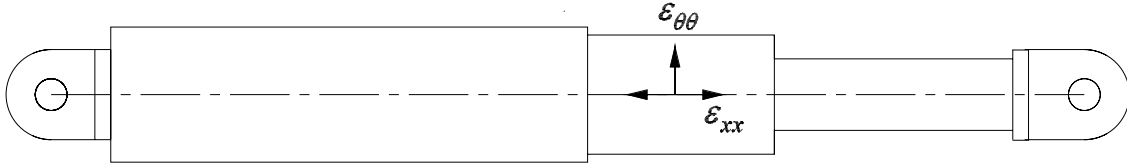


Fig. 2.1 Principal strains ϵ_{xx} and $\epsilon_{\theta\theta}$.

gauges are placed along the principal directions, and direct measurements of ϵ_{xx} and $\epsilon_{\theta\theta}$ are obtained. The principal stresses, σ_{xx} and $\sigma_{\theta\theta}$ may then be calculated from Hooke's law

$$\sigma_{xx} = \frac{E(\epsilon_{xx} + \nu\epsilon_{\theta\theta})}{1 - \nu^2} \quad (2.1a)$$

$$\sigma_{\theta\theta} = \frac{E(\epsilon_{\theta\theta} + \nu\epsilon_{xx})}{1 - \nu^2} \quad (2.1b)$$

where E and ν are the Young's modulus and Poisson's ratio of the steel of the damper housing. The force output of the damper is deduced directly as

$$P = A\sigma_{xx} = \frac{\pi}{4}\sigma_{xx}(d_o^2 - d_i^2) \quad (2.2)$$

where d_o and d_i are the inner and outer diameters of the damper housing. In terms of the experimentally measured strains, the force output is

$$P = \frac{\pi}{4}(d_o^2 - d_i^2) \frac{E(\epsilon_{xx} + \nu\epsilon_{\theta\theta})}{1 - \nu^2} \quad (2.3)$$

In addition to the strain measurements which will yield directly the measured forces that develop in the dampers, the project proposes the measurement of the piston's velocity. This can be either recovered by differentiating the displacement signal measured using a standard Linear Variable Displacement Transducer (LVDT) or obtained directly with commercially available velocity transducers. Velocity transducers designed to operate in harsh environments are commercially available. Further details on the instrumentation used in this project are offered later.

With the actual (measured) piston velocity, $\dot{u}(t)$, available the expected (theoretical) force output from the damper is

$$\bar{P}(t) = C_\alpha |\dot{u}(t)|^\alpha \text{sgn}[\dot{u}(t)] \quad (2.4)$$

The expected force output of the damper will then be compared with the experimentally measured force output of the damper given by Eq. (2.3), and one can directly detect if there is an appreciable drop in the damper force. In the event that a large drop in force between these two

$$\Delta P(t) = \bar{P}(t) - P(t) \quad (2.5)$$

(or between $\bar{P}(t)$ and the experimental force obtained during the production tests at the same piston velocity) is detected, say more than 15%, then one can pronounce the damper damaged. Of course, the fidelity of the theoretical force output is expected to have been validated during the production tests of the dampers.

Furthermore, if the force drop increases with the number of cycles, then the damage will be considered to be significant, and the dampers need to be replaced immediately. Alternatively, under cyclic loading, any significant departure of the recorded force–displacement loop shape from the anticipated shape established during production testing can be evaluated, and damage can be associated based on the distortion of the loops rather on the percentage of force drop.

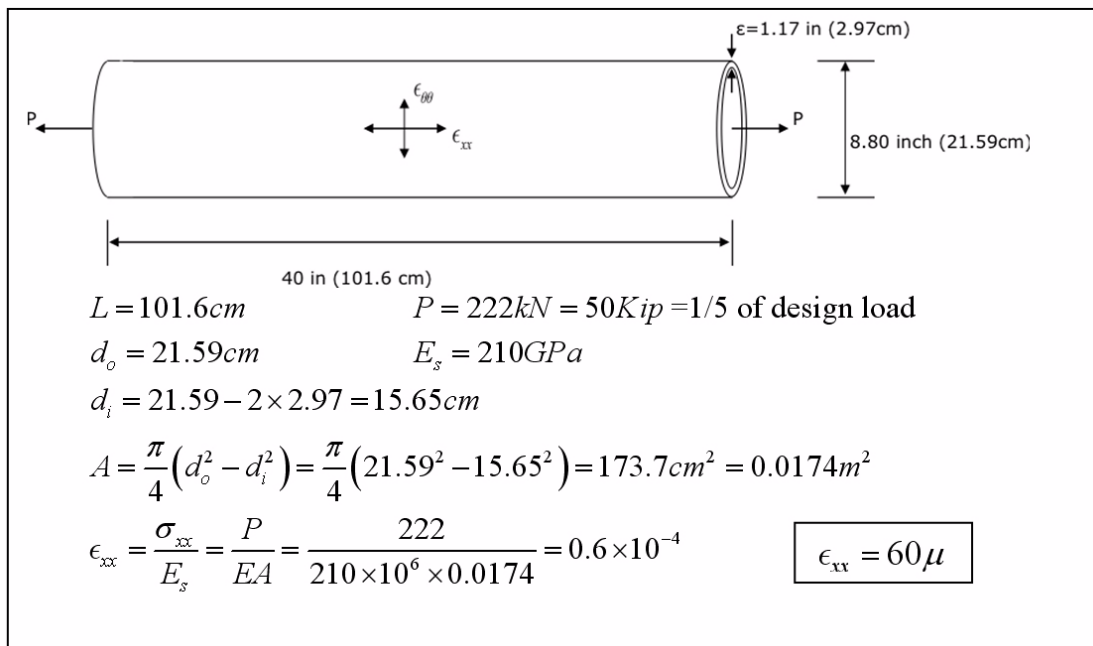


Fig. 2.2 Example: axial strain level along the damper shell of the 250-kip damper when stressed at 1/5 of its capacity = 50 kips.

2.3 DAMPER SPECIMENS

The experimental program included two fluid damper types: a 250-kip damper and a 450-kip damper. Both types of these dampers are double-ended, i.e., the piston rod extends in both chambers of the damper in order to achieve a symmetric mechanical behavior.

2.3.1 250-Kip Damper

Figure 2.3 shows a photograph of a 250-kip Taylor Devices fluid viscous damper installed on the damper testing machine at the Earthquake Simulator Laboratory of the Pacific Earthquake Engineering Research (PEER) Center, University of California, Berkeley. The testing machine consists of a self-equilibrating reaction frame with a dynamic, ± 12 -in. servo-hydraulic actuator that can deliver about 270 kips at 25 in/sec. The 250-kip damper considered in this study was origi-



Fig. 2.3 250-kip damper in the damper testing machine at the Pacific Earthquake Engineering Research Center laboratory, UC Berkeley.

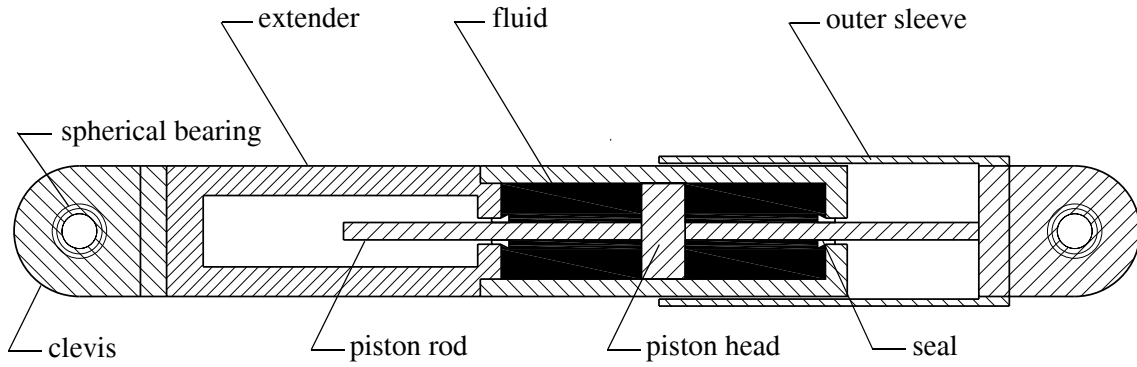


Fig. 2.4 Cross section of 250-kip damper.

nally one of two spare dampers provided for the 91/15 overpass in the Los Angeles area, the seismic response of which has been studied by Makris and Zhang (2004).

The 250-kip damper has a mid-stroke length of 72 in., and a maximum stroke of ± 8 in. The piston head has been designed with fluid flow orifice channels to deliver the nonlinear force-velocity relation given by Eq. (2.4), where $\alpha = 0.35$ and $C_\alpha = C_{0.35} = 60 \text{ kip}(\text{in}/\text{sec})^{0.35}$. Figure 2.4 shows a cross section of the 250-kip damper. The damper has an *extender* (spacer) circular tube with a cross sectional area $A_e = 35.7 \text{ in}^2$. Table 2.1 lists geometrical characteristics and

Table 2.1 Geometrical characteristics and mechanical properties of the two dampers considered in this study.

Quantity	250-kip damper	450-kip damper
Damping coefficient, C_α	$60 \text{ kip}(\text{sec}/\text{in})^{0.35}$	$118.6 \text{ kip}(\text{sec}/\text{in})^{0.30}$
Exponent, α	0.35	0.30
Thickness of damper housing, ϵ [in.]	1.170	1.825
Piston diameter, d_p [in.]	5.87	10.2
Rod diameter, d_r [in.]	2.23	3.72
Area of piston head, A_p [in ²]	23.19	70.84
Maximum stroke, U_0 [in.]	± 8.0	± 19.0
Cross-sectional area of extender, A_e [in ²]	35.7	57.1

mechanical properties of the damper. The damper had been previously used in an experimental study by Makris and Black (2005, 2007) at UC Berkeley that investigated the viscous heating of fluid dampers under wind and seismic loading.

The experimental program included tests on two of these dampers: one equipped with bondable strain gauges and one equipped with weldable strain gauges.

2.3.2 450-Kip Damper

Figure 2.5 shows a photograph of a 450-kip Taylor Devices fluid viscous damper installed on the damper testing machine at PEER's Earthquake Simulator Laboratory. The damper is identical to a *Type-A* damper used on the seismic retrofit project that included the addition of fluid viscous dampers on the west span of the San Francisco–Oakland Bay Bridge. installed The 450-kip damper has a mid-stroke length of 11 ft - 1 in., and a maximum stroke of ± 19 in. The piston head



Fig. 2.5 450-kip damper in the damper testing machine at the Pacific Earthquake Engineering Research Center laboratory, UC Berkeley.

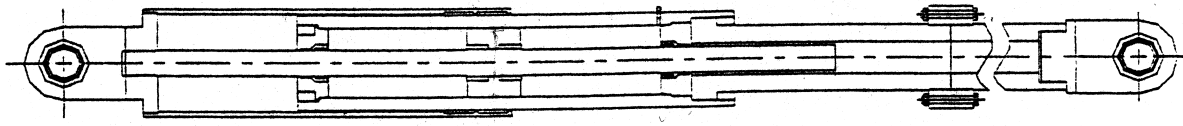


Fig. 2.6 Cross section of 450-kip damper.

has been designed with fluid flow orifice channels to deliver the nonlinear force-velocity relation given by Eq. (2.4), where $\alpha = 0.30$ and $C_\alpha = C_{0.30} = 118.6 \text{ kip}(\text{in}/\text{sec})^{0.30}$. Figure 2.6 shows a cross section of the 450-kip damper. The damper has an *extender* (spacer) circular tube with a cross sectional area $A_e = 57.1 \text{ in}^2$. The right column of Table 2.1 lists geometrical characteristics and mechanical properties of the damper.

2.4 EXPERIMENTAL PROGRAM

The objective of this series of experiments was to determine whether indeed the readings from strain gauges attached on the damper could be reliably used to accurately predict the damper force. The dampers were subjected to sinusoidal displacement signals given by

$$u(t) = u_0 \sin(2\pi ft) \quad (2.6)$$

with a wide range of displacement amplitudes, u_0 , and frequencies, f .

2.4.1 250-Kip Damper with Bondable Strain Gauges

One of the two available 250-kip Taylor Devices fluid dampers was tested first. The damper was equipped with conventional, adhesive-bonded strain gauges. A total of six strain-gauge rosettes were bonded on the specimen. Figure 2.7 shows a rosette bonded on the side of the damper casing closer to the extender (E-side) and a rosette bonded on the side of the damper casing closer to the actuator (A-side). Two more rosettes that are not visible in the photograph are bonded on the bottom of the damper casing, i.e., at 90 degrees, one on the E-side and one on the A-side. Figure 2.8 shows one of two rosettes that were bonded on the extender.

The relative displacement between the actuator clevis and a stationary point on the reaction frame of the testing machine was measured using a ± 3 in. Transtek Series 240 DCDT dis-

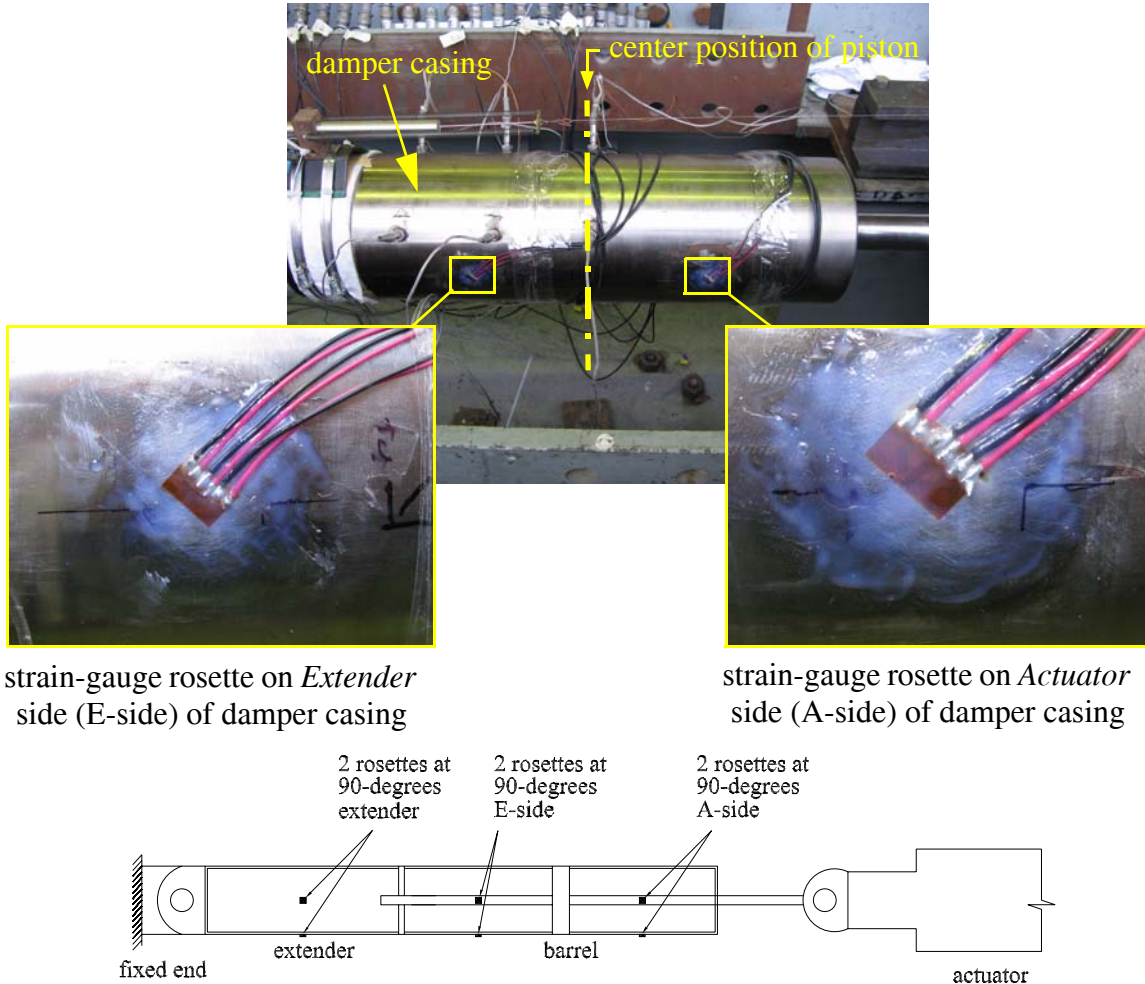


Fig. 2.7 Strain-gauge rosettes on the casing of the 250-kip damper.

placement transducer. This will henceforth be referred to as the *actuator displacement*. Another ± 3 in. Transtek Series 240 DCDT displacement transducer was used to measure the relative displacement between a point on the damper cover and a point on the damper barrel. This will henceforth be referred to as the *damper displacement*.

The 250-kip damper with bonded strain gauges was subjected to sinusoidal signals with various displacement amplitudes (ranging from 0.05 in. to 2.5 in.) and frequencies (from 0.25 Hz to 2 Hz), corresponding to velocity amplitudes, v_0 , ranging between 0.3 in/sec to 23.6 in/sec. Table 2.2 lists the tests conducted on the 250-kip damper equipped with bondable strain gauges, together with the number of cycles, displacement amplitude u_0 , frequency f , and corresponding velocity amplitude v_0 , of each test.



Fig. 2.8 Strain-gauge rosette on the extender of the 250-kip damper.

Table 2.2 Tests conducted on the 250-kip damper equipped with bondable strain gauges.

Test #	File Name	Freq. f [Hz]	Displacement, u_0 [in]			Velocity, v_0 [in/s]			Force, P [kips]		Cycles
			Target	Actual (+)	Actual (-)	Target	Actual (+)	Actual (-)	Actual (+)	Actual (-)	
27	09051402	0.5	1.00	0.96	-0.99	3.14	3.13	-3.18	104	-108	5
28	09051403	0.5	0.50	0.49	-0.53	1.57	1.72	-1.80	80	-82	5
29	09051404	0.5	0.25	0.20	-0.27	0.79	0.77	-0.79	54	-55	5
30	09051405	0.25	0.50	0.49	-0.56	0.79	0.83	-0.84	58	-60	5
31	09051406	0.25	0.50	0.52	-0.55	0.79	0.83	-0.86	57	-60	5
32	09051407	0.25	0.25	0.24	-0.32	0.39	0.41	-0.42	40	-42	5
33	09051408	1	0.25	0.19	-0.25	1.57	1.56	-1.60	67	-70	5
34	09051409	2	0.25	0.17	-0.19	3.14	3.23	-3.09	70	-73	5
35	09051410	1	0.05	0.06	-0.08	0.31	0.41	-0.33	27	-29	5
36	09051411	2	0.05	0.03	-0.07	0.63	0.52	-0.51	22	-24	5
37	09051412	1	0.10	0.13	-0.14	0.63	0.79	-0.77	48	-50	5
38	09051413	2	0.10	0.09	-0.12	1.26	1.18	-1.21	45	-47	5
39	09051414	0.5	1.00	0.96	-0.99	3.14	3.22	-3.30	100	-106	5
40	09051415	0.5	0.50	0.50	-0.52	1.57	1.63	-1.67	76	-80	5
41	09051416	0.5	0.25	0.22	-0.26	0.79	0.79	-0.81	54	-57	5
42	09051417	1.5	2.50	2.36	-2.42	23.56	19.16	-17.72	188	-180	5
43	09051418	1.5	2.50	2.45	-2.46	23.56	20.00	-18.61	190	-178	5

2.4.2 250-Kip Damper with Weldable Strain Gauges

The second of the two available 250-kip Taylor Devices fluid dampers was equipped with Micro-Measurements CEA-06-W250A-120 weldable strain gauges. These types of strain gauges are factory-prebonded with a high-performance adhesive to thin metal carriers. The metal carriers are spot welded around their perimeter to the specimen using a portable stored-energy hand-probe welder (Fig. 2.9). Weldable strain gauges are advantageous to bondable strain gauges in a bridge application because for the former the specimen requires minimal surface preparation; only a solvent cleaning and abrasion of the test surface with sandpaper or a small hand-held grinder is necessary. The welder unit weighs only 21 lb. and can be transported easily to the place of application. The welding unit incorporates a soldering gun to connect wires to terminals of the strain gauge. A clear and easy-to-follow, step-by-step procedure for attaching the gauges is provided by the manufacturer. After a few applications, the time required to layout, weld, and solder the terminals of a weldable strain gauge was less than 20 minutes. Lastly, protective coatings can be easily applied on the strain gauge to protect it against the harsh marine environment of a bridge. For example, a Vishay Micro-Measurements M-Coat A, followed by M-Coat B or M-Coat C, followed by M-Coat J will provide sufficient protection for the strain gauge.

Figure 2.10 shows one of several built-up rosettes consisting of weldable strain gauges. The arrangement of strain-gauge rosettes on the second 250-kip damper is identical to that shown



Fig. 2.9 Vishay Micro-Measurements 700 portable strain-gauge welding and soldering unit.

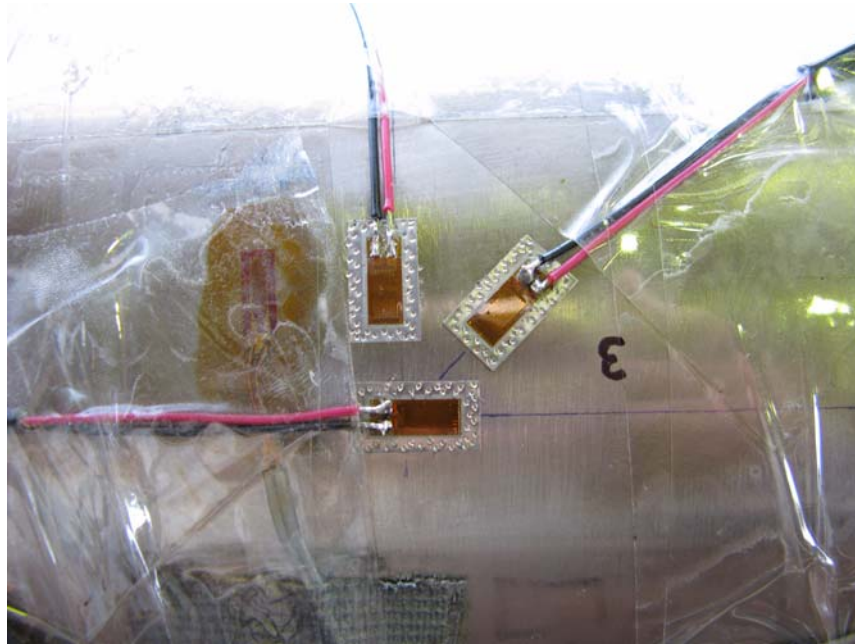


Fig. 2.10 A built-up rosette of weldable strain gauges.

in Fig. 2.7 for the bondable strain-gauge rosettes. Data from a total of 18 strain gauge channels (six rosettes) were collected during this series of tests. It is important to note at this point that, as the experiments confirmed, the use of this many strain gauges is unnecessary because there is a large degree of redundancy in the data collected.

As for the tests on the damper equipped with bondable strain gauges, the actuator and damper displacements was measured using two Transtek Series ± 3 in. 240 DCDT displacement transducers.

The 250-kip damper with weldable strain gauges was subjected to the same test protocol as the damper with bondable strain gauges. Table 2.3 lists the tests conducted on the 250-kip damper equipped with weldable strain gauges, together with the number of cycles, displacement amplitude u_0 , frequency f , and corresponding velocity amplitude v_0 , of each test.

2.4.3 450-Kip Damper

The third series of indoor tests on the damper testing machine at the Pacific Earthquake Engineering Research Center, University of California, Berkeley, was conducted on the 450-kip Taylor Devices fluid viscous damper with ± 19 in. displacement capacity.

Table 2.3 Tests conducted on the 250-kip damper equipped with weldable strain gauges.

Test #	File Name	Freq. f [Hz]	Displacement, u_0 [in]			Velocity, v_0 [in/s]			Force, P [kips]		Cycles
			Target	Actual (+)	Actual (-)	Target	Actual (+)	Actual (-)	Actual (+)	Actual (-)	
46	09063001	0.5	1.00	0.94	-1.00	3.14	3.14	-3.15	102	-109	5
47	09063002	0.5	0.50	0.48	-0.53	1.57	1.73	-1.75	79	-85	5
48	09063003	0.5	0.25	0.21	-0.26	0.79	0.79	-0.80	53	-55	5
49	09063004	0.25	0.50	0.51	-0.56	0.79	0.83	-0.85	57	-59	5
50	09063005	0.25	0.25	0.25	-0.31	0.39	0.40	-0.39	39	-43	5
51	09063006	1	0.25	0.19	-0.24	1.57	1.67	-1.63	67	-71	5
52	09063007	2	0.25	0.15	-0.20	3.14	3.09	-2.95	71	-74	5
53	09063008	1	0.10	0.12	-0.15	0.63	0.88	-0.86	51	-54	5
54	09063009	2	0.05	0.03	-0.05	0.63	0.49	-0.46	22	-26	5
55	09063010	1	0.10	0.13	-0.15	0.63	0.89	-0.86	51	-53	5
56	09063011	2	0.10	0.09	-0.11	1.26	1.15	-1.16	48	-50	5
57	09063012	0.5	1.00	0.94	-1.01	3.14	3.18	-3.21	98	-105	5
58	09063013	0.5	0.50	0.51	-0.53	1.57	1.63	-1.68	76	-79	5
59	09063014	0.5	0.25	0.22	-0.26	0.79	0.72	-0.73	54	-57	5
60	09063015	1.5	2.50	2.47	-2.52	23.56	21.05	-19.11	189	-189	5

The damper was equipped with a total of six weldable strain gauges measuring:

- longitudinal strain ϵ_{xx} on the top of the barrel
- hoop strain $\epsilon_{\theta\theta}$ on the top of the barrel
- longitudinal strain ϵ_{xx} on the side of the barrel
- hoop strain $\epsilon_{\theta\theta}$ on the side of the barrel
- longitudinal strain ϵ_{xx} on the top of the extender
- longitudinal strain ϵ_{xx} on the top of the extender

The locations of the strain gauges are indicated in Fig. 2.11.

Various options were considered to measure displacement and velocity. Since the force output of fluid dampers is a function of velocity, it is important to measure the velocity, either directly or by differentiating a measured displacement signal. The latter method often results in a noisy velocity signal, and filtering may be necessary to remove the noise to obtain a clean signal.

A challenge for the application at hand is the harsh environment that the displacement or

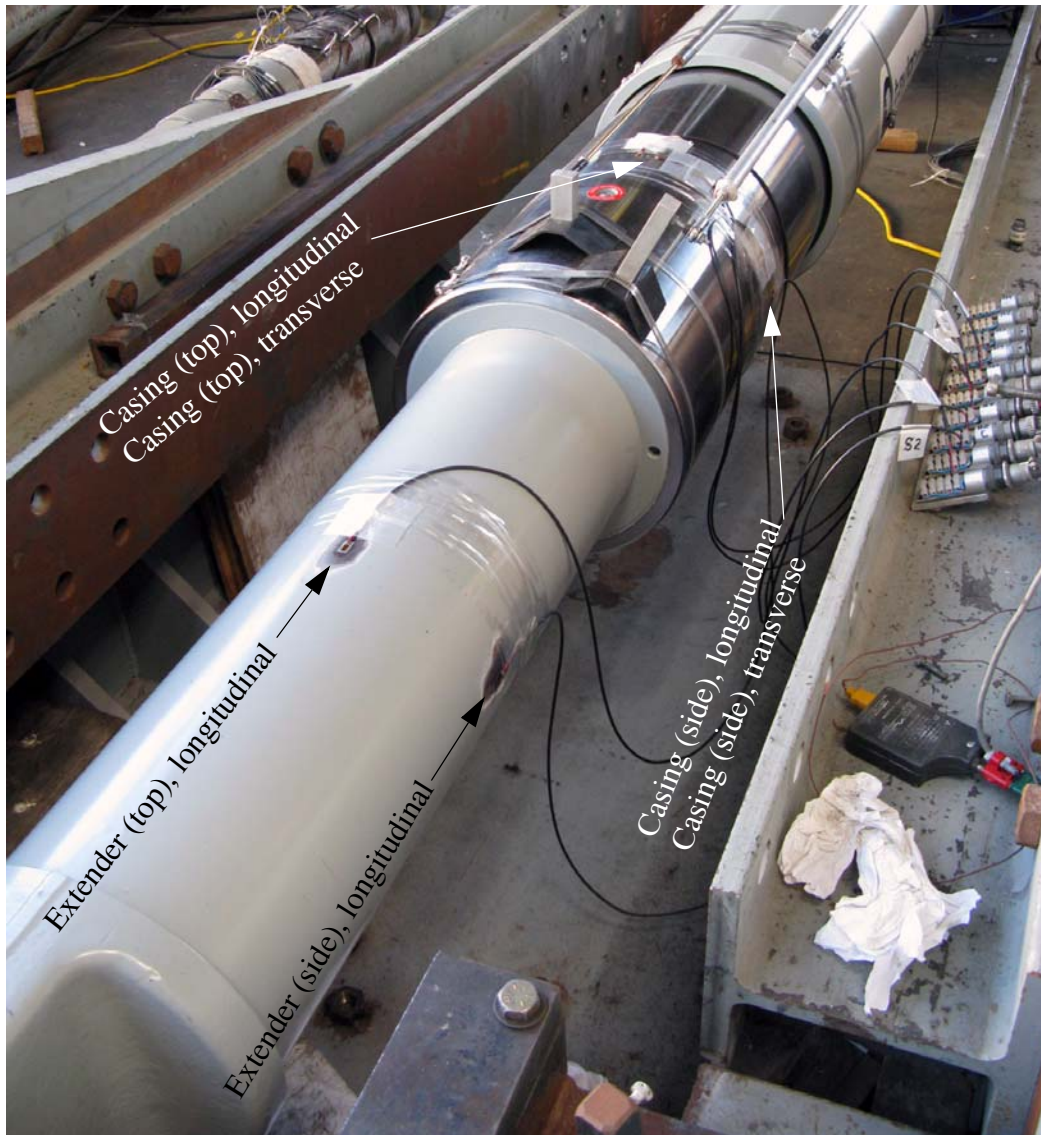


Fig. 2.11 Location of weldable strain gauges on the 450-kip damper.

velocity transducer will be exposed to. The displacement or velocity transducer used must be able to withstand a bridge's corrosive marine environment. For the tests that were conducted in an indoor setting, the following were used to measure displacement and velocity:

- A **Celesco PT5AV position and velocity combination transducer** (Fig. 2.12). This transducer features a precision plastic-hybrid potentiometer that provides accurate position feedback, while a self-generating DC tachometer provides a velocity signal that is proportional to the speed of the traveling measuring cable. The transducer has a ± 20 in. displacement range with ± 0.1 in. accuracy at full stroke. The maximum cable velocity is



Fig. 2.12 Celesco PT5AV position and velocity transducer.

300 in/sec. The rated life of the device is 500,000 cycles. The device enclosure is made from hard anodized aluminum, resistive to the elements. However, for a bridge application, the authors recommend the use of an additional plastic enclosure to protect the device from water. The measuring cable does not need to be protected, as the manufacturer provides cables from materials that resist corrosion. Also, the authors recommend that, upon installation, the measuring cable is angled slightly downward so that water that accumulates on the cable will not flow and enter the device but rather flow away towards the target. The authors recommend the use of this device in a bridge application, as it combines good accuracy, robust performance in a harsh marine environment, and relatively low cost (approximately \$900).

- A **Transtek 0127-0001 linear velocity transducer** (Fig. 2.13). This transducer provide a simple, accurate means of measuring instantaneous velocity. The velocity signal obtained directly with this transducer is significantly cleaner than that obtained by differentiating a displacement signal obtained with a displacement transducer. The motion of a magnetic rod through a pair of series opposed coils causes the transducer to output a DC voltage that varies linearly with the instantaneous velocity. The basic design permits operation without



Fig. 2.13 Transtek 0127-0001 linear velocity transducer and Novotechnik TLH-1000 position transducer.

external excitation (Transtek 2009). The device has a stroke range of ± 12 in. While this device provides accurate velocity readings with a clean signal, the authors believe that it would have to be hermetically enclosed to ensure its proper long-term operation in the marine environment of the bridge.

- **A Novotechnik TLH-1000 position transducer** (Figs. 2.13 and 2.14). These transducers are extremely accurate, having a resolution of 0.0004 in., however, on a bridge application that requires shielding from the marine environment, the fact that they have long guides (see Fig. 2.13) makes their use difficult and likely very costly. The transducer used in the indoor experiments has a stroke of ± 20 in., yet the company offers a wide range of strokes depending on the application (e.g., the transducer shown in Fig. 2.14 has a shorter stroke of ± 4.5 in.), up to ± 60 in. The device does not require external excitation to operate.

The 450-kip damper was subjected to sinusoidal signals with various displacement amplitudes (ranging from 0.05 in. to 5.0 in.) and frequencies (from 0.0667 Hz to 2 Hz), corresponding to velocity amplitudes ranging between 0.1 in/sec to 23.6 in/sec. Table 2.4 lists the tests conducted on the 450-kip damper, together with the number of cycles, displacement amplitude, frequency and corresponding velocity amplitude of each test.

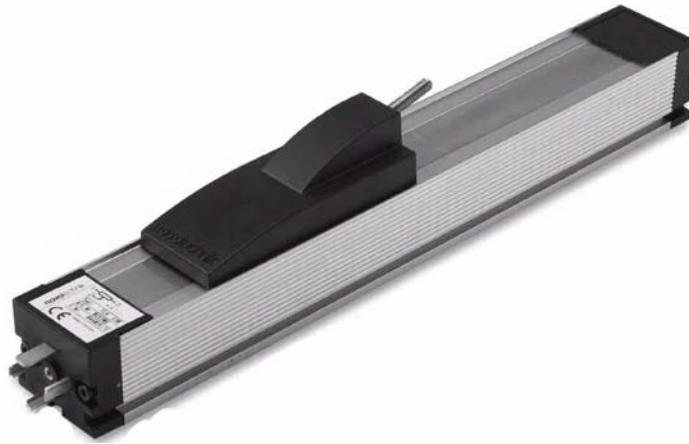


Fig. 2.14 Novotechnik TLH position transducer.

2.5 EXPERIMENTAL RESULTS

2.5.1 Results of Tests on the 250-Kip Damper Equipped with Bondable Strain Gauges

Table 2.2 lists the recorded peak displacement, velocity and force of all the tests conducted on the 250-kip damper equipped with bondable strain gauges at the PEER laboratory, UC Berkeley. Figures 2.15 and 2.16 show selected results of tests conducted on the 250-kip damper equipped with bondable strain-gauge rosettes (see Table 2.2). The left column shows graphs of results that were obtained from strain-gauge rosettes bonded on the damper casing, as shown in Fig. 2.7. The right column shows graphs of results obtained from rosettes bonded on the extender. The bottom-right corner of the figure serves as a legend explaining what each curve represents.

The displacement time histories shown are obtained from DCDTs attached on the damper and the actuator. In general, there is good agreement between the two recorded signals, except for differences attributed to slack (play) in the actuator and damper clevises and deformation of the testing machine. These differences are less pronounced for large-amplitude signals, implying that they are mostly caused by play in the clevises.

A total of 18 strain gauge channels (six rosettes) were recorded during the tests. On the left column, the graphs labelled ϵ_{xx} and $\epsilon_{\theta\theta}$ are the longitudinal and hoop strains recorded on the A-side and E-side (Fig. 2.7). The following channels are plotted:

Table 2.4 Tests conducted on the 450-kip damper.

Test #	File Name	Freq. f [Hz]	Displacement, u_0 [in]			Velocity, v_0 [in/s]			Force, P [kips]		Cycles
			Target	Actual (+)	Actual (-)	Target	Actual (+)	Actual (-)	Actual (+)	Actual (-)	
86	09110601	1.5	2.50	2.60	-2.73	23.56	19.00	-17.97	271	-280	5
87	09110602	1.5	2.50	2.60	-2.77	23.56	19.00	-18.23	269	-276	5
88	09110603	0.478	2.50	2.44	-2.43	7.51	7.70	-7.96	203	-202	6
89	09110604	0.478	5.00	4.94	-4.92	15.02	15.15	-15.15	256	-251	6
90	09110605	0.2	2.00	1.95	-1.93	2.51	2.62	-2.62	116	-114	4
91	09110606	0.2	2.16	2.11	-2.09	2.71	2.77	-2.77	121	-120	4
92	09110607	0.4	2.10	2.04	-2.02	5.28	5.27	-5.34	168	-167	4
93	09110608	0.6	2.10	2.03	-2.02	7.92	7.84	-7.99	199	-198	4
94	09110609	0.8	2.10	2.02	-2.02	10.56	10.55	-10.55	222	-217	4
95	09110610	1	2.10	2.01	-2.01	13.19	13.09	-13.09	239	-231	4
96	09110611	1.2	2.10	2.00	-2.01	15.83	14.97	-14.83	251	-241	4
97	09110612	0.067	0.375	0.35	-0.35	0.16	0.17	-0.17	18	-17	2
98	09110613	0.133	0.375	0.33	-0.37	0.31	0.34	-0.34	29	-28	2
99	09110614	0.067	0.75	0.75	-0.75	0.31	0.35	-0.35	29	-28	2
100	09110615	0.133	0.75	0.74	-0.74	0.63	0.68	-0.68	46	-46	2
101	09110616	0.067	1.50	1.54	-1.53	0.63	0.67	-0.67	47	-47	2
102	09110617	0.133	1.50	1.52	-1.53	1.26	1.34	-1.34	76	-75	2
103	09110618	0.067	0.25	0.22	-0.24	0.10	0.12	-0.12	15	-15	2
104	09110619	0.133	0.25	0.24	-0.20	0.21	0.23	-0.23	22	-22	2
105	09111001	0.5	1.00	1.03	-0.99	3.14	3.45	-3.45	146	-148	5
106	09111002	0.5	0.50	0.56	-0.51	1.57	1.95	-1.95	106	-106	5
107	09111003	0.5	0.25	0.27	-0.24	0.79	0.95	-0.99	70	-69	5
108	09111004	0.25	0.50	0.56	-0.53	0.79	0.94	-0.94	72	-71	5
109	09111005	1	0.25	0.30	-0.23	1.57	1.95	-1.95	108	-107	5
110	09111006	0.25	0.25	0.29	-0.27	0.39	0.49	-0.49	47	-46	5
111	09111007	2	0.25	0.33	-0.31	3.14	4.56	-4.71	159	-157	5
112	09111008	2	0.05	0.11	-0.07	0.63	1.43	-1.43	67	-63	5
113	09111009	1	0.10	0.13	-0.09	0.63	0.98	-0.92	62	-62	5
114	09111010	2	0.10	0.17	-0.12	1.26	2.00	-2.00	97	-95	5
115	09111011	0.5	1.00	1.02	-1.00	3.14	3.57	-3.57	145	-145	5
116	09111012	0.5	0.50	0.55	-0.52	1.57	1.96	-1.96	102	-103	5
117	09111013	0.5	0.25	0.28	-0.22	0.79	0.94	-0.94	71	-69	5
118	09111014	1.5	2.50	2.49	-2.47	23.56	18.48	-16.94	273	-279	5
119	09111015	1.5	2.50	2.64	-2.76	23.56	18.74	-17.97	269	-276	5

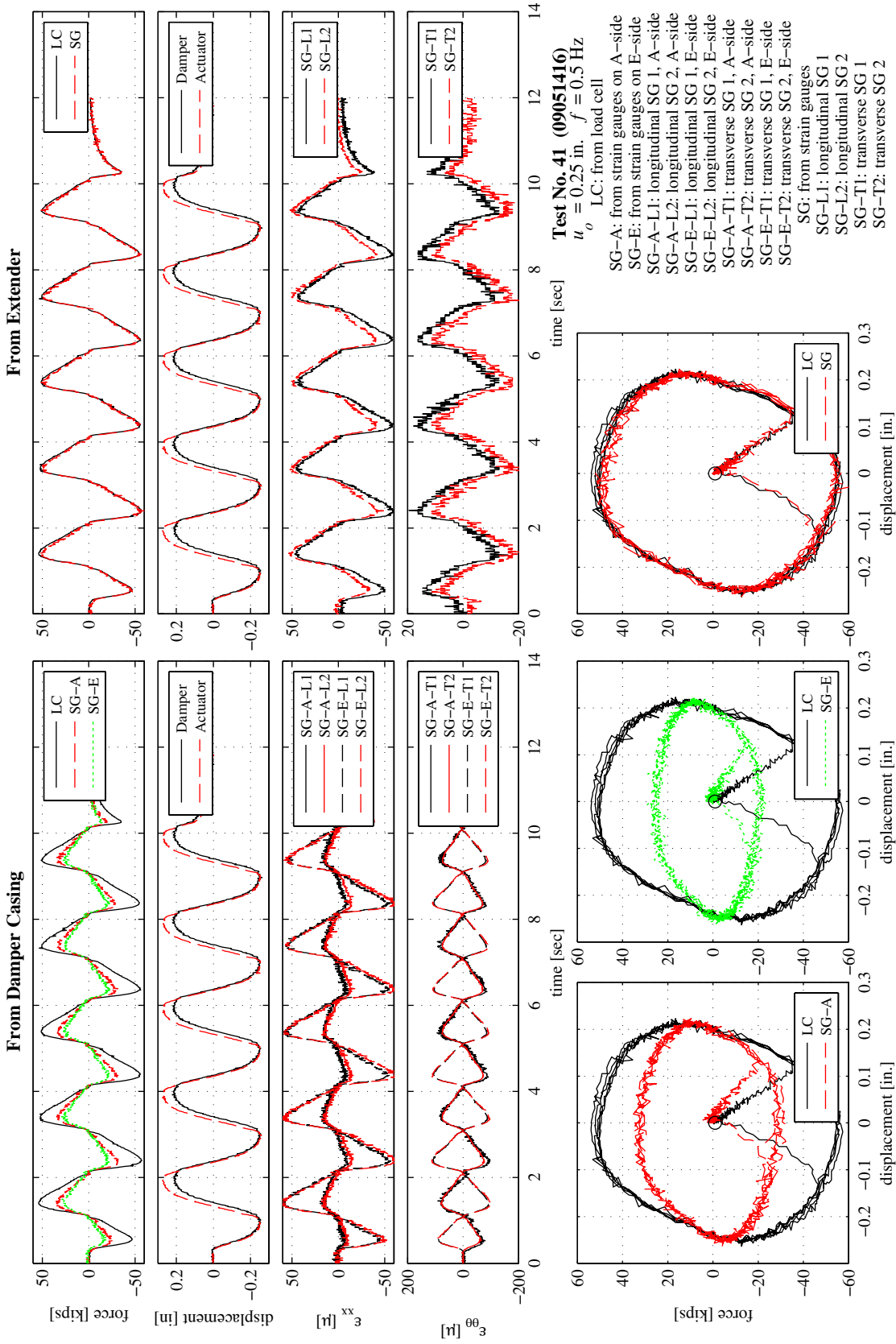


Fig. 2.15 Results of Test No. 41 on the 250-kip damper equipped with bondable strain gauges.

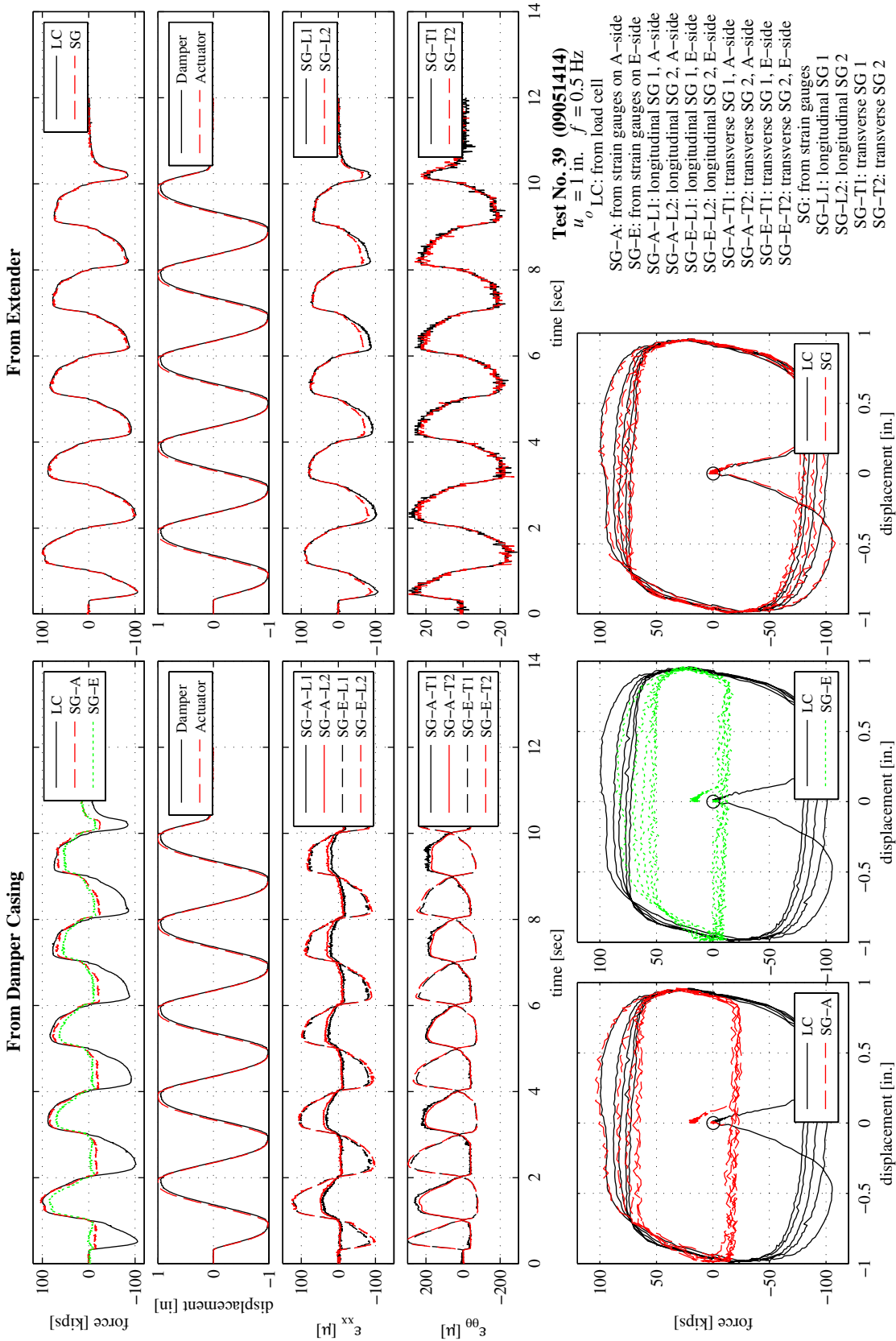


Fig. 2.16 Results of Test No. 39 on the 250-kip damper equipped with bondable strain gauges.

- SG-A-L1: longitudinal strain recorded from rosette 1 on A-side of damper casing
- SG-A-L2: longitudinal strain recorded from rosette 2 on A-side of damper casing
- SG-E-L1: longitudinal strain recorded from rosette 1 on E-side of damper casing
- SG-E-L2: longitudinal strain recorded from rosette 2 on E-side of damper casing
- SG-A-T1: transverse (hoop) strain recorded from rosette 1 on A-side of damper casing
- SG-A-T2: transverse (hoop) strain recorded from rosette 2 on A-side of damper casing
- SG-E-T1: transverse (hoop) strain recorded from rosette 1 on E-side of damper casing
- SG-E-T2: transverse (hoop) strain recorded from rosette 2 on E-side of damper casing

As shown in the graphs, some noise is embedded in the signals, yet it was not deemed necessary to filter the strain gauge data. The peak recorded strains from all the tests ranged between about 20 and 750 μ (micro-strain).

In the event that the damper is stressed purely axially without inducing any end moments and shear forces, the longitudinal and tangential strain gauges measure principal strains. The spherical bearing mountings of the damper's clevises eliminate the developments of any end moment or shear force. The strain rosette arrangement shown in Figs. 2.7 and 2.8 was used to check that the longitudinal and transverse strains were indeed principal (Timoshenko and Goodier 1970).

The recorded longitudinal, ϵ_{xx} , and transverse strains, $\epsilon_{\theta\theta}$, were used to estimate the force on the actuator. The average of SG-A-L1 and SG-A-L2 was taken as the ϵ_{xx} on the A-side of the damper casing, and the average of SG-A-T1 and SG-A-T2 was taken as the $\epsilon_{\theta\theta}$ on the A-side of the damper casing. These values of ϵ_{xx} and $\epsilon_{\theta\theta}$ were plugged in Eq. (2.3) to compute the force P on the A-side of the damper casing. Similarly, the ϵ_{xx} on the E-side of the damper casing was taken as the average of SG-E-L1 and SG-E-L2, and the $\epsilon_{\theta\theta}$ as the average of SG-E-T1 and SG-E-T2. Plugging into Eq. (2.3) provided an estimate of the force P on the E-side of the damper casing.

The time histories for the estimated force P on the A-side (plotted in Figs. 2.15 and 2.16 as SG-A) and on the E-side (plotted as SG-E) are compared to the force time histories recorded with the load cell. It can be seen on the top graph (left column), which compares time histories of the force, and the two bottom graphs (left column), which compare hysteresis loops, that the estimated force computed from strain gauge readings on the damper casing can deviate substantially from the force recorded using load cells.

Figure 2.17 shows schematically the stressing of the damper casing during tension and compression of the piston rod. When the piston rod is in tension, Fig. 2.17(a), the damper casing is subjected to longitudinal tension, and both longitudinal and tangential stresses develop during the bursting of the barrel. On the other hand, when the piston rod is in compression, Fig. 2.17(b), the compressive force does not go through the barrel casing, but rather it is transferred directly at the end of the damper (extender) via the pressurized fluid at the back chamber. Therefore, only tangential (hoop) stresses develop during the bursting of the damper. Consequently, we conclude that strain gauges when installed on the damper casing can only capture the force that induces tension on the damper; even then, the tension force predicted using the strain gauges deviates from that recorded using the load cell. Therefore, strain gauges should *not* be attached on the damper casing, since they result in an inaccurate estimate of the force.

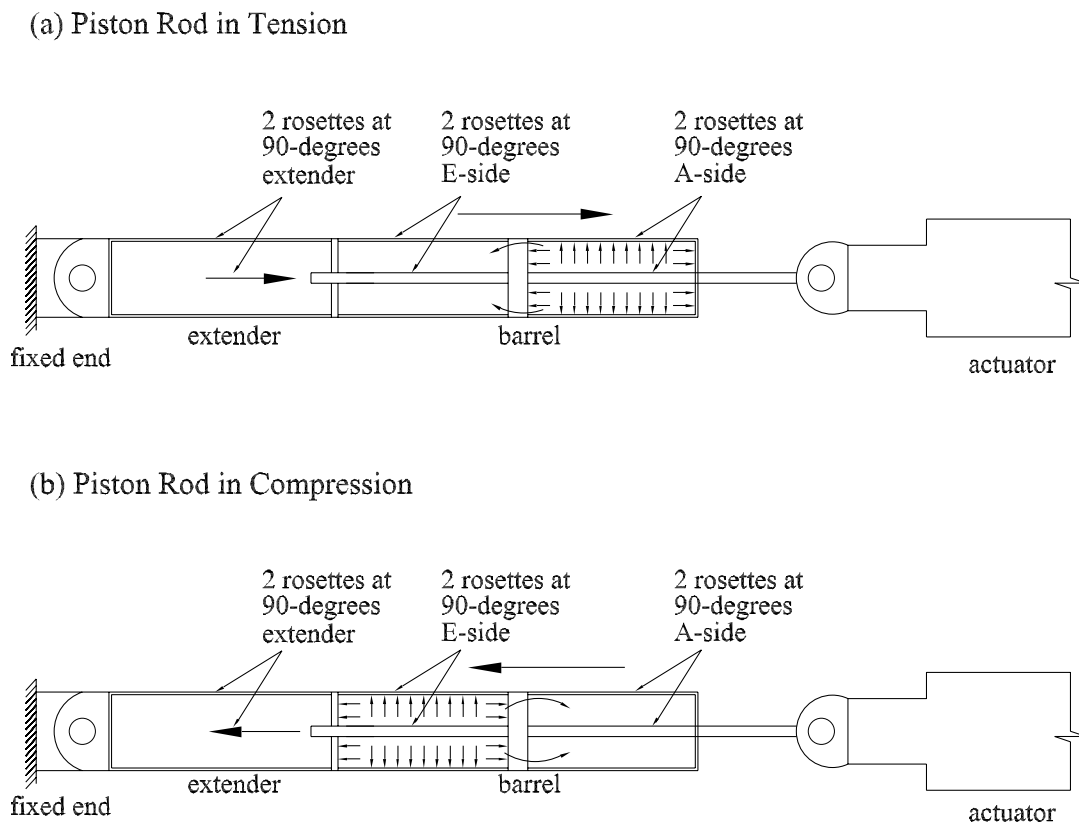


Fig. 2.17 Schematic of the cross-section of a fluid damper showing the stressing of the damper casing during (a) tension of the piston rod, and (b) compression.

The right column of Figs. 2.15 and 2.16 shows results obtained from rosettes bonded to extender piece (see Fig. 2.8):

- SG-L1: longitudinal strain recorded from rosette 1 on extender
- SG-L2: longitudinal strain recorded from rosette 2 on extender
- SG-T1: transverse strain recorded from rosette 1 on extender
- SG-T2: transverse strain recorded from rosette 2 on extender

The estimated force labelled SG on the force time history and hysteresis loops is obtained from Eq. (2.3), where ϵ_{xx} is the average of SG-L1 and SG-L2, and $\epsilon_{\theta\theta}$ is the recorded signal from SG-T2. The reason why only the hoop strain of the second rosette on the extender piece is used is because some irregularities were observed in the recorded signal of SG-T1 (as can be seen, for example, in Fig. 2.20, which plots results only from the extender piece). These could possibly be the result of slipping.

Figure 2.15 shows the results for Test No. 41, with $f = 0.5$ Hz and target displacement amplitude $u_0 = 0.25$ in. The recorded peak displacement was $+0.22/-0.26$ in., and the recorded peak velocity was $+0.79/-0.81$ in/sec, which was very close to the target of 0.79 in/sec. The recorded peak force was $+54/-57$ kips. A comparison of the plotted force time histories and hysteretic loops shown on the right columns shows that the strains recorded from the extender resulted into damper forces that are in very good agreement with the forces recorded from the load cell. The results are also very accurate for Test No. 39, shown in Fig. 2.16, with the same frequency but target $u_0 = 1.0$ in. (and recorded $+0.96/-0.99$ in.). The peak velocities recorded for this test were $+3.22/-3.30$ in/sec, and the peak force was $+100/-106$ kips. Figure 2.18 shows displacement, velocity, and force time histories for Test No. 39, indicating that the force follows the velocity.

The accuracy of the predictions are good even for very small displacement amplitudes, as shown, for example, in Fig. 2.19, which plots results from the extender piece for Test No. 38 with target $u_0 = 0.1$ in., and $f = 2$ Hz. The top and bottom graphs, which plot the force time history and the hysteretic loops, respectively, show that the predictions for force using the recorded strains are very close to the readings from the load cell.

Lastly, Fig. 2.20 shows results for Test No. 43, which had the largest displacement amplitude (target $u_0 = 2.5$ in. and $f = 1.5$ Hz). The actuator was unable to deliver the target

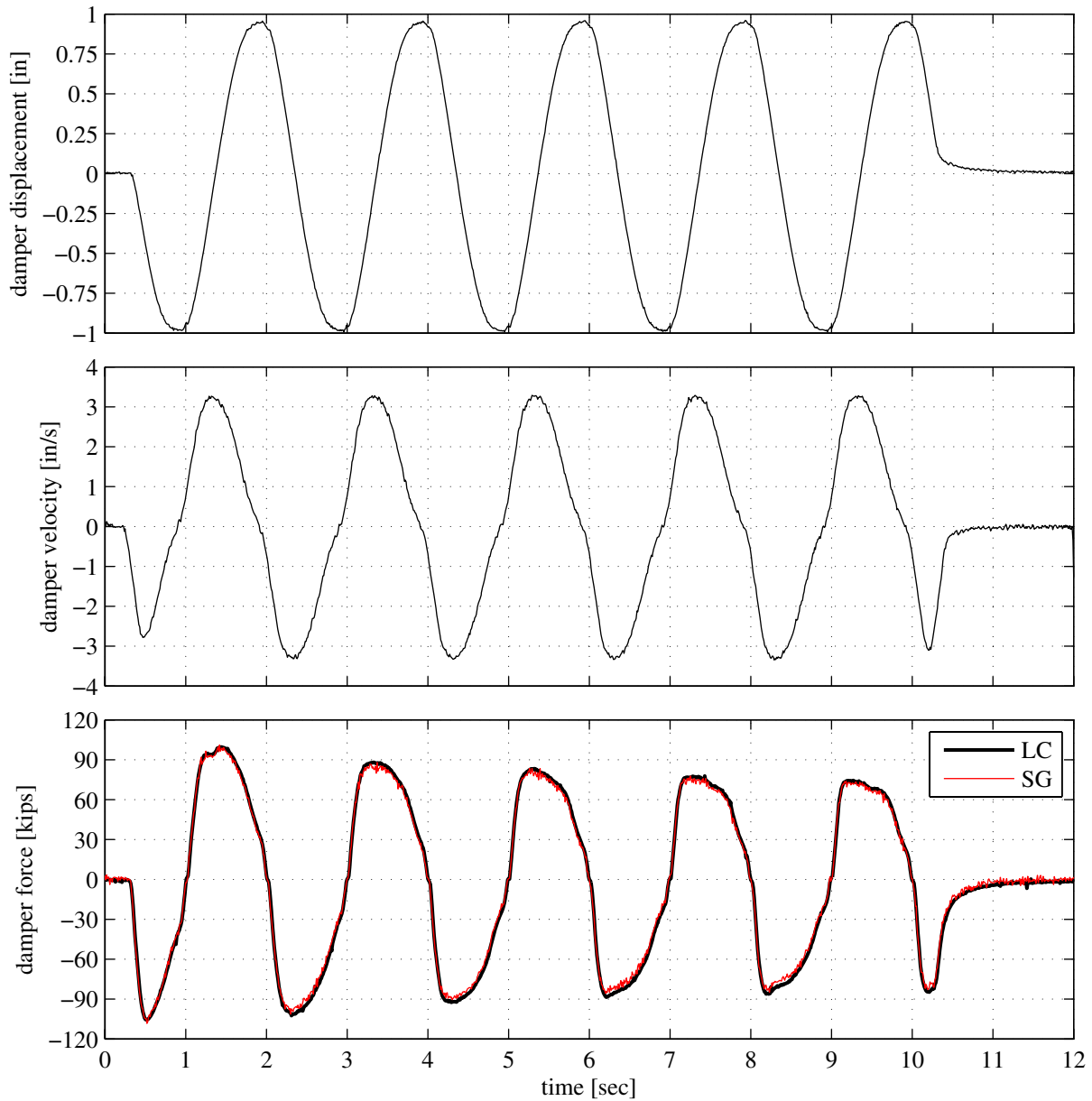


Fig. 2.18 Displacement, velocity and force histories for Test No. 39 on the 250-kip damper.

$v_0 = 23.6$ in/sec. Instead, the peak velocity recorded was $+20.0/-18.6$ in/sec, and the peak force recorded was $+190/-178$ kips. Again the predictions using the recorded strains from the extender piece are very accurate.

The results from the experimental program indicate that with commercially available conventional, bondable strain gauges one can accurately monitor the force output of fluid dampers installed on the field over a wide range of velocity inputs. The gauges should not be placed on the

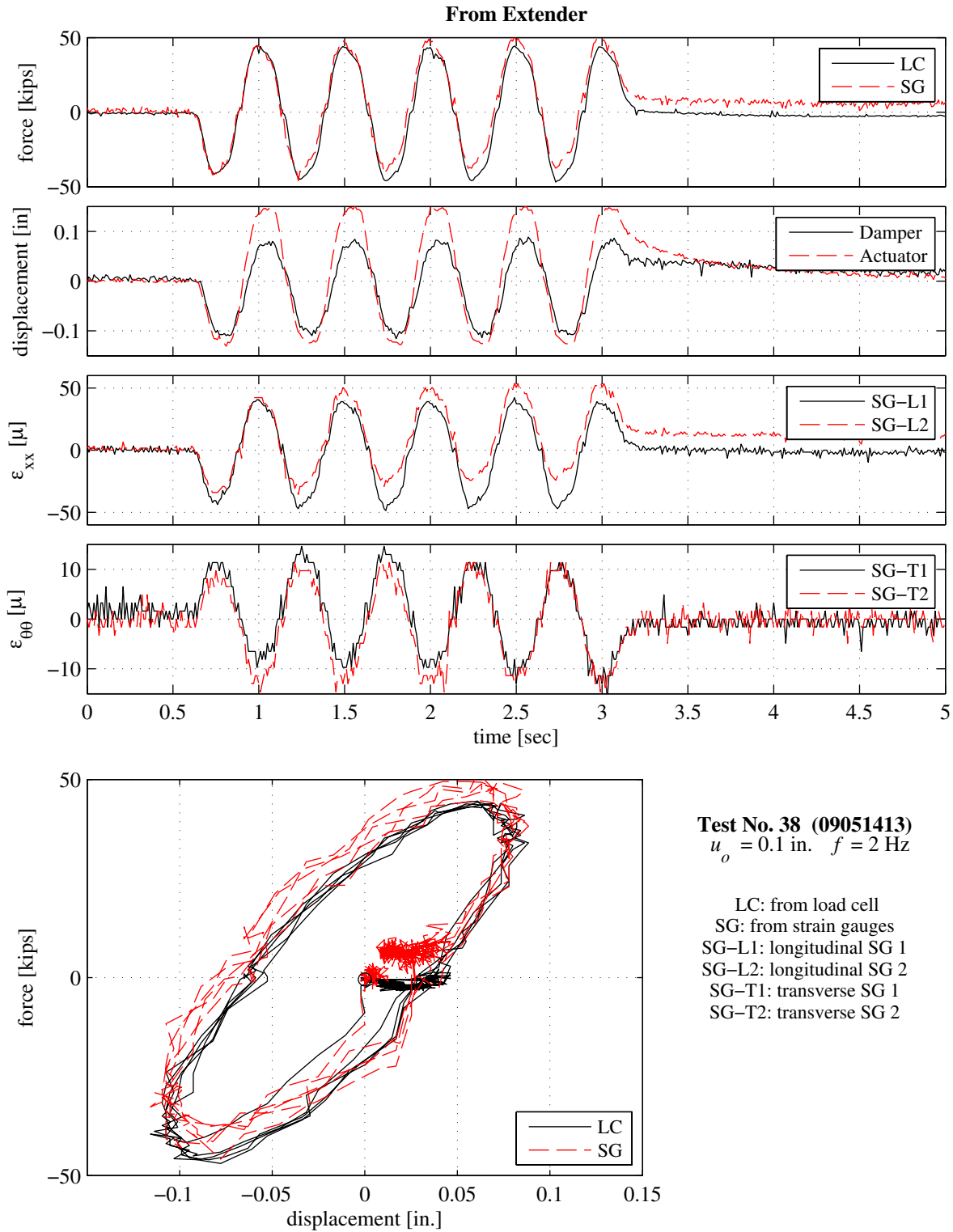


Fig. 2.19 Results of Test No. 38 on the 250-kip damper equipped with bondable strain gauges.

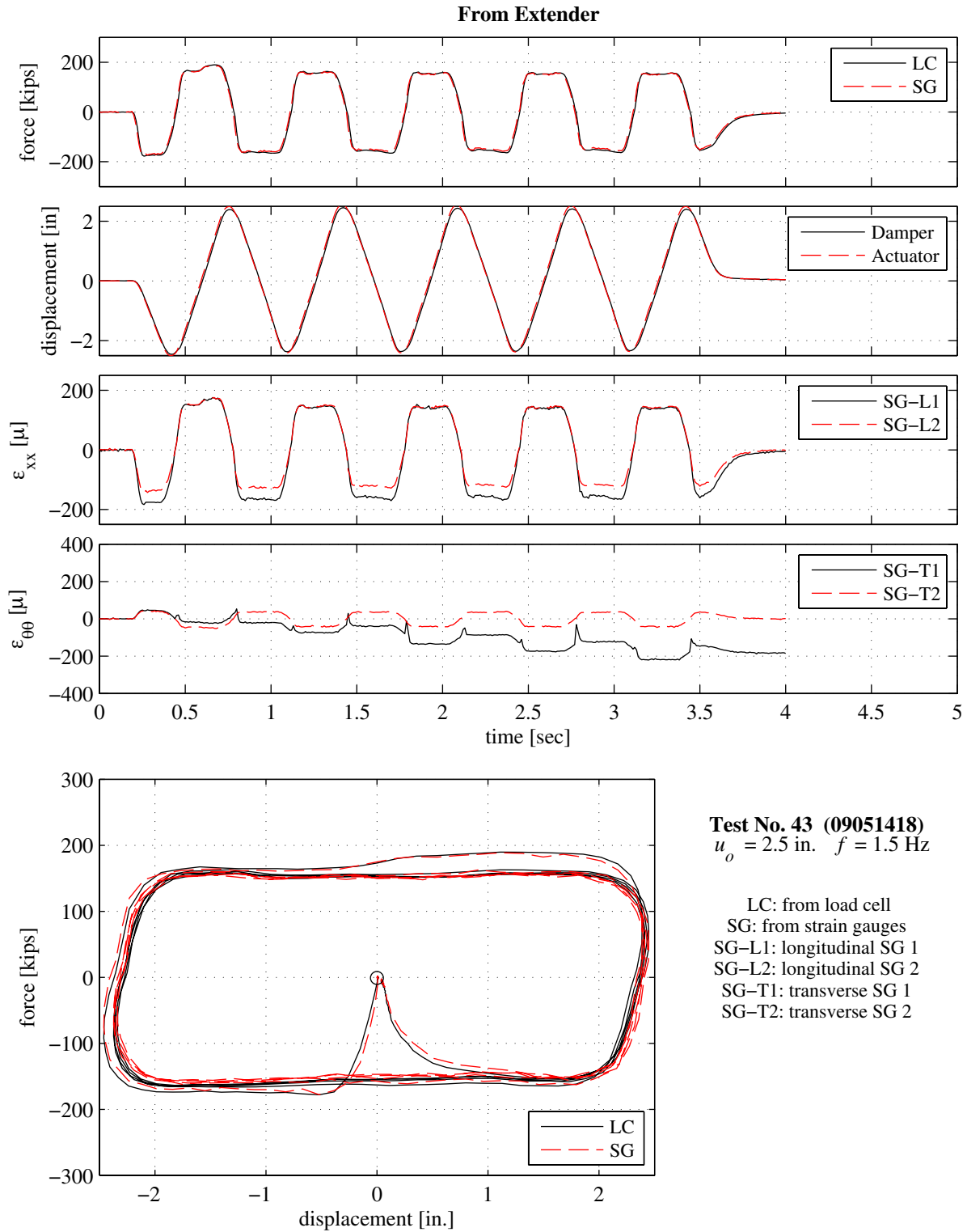


Fig. 2.20 Results of Test No. 43 on the 250-kip damper equipped with bondable strain gauges.

damper casing; instead they should be placed on the extender piece, preferably near mid-length to avoid end-effects. Since the pin connections of the damper feature spherical bearings, no moments and shears are theoretically present in the damper except due to its self weight. However, if the bushings cease, and shears and moments act on the damper, a strain-gauge rosette is necessary to capture them. It is recommended to install two rosettes on each damper for the sake of redundancy and to capture any such shears/moments if they occur.

2.5.2 Results of Tests on the 250-Kip Damper Equipped with Weldable Strain Gauges

Table 2.3 lists the recorded peak displacement, velocity, and force of all the indoor tests conducted on the 250-kip damper equipped with weldable strain-gauge rosettes. Figures 2.21 to 2.24 plot results of four tests, where the data have been obtained from strain gauges that were welded in a rosette-pattern onto the extender. The bottom-right corner of the figure serves as a legend explaining what each abbreviation represents. The arrangement of weldable rosettes on the damper was identical to that on the 250-kip damper equipped with bondable strain gauge, described in the previous section. The results are fairly repeatable, with the weldable strain gauges in some instances capturing the force with higher accuracy than the conventional bondable strain gauges.

Figures 2.21 to 2.24 show the results of Test Nos. 48, 46, 56, and 60, which as can be seen in Tables 2.2 and 2.3 have the same u_0 and f as Test Nos. 41, 39, 38, and 43 (shown in Figs. 2.15, 2.16, 2.19, and 2.20), discussed in the previous section. The force predicted using strain readings is very close to the force recorded using a load cell.

Their high performance, together with their versatility and ease of application, makes weldable strain gauges preferred to bondable ones for applications on a bridge environment. As mentioned earlier, it is recommended to install two (built-up) strain-gauge rosettes for the sake of redundancy but also to capture any accidental moments/shears in the damper. The rosettes should be welded on the extender piece, preferably near its mid-length so as to avoid end-effects. The force on the damper is

$$P = EA_e \epsilon_{xx} \quad (2.7)$$

where A_e is the cross-sectional area of the extender, and ϵ_{xx} is the average reading of the longitudinal gauges attached.

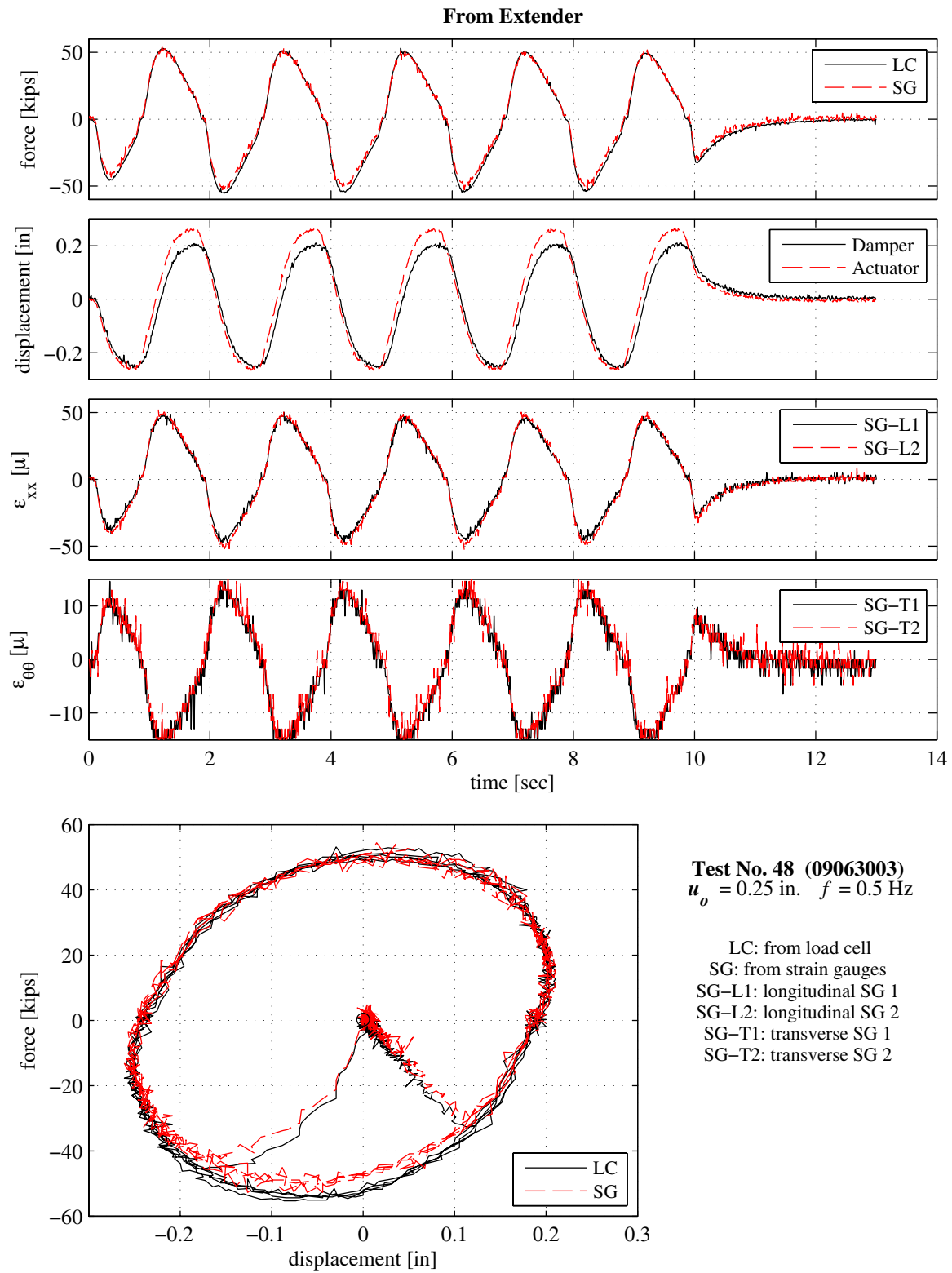


Fig. 2.21 Results of Test No. 48 on the 250-kip damper equipped with weldable strain gauges.

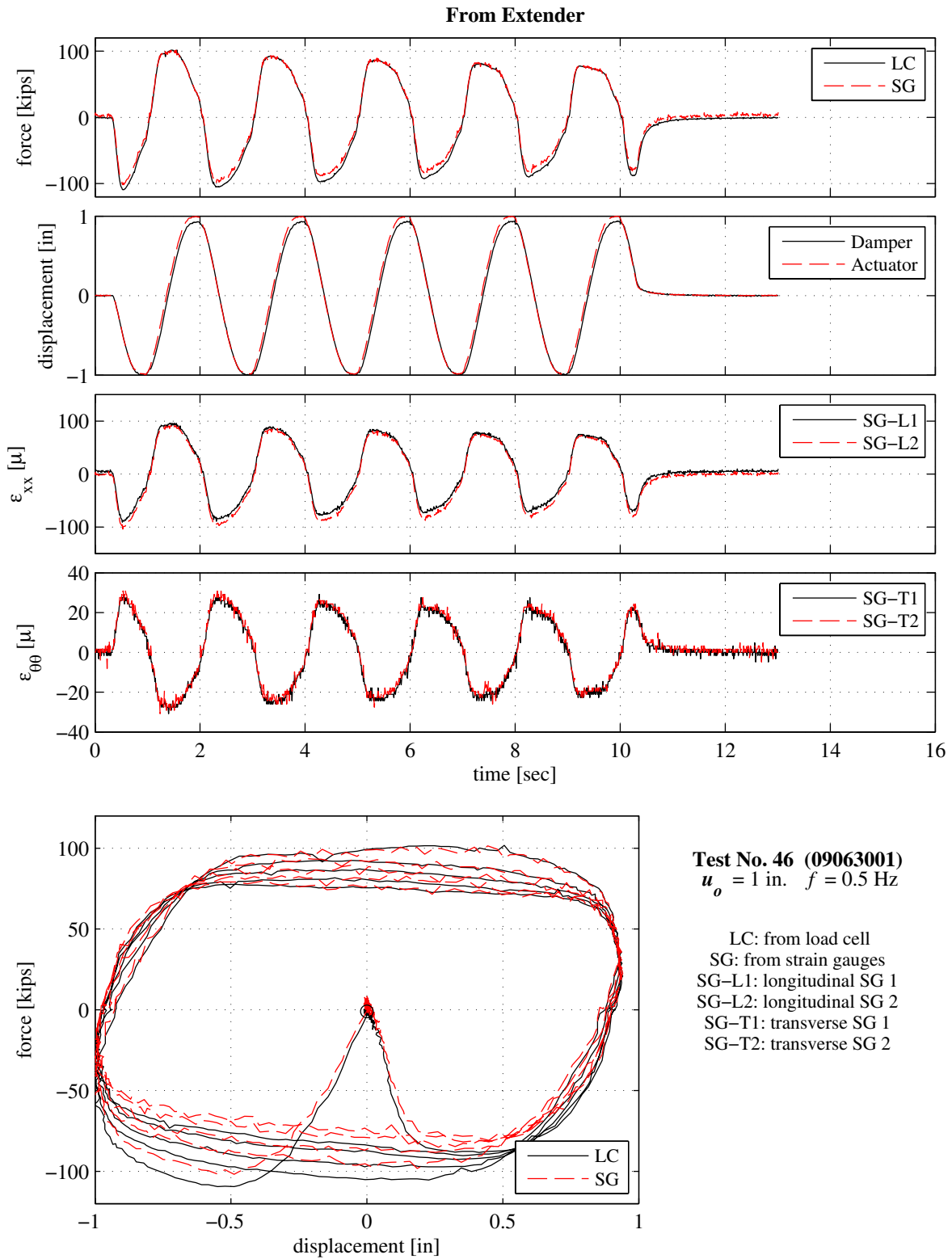


Fig. 2.22 Results of Test No. 46 on the 250-kip damper equipped with weldable strain gauges.

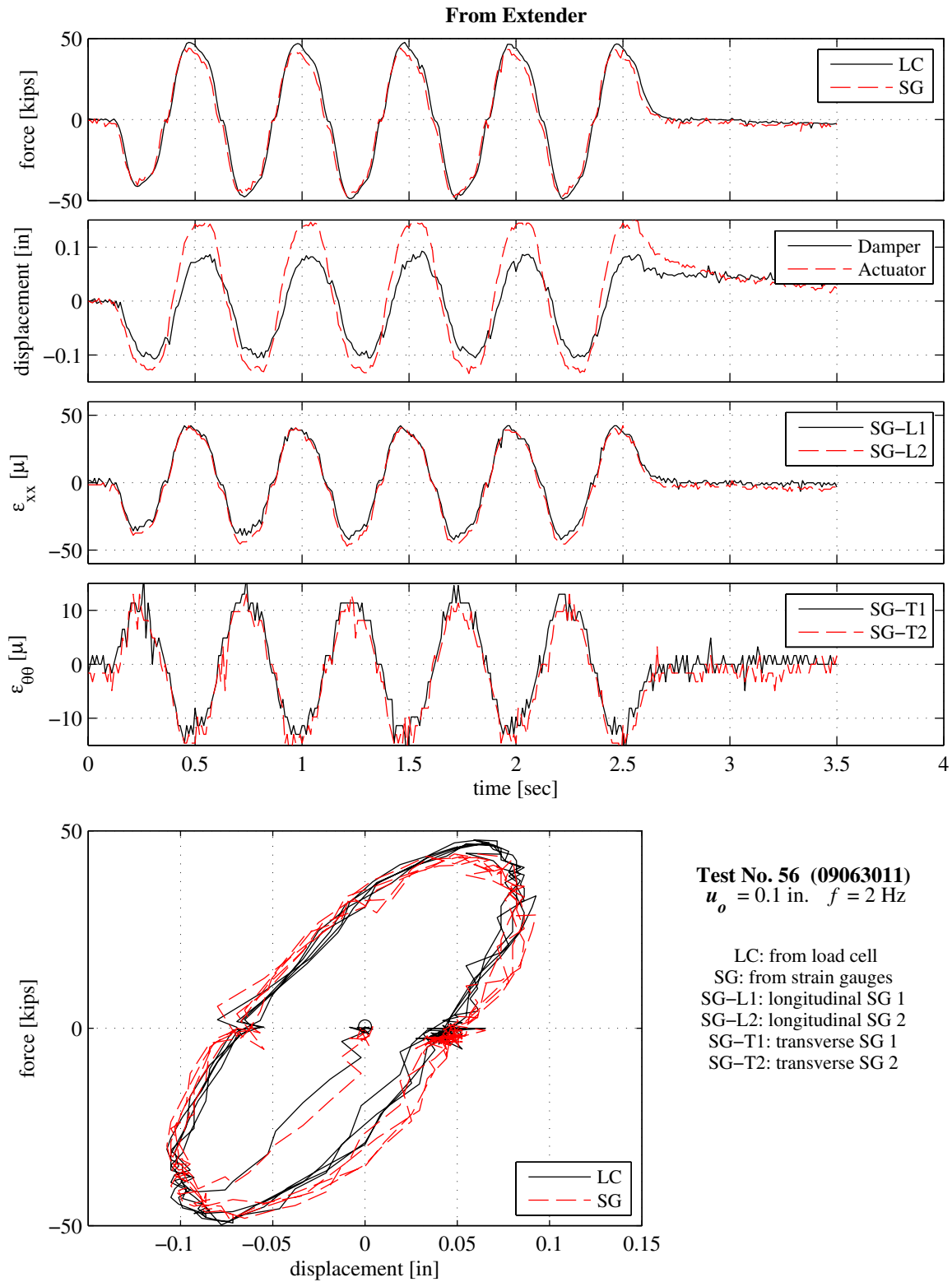


Fig. 2.23 Results of Test No. 56 on the 250-kip damper equipped with weldable strain gauges.

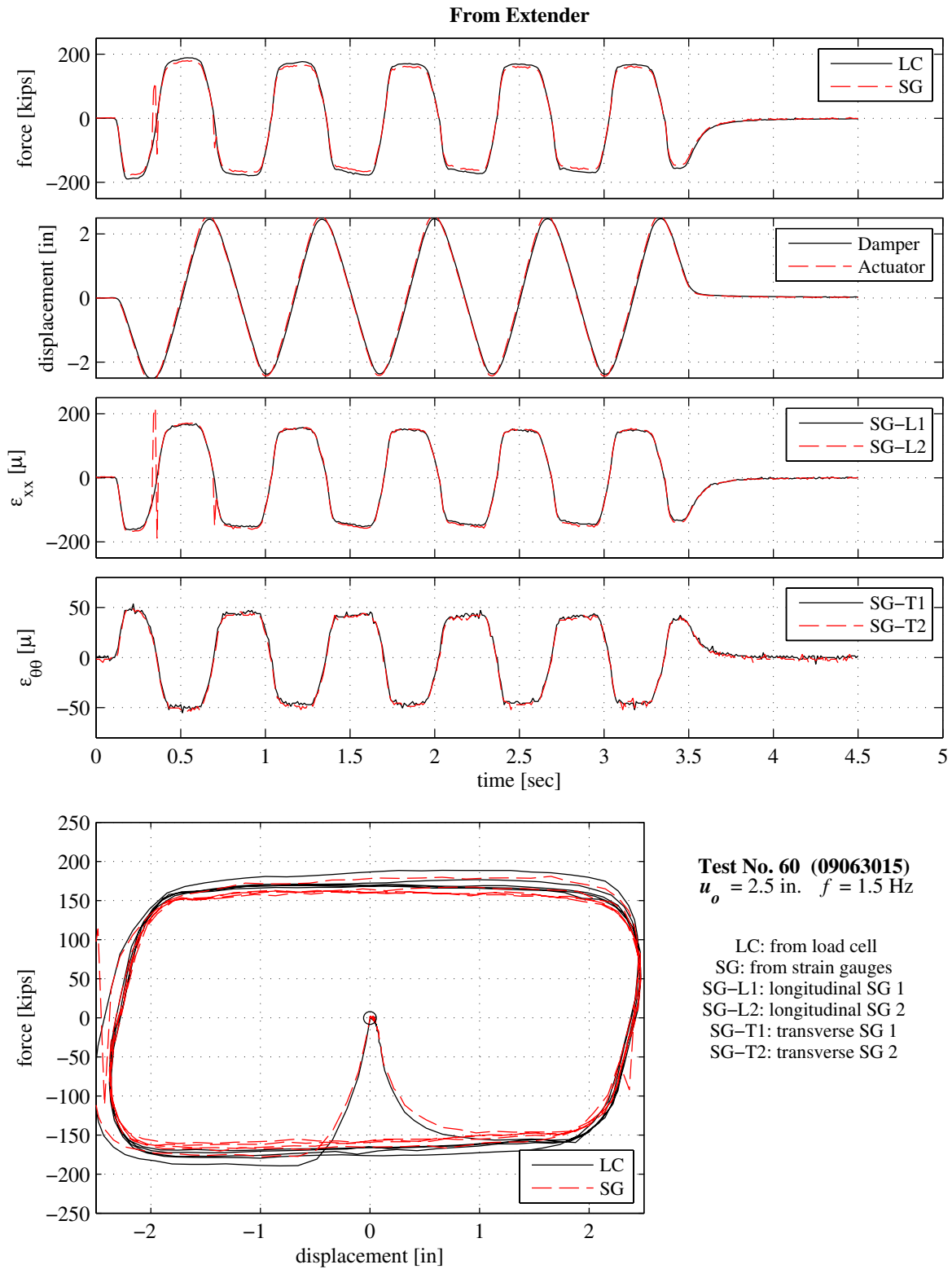


Fig. 2.24 Results of Test No. 60 on the 250-kip damper equipped with weldable strain gauges.

2.5.3 Results of Tests on the 450-Kip Damper

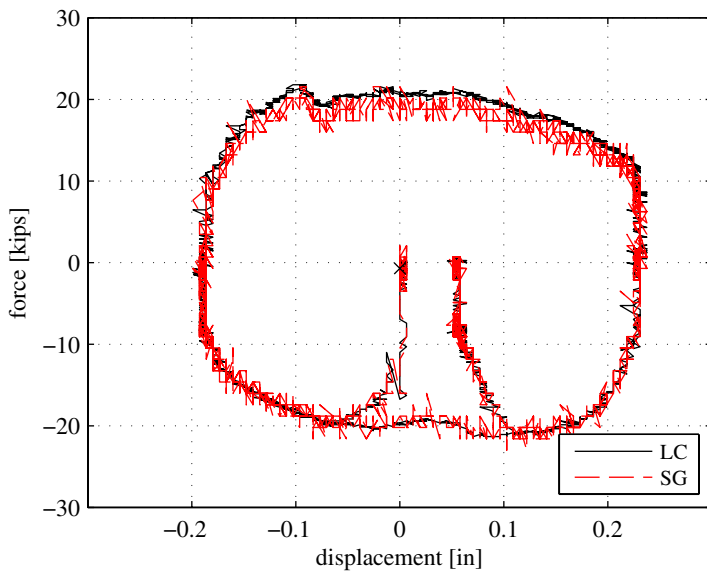
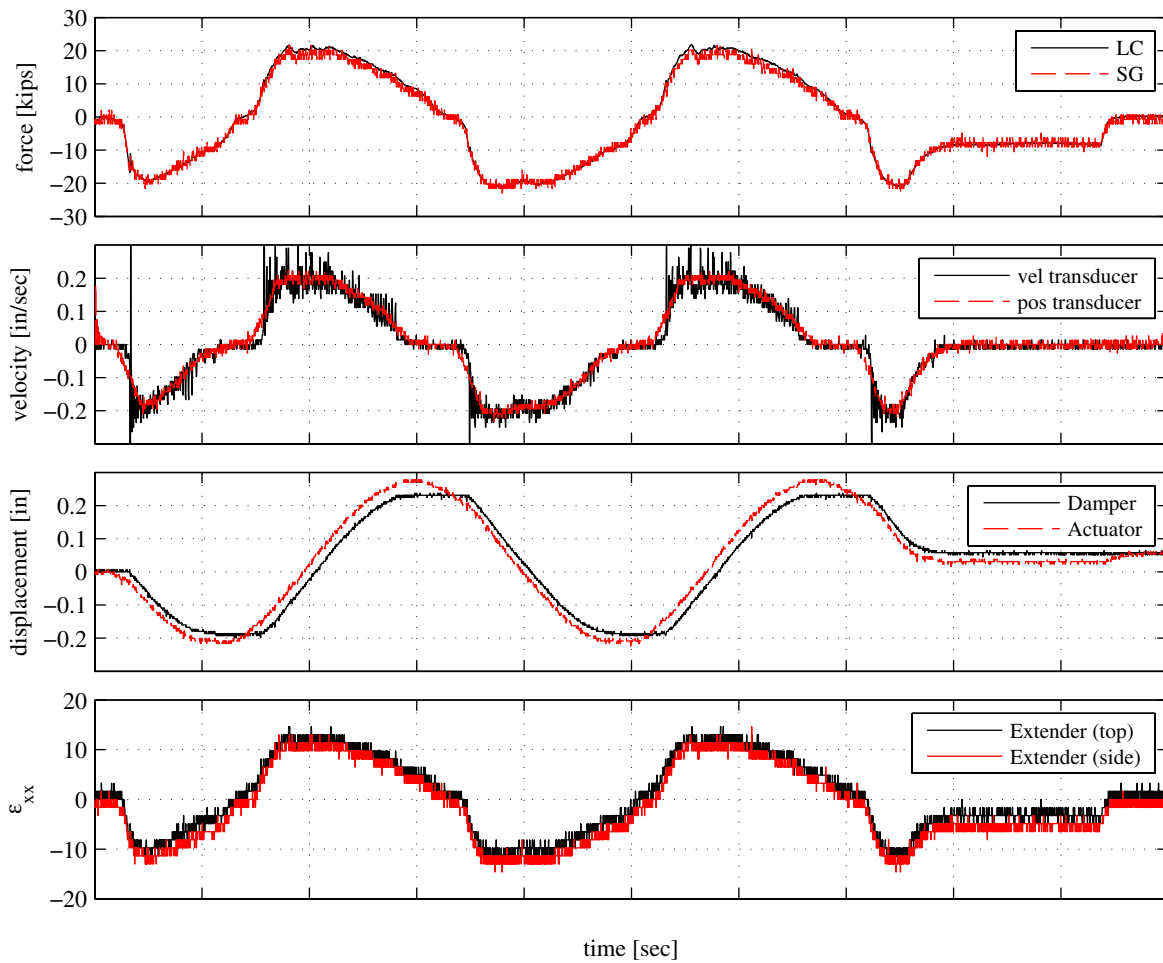
Table 2.4 lists the recorded peak displacement, velocity, and force of all the indoor tests conducted on the 450-kip damper equipped with weldable strain gauges in the locations shown in Fig. 2.11. Figures 2.25 to 2.27 show results of three experiments. The top graph shows the force output of the damper. The solid line, designated LC, shows the force recorded using the load cell, while the dashed line, designated SG, shows the force as computed using the recorded strain histories. The average of the longitudinal strain readings from the top and side strain gauges on the extender were used to compute the force, $P = A_e E (\epsilon_{xx}^{\text{top}} + \epsilon_{xx}^{\text{side}}) / 2$.

The second graph shows the velocity of the damper. The solid line shows the velocity history as recorded using the Transtek 0127-0001 velocity transducer (Fig. 2.13), while the dashed line shows the velocity history that results after differentiating the displacement signal obtained using the Novotechnik TLH-1000 position transducer. Note that to obtain a clean velocity signal, after differentiation of the displacement signal, it was necessary to filter the resulting signal. More filtering was necessary for smaller velocity-amplitude motions. Some signal noise was detected even on the data collected using the velocity transducer, which again is more pronounced under low-amplitude excitations. The noise in directly measured velocity signal is certainly less than the noise in an unfiltered differentiated displacement signal, but filtering is still necessary nevertheless. Since filtering may be necessary either way, it is perhaps better to simply use one position transducer to measure directly displacement, and obtain the velocity by differentiating and filtering the resulting signal.

The third graph in Figs. 2.25 to 2.27 shows the displacement history for the test. The solid line shows the displacement recorded using a DCDT attached on the actuator, while the dashed line shows the displacement recorded using the Novotechnik TLH-1000 position transducer attached on the damper.

The fourth graph shows recorded longitudinal strains, ϵ_{xx} , from weldable strain gauges attached on the top and side of the extender.

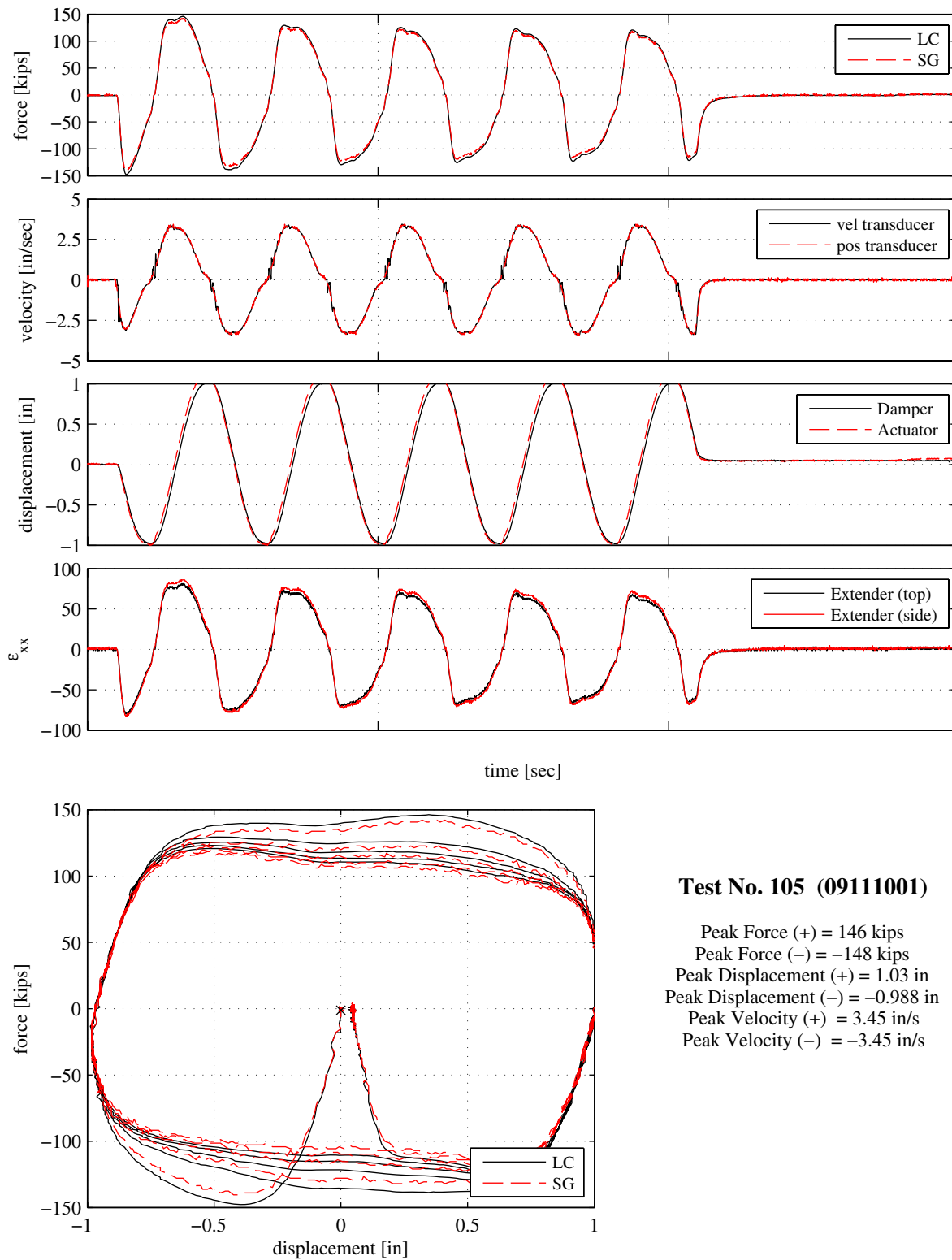
The bottom graph shows the hysteretic loops for the test. The solid line shows the force recorded with the load cell versus the damper displacement recorded with the Novotechnik position transducer, while the dashed line shows the force computed from the strain-gauge readings



Test No. 104 (09110619)

Peak Force (+) = 21.8 kips
 Peak Force (-) = -21.6 kips
 Peak Displacement (+) = 0.237 in
 Peak Displacement (-) = -0.199 in
 Peak Velocity (+) = 0.233 in/s
 Peak Velocity (-) = -0.233 in/s

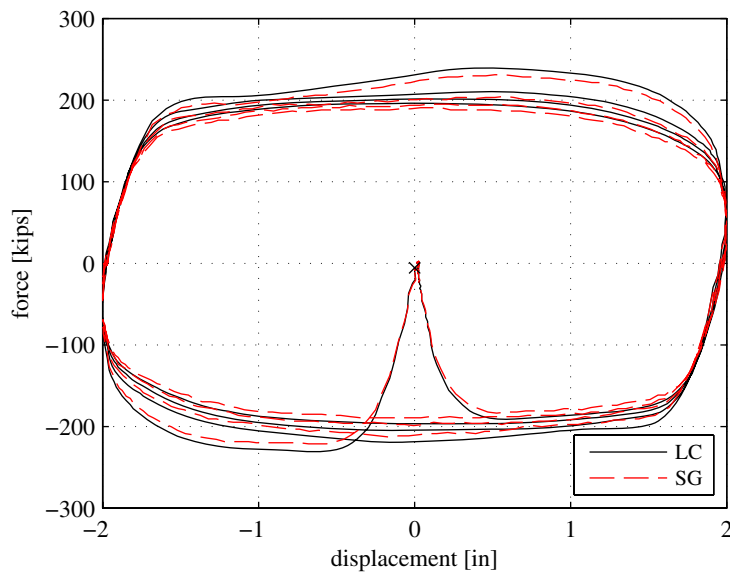
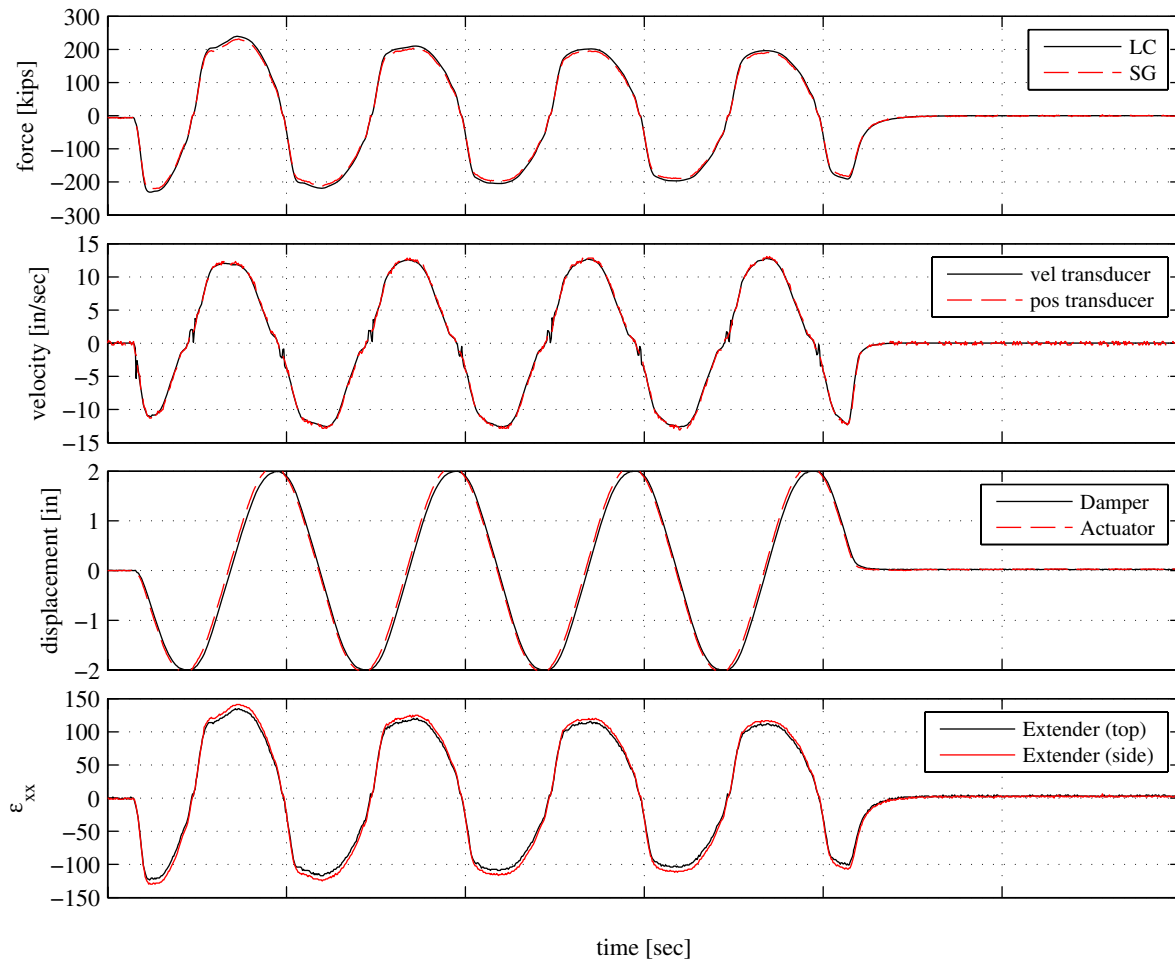
Fig. 2.25 Results of Test No. 104 on the 450-kip damper.



Test No. 105 (09111001)

Peak Force (+) = 146 kips
 Peak Force (-) = -148 kips
 Peak Displacement (+) = 1.03 in
 Peak Displacement (-) = -0.988 in
 Peak Velocity (+) = 3.45 in/s
 Peak Velocity (-) = -3.45 in/s

Fig. 2.26 Results of Test No. 105 on the 450-kip damper.



Test No. 95 (09110610)

- Peak Force (+) = 239 kips
- Peak Force (-) = -231 kips
- Peak Displacement (+) = 2.01 in
- Peak Displacement (-) = -2.01 in
- Peak Velocity (+) = 13.1 in/s
- Peak Velocity (-) = -13.1 in/s

Fig. 2.27 Results of Test No. 95 on the 450-kip damper.

versus the same damper displacement.

The bottom-right corner of the figure shows the maximum and minimum force recorded using the load cell, the maximum and minimum displacement recorded using the Novotechnik position transducer, and the maximum and minimum velocity recorded using the Transtek velocity transducer.

As shown in the graphs, some noise is embedded in the signals, yet it was not deemed necessary to filter the strain gauge data, even under very low-amplitude excitation signals. The peak recorded strains ranged between about 5 and 250 μ (micro-strain). The ability to resolve strain readings down to such low numbers is very important, especially in bridge applications where data are recorded under ambient conditions.

Figure 2.25 shows results of Test No. 104 with target $u_0 = 0.25$ in. and $f = 0.133$ Hz; the recorder peak displacement was +0.24/−0.20 in. For this very slow test, the recorded peak velocity was +0.23/−0.23 in/sec, and the peak force was +22/−22 kips. The top and bottom graphs of the figure, which plot the time history force and the hysteretic loops, show that the predicted force using strain readings is very close to the force recorded using the load cell. Figure 2.26, which shows results of Test No. 105 with target $u_0 = 1.00$ in. and $f = 0.5$ Hz (recorded u_0 was +1.03/−0.99 in., v_0 was +3.45/−3.45 in/sec, and peak P was +146/−148 kips), indicate that the recorded strain readings yield again very accurate predictions of the force. Lastly, Fig. 2.27, which shows results of Test No. 95 with target $u_0 = 2.1$ in. and $f = 1$ Hz (recorded u_0 was +2.01/−2.01 in., v_0 was +13.09/−13.09 in/sec, and peak P was +239/−231 kips), demonstrates that the method also gives very reliable predictions for fast tests.

The results from the experimental program on the 450-kip damper using weldable strain gauges to record strain proved that the method is a very reliable way to estimate the force output of the damper, even under very low amplitude excitations. We were able to resolve strains down to 5 μ , corresponding to a force of about 15 kips. It is recommended that two weldable strain-gauge rosettes are attached at mid-length (in order to avoid end effects) of the extender piece to measure strain. The force could then be estimated using the formula, $P = A_e E \epsilon_{xx}$, where A_e is the cross-sectional area of the extender, and ϵ_{xx} is the average reading of longitudinal strain.

2.6 CHOICE OF POSITION TRANSDUCER AND SMOOTHING OF DATA

To measure position and velocity, a single position transducer could be used to measure position; the velocity could be obtained by differentiating the position signal and filtering it to reduce inherit noise. Alternatively, a device like the Celesco PT5AV transducer (Fig. 2.12) with separate outputs for position and velocity could be used. This device was used in the outdoor tests (Chapter 3) and proved to perform very satisfactorily. For low readings of velocity, it was found necessary to filter the velocity signal to eliminate noise regardless of whether the signal was obtained directly from the velocity output of the device or indirectly from differentiating the recorded displacement signal. Figure 2.28 shows the velocity signals for the tests shown in Figs. 2.21 to 2.24, which were conducted on the 250-kip damper with weldable strain gauges. The noisy signal shown with a thin line is obtained by differentiating the displacement signal. The smooth signal shown with a thick line is obtained by taking a simple moving average (SMA) with span N . This was done in MATLAB (Mathworks 2007) using the *smooth* function. The span N of the moving average had to be changed from test to test in order to achieve smooth velocity signals.

Too little smoothing results in a very noisy signal and large overestimates of the velocity, while too much smoothing results in underestimates of the velocity. Thus, caution must be exercised when filtering the velocity signal. The type and amount of filtering will depend on the application at hand. Different recording sensors, cables, connectors, and data acquisitions systems will require different filtering for different bridges. The possibility of using a *band-pass filter* (not examined in this study) should be considered. The center frequency of the band-pass filter should be the natural frequency of the bridge measured under ambient conditions, and the bandwidth of the filter should be gradually decreased until a clean signal results.

As mentioned earlier, it was observed that while the strain histories were slightly noisy, it was not necessary to filter them in order to obtain accurate forces.

2.7 FORCE AT LOW VELOCITIES

Some of the tests on the 450-kip damper were conducted in order to investigate its force response to low velocities and to see if this is close to the “target” value $C_\alpha |\dot{u}(t)|^\alpha$, where C_α and α (pro-

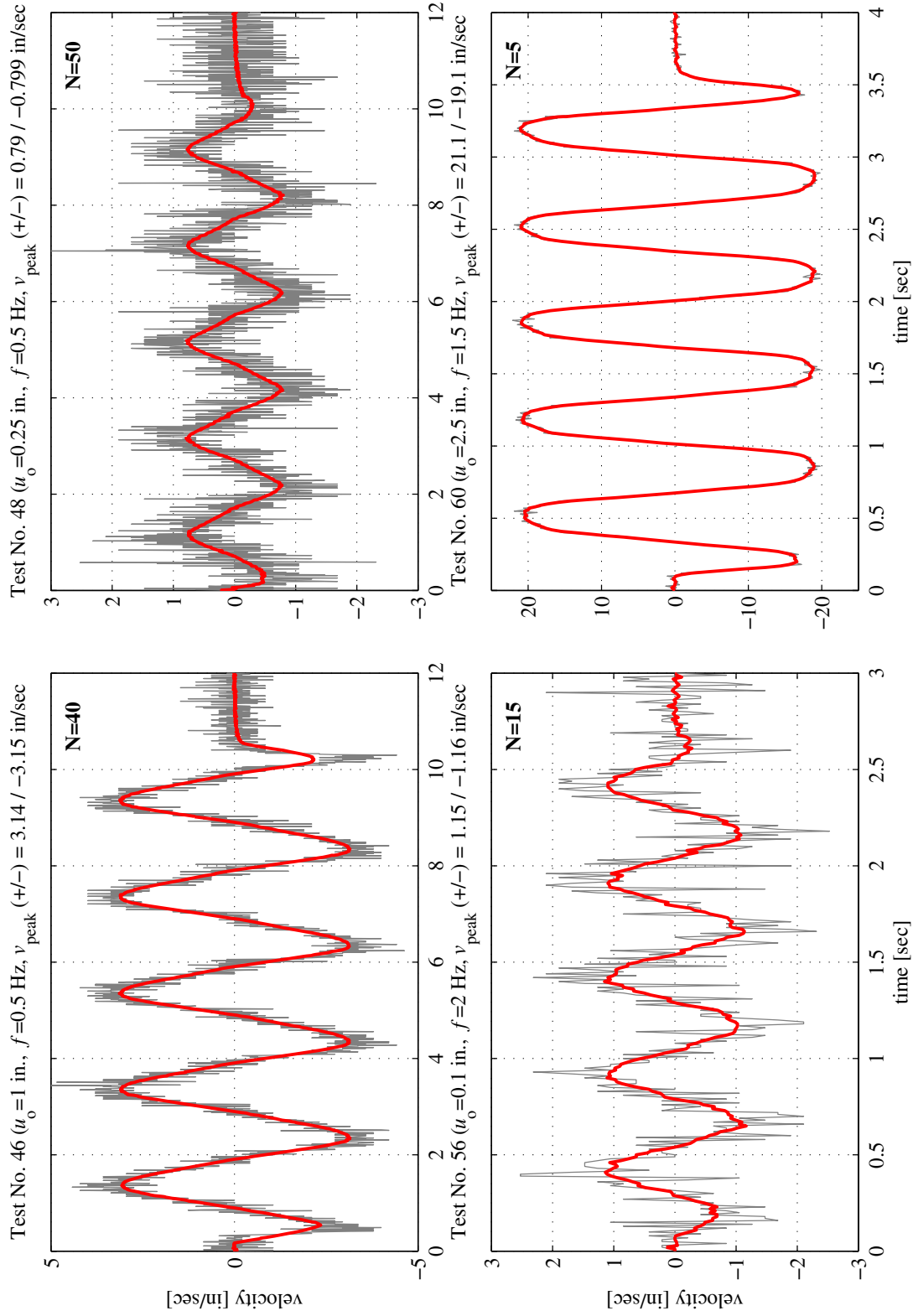


Fig. 2.28 The thin line shows the velocity signal obtained by differentiating the displacement signal, while the bold line shows the smoothed signal obtained after taking the simple moving average with span N of that velocity signal. v_{peak} is the peak of the smoothed signal.

vided by the manufacturer) characterize the behavior at seismic design velocities. If the input signal is $u(t) = u_0 \sin(2\pi ft)$, then the velocity amplitude is given by $v_0 = 2\pi f u_0$. Table 2.5 lists the measured peak velocity and force in the positive and negative directions for every test conducted on the 450-kip damper. Also listed is the target force $\bar{P} = C_\alpha v_0^\alpha$,

$$\bar{P} = 118.6 \text{ kips} \left(\frac{\text{sec}}{\text{in}} \right)^{0.3} v_0^{0.3} \quad (2.8)$$

Figure 2.29 shows the experimental peak force versus velocity together with the target force, shown with a bold solid line. The top graph presents the results on linear axes, while the bottom graph presents them on log-log axes. Figure 2.29 also shows with a thin gray line the formula obtained by a least-squares power fit of the data from tests with velocity slightly less than 8 in/sec and above (i.e., the bottom section of Table 2.5, starting with Test No. 88),

$$\hat{P} = 91.91 v_0^{0.3733}, \quad 8 < v_0 < 20 \quad (2.9)$$

where v_0 is in in/sec and \hat{P} in kips. The difference between the values of force given by Eqs. (2.8) and (2.9) is 10.8% at 8 in/sec and less than 9% for $v_0 > 10$ in/sec. It is therefore concluded that for higher velocities, the experimental results are in fairly good agreement with the target force.

At low velocities, however, Fig. 2.29 shows that the difference between the measured, P , and expected, \bar{P} , values for the force deviate dramatically. The difference becomes exceedingly pronounced as the velocity decreases. The last column of Table 2.5, which lists numerical values of the error, shows that the error can exceed 300% at velocities around 0.1 in/sec.

It is concluded that if the in-situ method proposed in this study is to be implemented to compare the measured force to a target force in order to draw conclusions on whether the performance of a damper on the field is acceptable, it is imperative to have an accurate characterization of the damper's force output at low velocities; and not assume that the behavior at seismic design velocities also applies at low velocities. Consequently, dampers to be health monitored on a bridge need to be tested not only at design velocities, but also at the range of low velocities that the bridge is expected to experience under service conditions.

For example, Fig. 2.29 shows with a thick gray line a formula obtained by least-squares fit for the low-velocity tests (tests listed on the top section of Table 2.5, down to, and including, Test No. 114), given by

Table 2.5 Velocity dependence of force and error between target and experimental force.

Test No.	Measured Peak Velocity v_o [in/s]		Measured Peak Force, P [kips]		Target Peak Force, \bar{P} [kips]		$\frac{ P - \bar{P} }{P}$
	(+)	(-)	(+)	(-)	(+)	(-)	max of (+)/(-) [%]
103	0.12	0.12	15	15	63	63	317
97	0.17	0.17	17	18	69	70	308
104	0.23	0.23	22	22	77	77	256
98	0.34	0.34	28	29	86	86	211
99	0.35	0.35	28	29	87	87	204
110	0.49	0.49	46	47	96	96	109
101	0.67	0.67	47	47	105	105	124
100	0.68	0.68	46	46	106	106	131
108	0.94	0.94	71	72	116	116	64
117	0.94	0.94	69	71	117	117	68
113	0.92	0.98	62	62	116	118	90
107	0.99	0.95	69	70	118	117	72
102	1.34	1.34	75	76	129	129	73
112	1.43	1.43	63	67	132	132	108
106	1.95	1.95	106	106	145	145	37
109	1.95	1.95	107	108	145	145	35
116	1.96	1.96	103	102	145	145	43
114	2.00	2.00	95	97	146	146	54
90	2.62	2.62	114	116	158	158	38
91	2.77	2.77	120	121	161	161	34
105	3.45	3.45	148	146	172	172	17
115	3.57	3.57	145	145	174	174	20
111	4.71	4.56	157	159	189	187	20
92	5.34	5.27	167	168	196	195	17
88	7.96	7.70	202	203	221	219	9
93	7.99	7.84	198	199	221	220	12
94	10.55	10.55	217	222	240	240	11
95	13.09	13.09	231	239	257	257	11
96	14.83	14.97	241	251	266	267	11
89	15.15	15.15	251	256	268	268	7
118	16.94	18.48	279	273	277	285	4
119	17.97	18.74	276	269	282	286	6
86	17.97	19.00	280	271	282	287	6
87	18.23	19.00	276	269	283	287	6

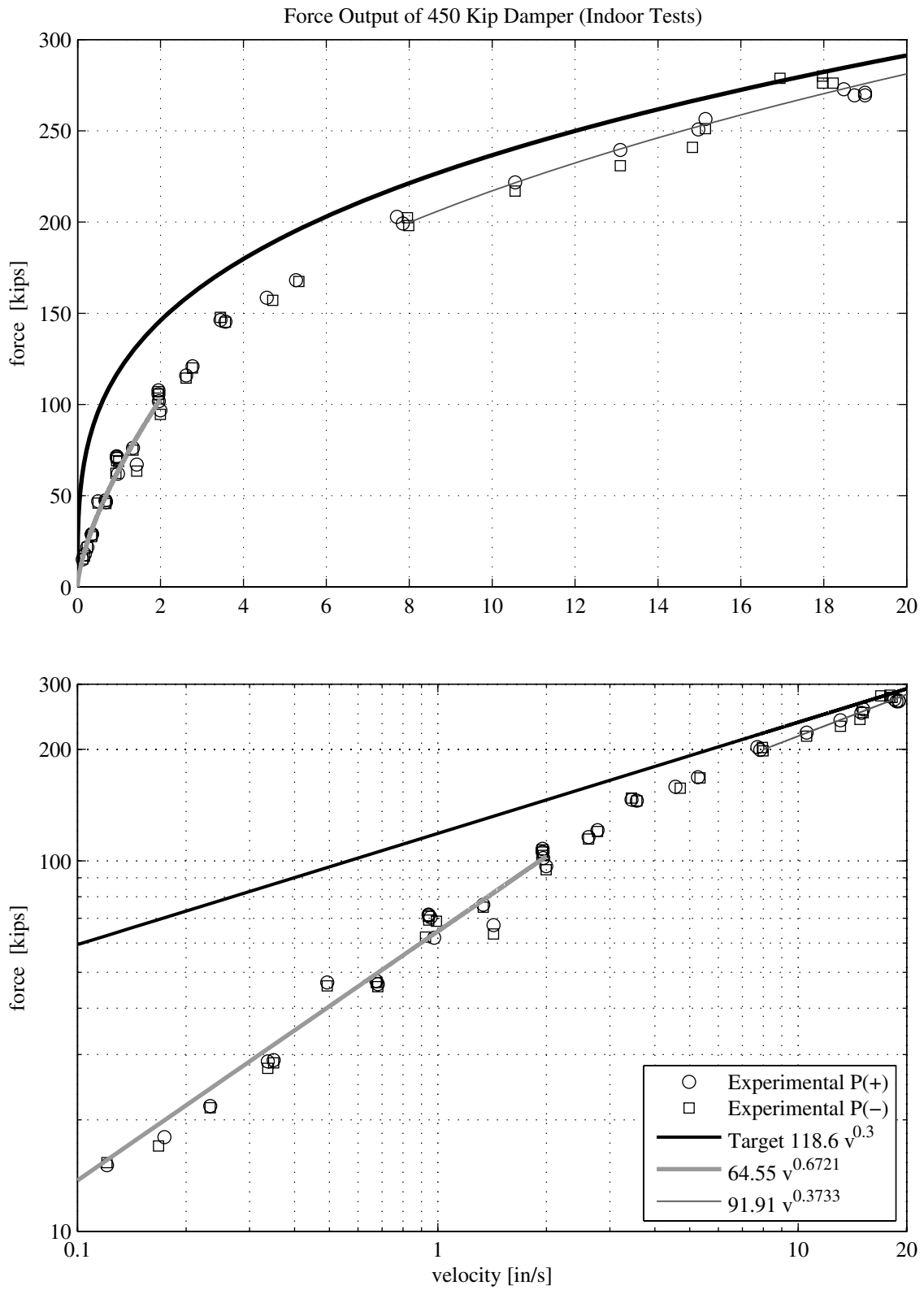


Fig. 2.29 Force output of 450-kip damper.

$$\hat{P} = 64.55v_0^{0.6721}, 0.1 < v_0 < 2.0 \quad (2.10)$$

where v_0 is in in/sec and \hat{P} in kips.

3 Outdoor Experiments on 450-Kip damper

The indoor experimental program demonstrated that commercially available strain gauges, both the bondable and weldable kind, can reliably be used to accurately monitor the force output of fluid dampers installed on the field over a wide range of velocity inputs. It was concluded that gauges should not be placed on the damper casing but rather on the extender piece, preferably near mid-length to avoid end-effects.

An experimental program that consisted of testing the second of the two available 450-kip dampers (the first was used in the indoor tests), described in Chapter 2, on a testing machine that was built for the purposes of this project outside of the testing laboratory at the Pacific Earthquake Engineering Research Center, University of California, Berkeley. The purpose of this series of experiments was to investigate possible changes in the force output of the damper over time under service loading conditions, where the frequency and amplitude of the displacement cycles are very small. In addition, the damper was again instrumented with displacement transducers as well as strain gauges, to examine the effect of environmental conditions on them. In an effort to replicate actual conditions on a bridge, the setup was located very near the bay, approximate distance 1/3 mile, and exposed to wind coming in from the bay (See Fig. 3.1).

3.1 EXPERIMENTAL PROGRAM

Figure 3.2 is a schematic of the setup for the outdoor tests on the 450-kip damper. The reaction frame, shown in Fig. 3.3 before any modifications, was salvaged from the PEER laboratory yard, where it was laying around after it had been used in past experiments. Some modifications were necessary to make it adopt the damper and actuator. An actuator clevis, a backside clevis, pins, retainer plates, an actuator bracket and a fixed mount were designed in-house and sent out for fab-

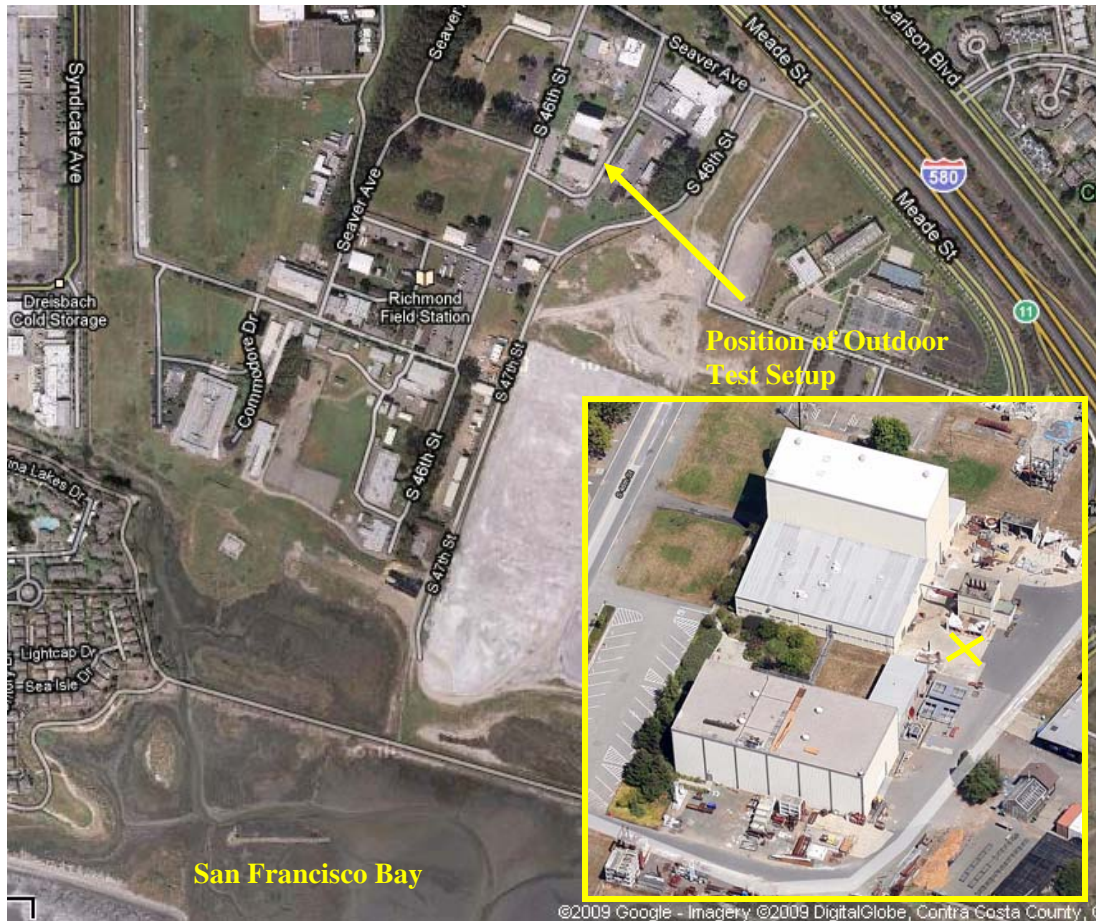


Fig. 3.1 The outdoor test setup is approximately 1/3 mile from the San Francisco Bay. The X in the smaller photograph marks the location of the test setup outside the PEER laboratory at the Richmond Field Station, University of California, Berkeley (Images from Google Maps).

rication. The reaction frame featuring an MTS 244 hydraulic actuator with ± 3 in. stroke and 55-kip force capacity was then assembled.

Figure 3.4 shows a cart with the ATS controller and 16-channel data acquisition system used. In the early phase of testing (up to Test No. 241) only the force and actuator displacement were recorded, while in the later phases (from Test No. 242 on), all 16 channels were used to record a multitude of responses, including strains, displacement from an additional transducer mounted on the damper, and temperature from three thermocouples. One was located on the reaction frame to measure ambient temperature and the other two on the barrel of the damper at distances of 5.0 inches and 13.5 inches from the mid-stroke position of the damper piston. It was not possible to

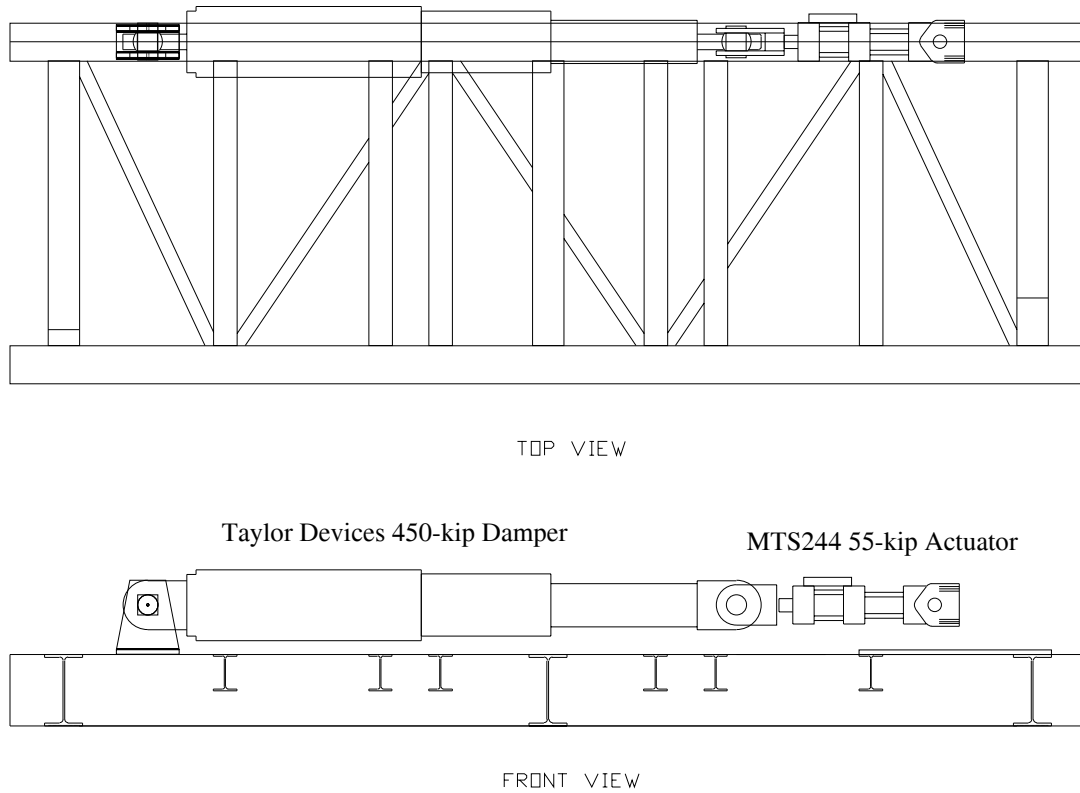


Fig. 3.2 Outdoor test setup.

locate a thermocouple closer to the mid-stroke position due to the cover of the damper. The thermocouples were protected from weather by multiple layers of adhesive vinyl tape and were unaffected by heavy rainfall during the duration of the testing program. Table 3.1 lists the 16 channels used during the later phase of the outdoor testing.

Figure 3.5 shows the experimental setup of the outdoor tests, with arrows indicating the locations of the various pieces of instrumentation used. The position transducers used are the Celesco PT5AV and Novotechnik TLH, which have been described in Chapter 2. The Celesco position/velocity transducer was covered with a clear plastic bag, which proved sufficient to keep it operational without problems even during days with massive rainfall. The manufacturer rates the device suitable for wet conditions. In a bridge application, the authors recommend a protective plastic enclosure with holes for the potentiometer wire and connecting cables. It is also recommended that the extended potentiometer wire is slightly inclined so that water that pours on it will trickle away from the device.



Fig. 3.3 Old frame salvaged from the PEER laboratory yard for use in the outdoor testing program.



Fig. 3.4 ATS controller and data acquisition cart; portable hydraulic pump.

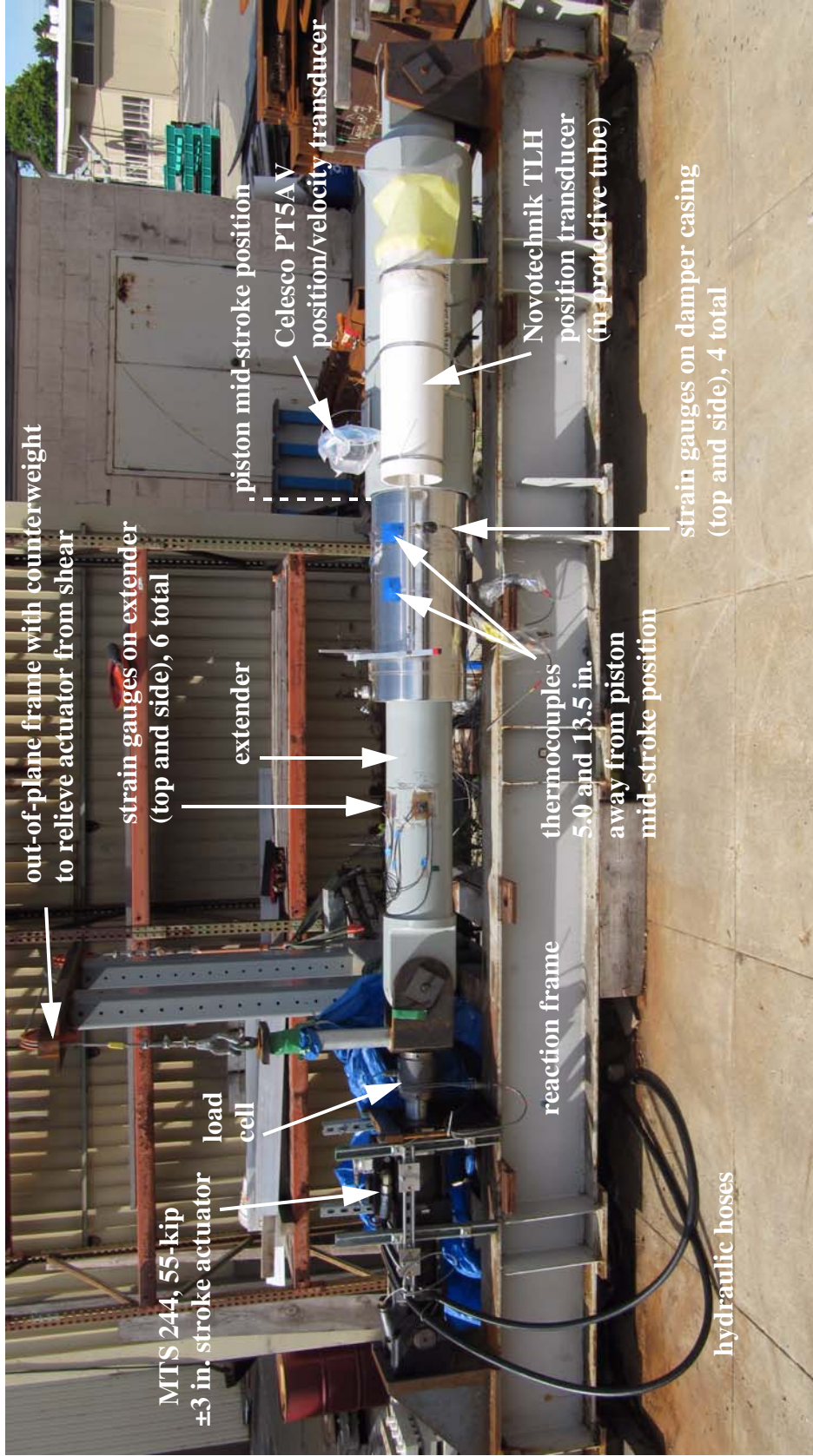


Fig. 3.5 Fully instrumented 450-kip damper mounted on the outdoor testing machine at the PEER laboratory, University of California, Berkeley.

Table 3.1 Channel list for outdoor tests on 450-kip damper.

Channel	Quantity measured
1	Force from load cell
2	Actuator displacement, up to Test No. 307 / Damper displacement, Test No. 308 on
3	Extender (top) longitudinal strain
4	Extender (top) transverse strain
5	Extender (top) 45-deg strain
6	Extender (side) longitudinal strain
7	Extender (side) transverse strain
8	Extender (side) 45-deg strain
9	Damper casing (top) longitudinal strain
10	Damper casing (top) transverse strain
11	Damper casing (top) 45-deg strain
12	Damper casing (side) transverse strain
13	Damper displacement
14	Temperature on damper casing 5.0 in. away from piston mid-stroke position
15	Temperature on damper casing 13.5 in. away from piston mid-stroke position
16	Outdoor (ambient) temperature

The Novotechnik TLH position transducer is not recommended for wet/humid environments. It was only installed in the late phases of testing in order to be used as a control displacement device mounted directly on the damper. Until that point, an LVDT displacement transducer (not visible in Fig. 3.5) mounted on the actuator was used as a control device. As it can be seen in the figure, the Novotechnik was protected by a plastic tube from rainfall.

Built-up rosettes of weldable strain gauges were attached on the damper extender at its mid-length, as shown in Fig. 3.5, one on the top of the extender and one at its side. Figure 3.6 is a close-up photograph of a rosette that has been covered with coatings to protect it from the environmental conditions. Below the rosette, a single weldable strain gauge that measures longitudinal strain can be seen. This gauge has been covered with a transparent coat only (i.e., the first coat of a three-different-coat procedure). This photograph was taken at a later time when the wireless

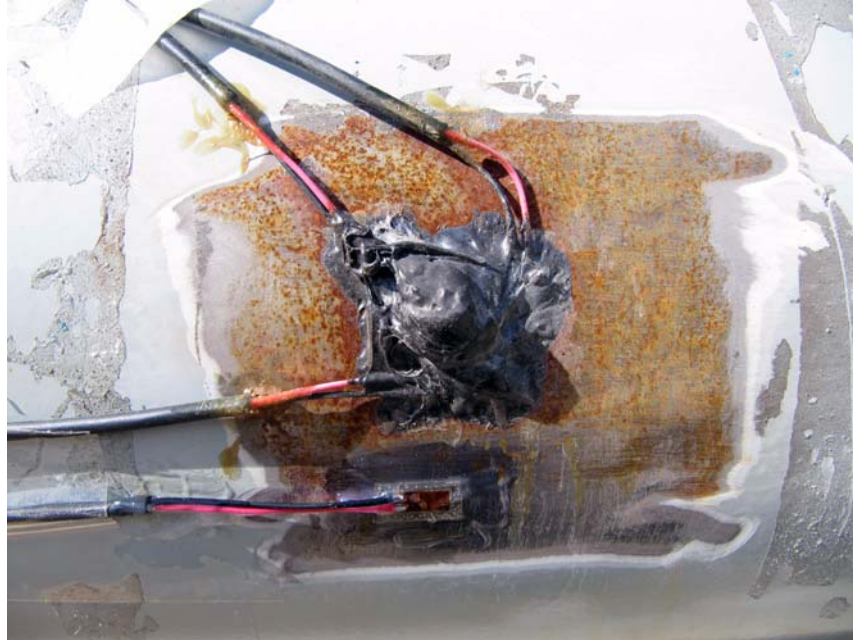


Fig. 3.6 Built-up rosette of weldable strain gauges covered with Vishay Micro-Measurements protective M-Coat A, B and J. Below the rosette is a single weldable gauge (longitudinal strain) that is only covered with the transparent M-Coat A.

Opto22 system was tested, and a parallel network of strain gauges was attached on the damper. The single gauge with the transparent coat is part of this parallel network of gauges. The three coats of protection applied, and which are recommended for a bridge application, consisted of Vishay Micro-Measurements *M-Coat A*, *M-Coat B*, and *M-Coat J*.

The first coat, M-Coat A, is a transparent, air-drying, solvent-thinned (xylene) polyurethane. It is the general-purpose coating in (indoor) lab applications and can be used as a base coating for field applications. It must be fully cured before application of other coatings. By itself, it has fair moisture resistance, and it is not readily attacked by many solvents. Dries tack-free at room temperature in 20 minutes and is completely dry in two hours. The normal curing time is 24 hours at room temperature.

The second coat, M-Coat B, is an air-drying solvent-thinned (MEK) nitrile rubber. It forms a flexible rubbery coating. It has excellent resistance to gasoline, kerosene, and commercial oils. It air-dries in one hour at 75°F. The normal curing time is 24 hours at room temperature. Vishay Micro-Measurements M-Coat C could be used instead of B.

The third coat, M-Coat J, is a two-part polysulfide liquid polymer compound. It is a tough, flexible coating and offers very good salt-water immersion protection. Moreover, it offers good protection against oil, grease, most acids and alkalies, and most solvents. Normal curing time is 24 hours.

The manufacturers instructions, while simple, must be carefully followed in applying these coats to ensure proper environmental protection. Appendix A offers more information that can be used to aid in the installation and protection of weldable strain gauges. The information was collected from Vishay Micro-Measurements literature. Protection of the lead wires at least up to 1.0 in. away from the gauge terminals is necessary since a common cause of failure in strain gage installations is penetration by water or other liquids at the lead-wire entrance to the coating.

The testing program was carried out over the first six months of 2010 during a period with several large storms that produced very heavy rain. All of the instrumentation that would be used on a damper on a bridge functioned without problems during this period, the only significant impact of the weather was to the load cell, that would not be used in the field.

Table 3.2 lists the displacement amplitudes, u_0 , (labelled *signal input*) and periods, T , for all the outdoor tests with signal displacement $u(t) = u_0 \sin(2\pi t / T)$. The nomenclature for file-name in Table 3.2 is as follows: first two digits are the year, next two are the month, next two are the date, and last two are the test number in that day. For example, Test No. 342 was the 4th test conducted on May 25, 2010. The table also lists the beginning cycle, the total number of cycles, the cumulative distance travelled, and the data sampling rate.

3.2 RESULTS OF OUTDOOR TESTS

Figures 3.7 and 3.8 show results of two typical outdoor experiments on the 450-kip damper. Figure 3.7 shows the results of the first 60 seconds of Test No. 194, one of the tests with low displacement and velocity amplitudes. The test, which had a total of 400 cycles, had an input signal with displacement amplitude 0.5 in. and period of 30 sec. The peak recorded displacement was +0.505/−0.493 in., and the peak recorded velocity was +0.106/−0.108. Figure 3.8, on the other hand, shows a fast, large-amplitude tests (Test No. 272) which had a input signal with displacement amplitude 1.5 in. and period of 15 sec. The test ran for 1600 cycles. The peak recorded displacement was +1.51/−1.50 in., while the peak recorded velocity was +0.616/−0.624 in/sec. Note

Table 3.2 Outdoor tests conducted on the 450-kip damper.

Test No.	File Name	Beginning Cycle Count	Cycles	Signal Input (+/- in)	Signal Period (sec)	Cumulative Distance (miles)	Scan Rate (Hz)
124	10021104	40	10	1.10	15.0	0.003	10
125	10021105	50	10	1.05	15.0	0.004	10
128	10021108	62	10	1.05	15.0	0.005	10
129	10021109	72	10	1.00	15.0	0.005	2
130	10021110	82	10	1.00	15.0	0.006	10
131	10021111	92	10	1.00	15.0	0.007	10
132	10021112	102	10	1.00	15.0	0.007	2
133	10021201	112	10	1.00	15.0	0.008	10
134	10021202	122	500	1.00	15.0	0.040	2
135	10021203	622	10	1.00	15.0	0.040	10
136	10021204	632	500	1.00	15.0	0.072	2
137	10021205	1132	10	1.00	15.0	0.072	10
138	10021206	1142	500	1.00	15.0	0.104	2
139	10021301	1642	10	1.00	15.0	0.105	10
140	10021302	1652	500	1.00	15.0	0.136	2
141	10021303	2152	10	1.00	15.0	0.137	10
142	10021304	2162	500	1.00	15.0	0.168	2
143	10021305	2662	10	1.00	15.0	0.169	10
144	10021306	2672	500	1.00	15.0	0.201	2
145	10021307	3172	10	1.00	15.0	0.201	10
146	10021501	3182	10	1.00	15.0	0.202	10
147	10021502	3192	800	1.00	15.0	0.252	2
148	10021601	3992	10	1.00	15.0	0.253	10
149	10021602	4002	400	1.00	15.0	0.278	2
150	10021603	4402	10	1.00	15.0	0.279	10
151	10021604	4412	175	1.00	15.0	0.290	2
152	10021605	4587	10	1.00	15.0	0.291	10
153	10021606	4597	640	1.00	15.0	0.331	2
154	10021607	5237	10	1.00	15.0	0.332	10
155	10021608	5247	70	0.50	30.0	0.334	2
156	10021701	5317	10	1.00	15.0	0.334	10
157	10021702	5327	400	0.50	30.0	0.347	2
158	10021703	5727	10	1.00	15.0	0.348	10
159	10021704	5737	110	0.50	30.0	0.351	2
160	10021705	5847	400	0.50	30.0	0.364	2
161	10021706	6247	10	1.00	15.0	0.364	10
162	10021707	6257	400	0.50	30.0	0.377	2
163	10021801	6657	10	1.00	15.0	0.378	10
164	10021802	6667	400	0.50	30.0	0.390	2
165	10021803	7067	10	1.00	15.0	0.391	10
166	10021804	7077	400	0.50	30.0	0.404	2
167	10021805	7477	10	1.00	15.0	0.404	10
168	10021806	7487	10	0.50	30.0	0.404	10
169	10021807	7497	400	0.50	30.0	0.417	2
170	10021808	7897	10	0.50	30.0	0.417	10
171	10021901	7907	10	0.50	30.0	0.418	10
173	10021903	8317	10	0.50	30.0	0.431	10
174	10021904	8327	400	0.50	30.0	0.443	2
175	10021905	8727	10	0.50	30.0	0.444	10
176	10021906	8737	313	0.50	30.0	0.453	2
177	10021907	9050	10	0.50	30.0	0.454	10
178	10022201	9060	10	0.50	30.0	0.454	10

Table 3.2(cont.) Outdoor tests conducted on the 450-kip damper.

Test No.	File Name	Beginning Cycle Count	Cycles	Signal Input (+/- in)	Signal Period (sec)	Cumulative Distance (miles)	Scan Rate (Hz)
179	10022202	9070	400	0.50	30.0	0.467	2
180	10022203	9470	10	0.50	30.0	0.467	10
181	10022204	9480	400	0.50	30.0	0.480	2
182	10022205	9880	10	0.50	30.0	0.480	10
183	10022206	9890	400	0.50	30.0	0.493	2
184	10022207	10290	10	0.50	30.0	0.493	10
185	10022301	10300	10	0.50	30.0	0.493	10
186	10022302	10310	400	0.50	30.0	0.506	2
187	10022303	10710	10	0.50	30.0	0.506	10
188	10022304	10720	400	0.50	30.0	0.519	2
189	10022305	11120	10	0.50	30.0	0.519	10
190	10022306	11130	400	0.50	30.0	0.532	2
191	10022307	11530	10	0.50	30.0	0.532	10
192	10022401	11540	10	0.50	30.0	0.532	10
193	10022501	11550	10	0.50	30.0	0.533	10
194	10022502	11560	400	0.50	30.0	0.545	2
195	10022503	11960	10	0.50	30.0	0.546	10
196	10022601	11970	10	0.50	30.0	0.546	10
197	10022602	11980	400	0.50	30.0	0.559	2
198	10022603	12380	10	0.50	30.0	0.559	10
199	10022604	12390	400	0.50	30.0	0.572	2
200	10022605	12790	10	0.50	30.0	0.572	10
201	10022606	12800	350	0.50	30.0	0.583	2
202	10022607	13150	10	0.50	30.0	0.583	10
203	10022701	13160	10	0.50	30.0	0.584	10
204	10022702	13170	400	0.50	30.0	0.596	2
205	10022703	13570	10	0.50	30.0	0.596	10
213	10030401	14111	10	0.50	30.0	0.614	10
214	10030402	14121	400	0.50	30.0	0.626	2
215	10030501	14521	10	0.50	30.0	0.626	10
216	10030502	14531	400	0.50	30.0	0.639	2
217	10030503	14931	10	0.50	30.0	0.639	10
218	10030504	14941	400	0.50	30.0	0.652	2
219	10030505	15341	10	0.50	30.0	0.652	10
220	10030506	15351	400	0.50	30.0	0.665	2
221	10030507	15751	10	0.50	30.0	0.665	10
222	10030801	15761	10	0.50	30.0	0.666	10
223	10030802	15771	400	0.50	30.0	0.678	2
224	10030803	16171	10	0.50	30.0	0.679	2
225	10030804	16181	10	0.50	30.0	0.679	10
226	10030805	16191	400	0.50	30.0	0.692	2
227	10030806	16591	10	0.50	30.0	0.692	10
228	10030807	16601	300	0.50	30.0	0.701	2
229	10030808	16901	10	0.50	30.0	0.702	10
230	10030901	16911	10	0.50	30.0	0.702	10
231	10030902	16921	400	0.50	30.0	0.715	2
233	10030904	17331	80	0.50	30.0	0.717	2
234	10030905	17411	10	1.00	30.0	0.718	10
235	10030906	17421	360	1.05	20.0	0.742	2
236	10031001	17781	350	1.55	20.0	0.776	2
237	10031002	18131	500	1.55	20.0	0.825	2
238	10031101	18631	20	1.55	20.0	0.827	10

Table 3.2(cont.) Outdoor tests conducted on the 450-kip damper.

Test No.	File Name	Beginning Cycle Count	Cycles	Signal Input (+/- in)	Signal Period (sec)	Cumulative Distance (miles)	Scan Rate (Hz)
239	10031102	18651	20	1.55	20.0	0.829	10
240	10031103	18671	20	1.55	15.0	0.831	10
241	10031104	18691	20	1.55	15.0	0.833	10
242	10031801	18711	10	1.00	20.0	0.834	10
243	10031802	18721	110	1.00	20.0	0.840	2
244	10031803	18831	121	1.55	15.0	0.852	2
245	10031804	18952	100	1.55	15.0	0.862	2
246	10031901	19052	10	1.00	20.0	0.863	10
247	10031902	19062	20	1.55	15.0	0.865	10
248	10031903	19082	289	1.55	15.0	0.893	2
249	10031904	19371	800	1.55	15.0	0.971	2
250	10031905	20171	20	1.55	20.0	0.973	10
251	10031906	20191	120	1.55	20.0	0.985	2
252	10031907	20311	20	1.55	20.0	0.987	10
253	10031908	20331	169	1.55	20.0	1.003	2
254	10031909	20500	370	1.55	20.0	1.040	2
255	10032201	20870	10	1.00	20.0	1.040	10
256	10032202	20880	900	1.00	20.0	1.097	2
257	10032301	21780	10	1.00	30.0	1.098	10
258	10032302	21790	600	1.00	30.0	1.136	2
259	10032401	22390	10	1.00	15.0	1.136	10
260	10032402	22400	1200	1.00	15.0	1.212	2
263	10032601	24210	10	1.50	30.0	1.271	10
264	10032602	24220	600	1.50	30.0	1.328	2
265	10032901	24820	10	1.50	20.0	1.328	10
266	10032902	24830	1200	1.50	20.0	1.442	2
269	10033003	26044	10	1.50	20.0	1.444	10
270	10033004	26054	1200	1.50	20.0	1.558	2
271	10033101	27254	10	1.50	15.0	1.559	10
272	10033102	27264	1600	1.50	15.0	1.710	2
273	10033103	28864	10	1.50	15.0	1.711	10
274	10033104	28874	20	1.50	15.0	1.713	2
275	10040101	28894	10	1.50	15.0	1.714	10
276	10040102	28904	7	1.50	15.0	1.715	2
277	10040103	28911	10	1.50	15.0	1.716	2
278	10040104	28921	1600	1.50	15.0	1.867	10
279	10040201	30521	10	1.50	15.0	1.868	2
280	10040202	30531	853	1.50	15.0	1.949	10
283	10041401	32984	10	1.50	15.0	2.102	10
284	10041402	32994	1600	1.50	15.0	2.253	2
285	10041501	34594	10	1.50	15.0	2.254	10
286	10041502	34604	1600	1.50	15.0	2.406	2
287	10041901	36204	10	1.50	15.0	2.407	10
288	10041902	36214	1600	1.50	15.0	2.558	2
289	10042101	37814	10	1.50	15.0	2.559	10
290	10042102	37824	1600	1.50	15.0	2.710	2
291	10042103	39424	432	1.50	15.0	2.751	2
292	10042601	39856	10	1.50	15.0	2.752	10
293	10042602	39866	1600	1.50	15.0	2.904	2
295	10050301	41467	10	1.50	15.0	2.905	10
296	10050302	41477	1600	1.50	15.0	3.056	2
297	10050303	43077	937	1.50	15.0	3.145	2

Table 3.2(cont.) Outdoor tests conducted on the 450-kip damper.

Test No.	File Name	Beginning Cycle Count	Cycles	Signal Input (+/- in)	Signal Period (sec)	Cumulative Distance (miles)	Scan Rate (Hz)
298	10050401	44014	10	1.50	15.0	3.146	10
299	10050402	44024	1271	1.50	15.0	3.266	2
300	10050501	45295	10	1.50	15.0	3.267	10
301	10050502	45305	1600	1.50	15.0	3.419	2
302	10050601	46905	10	1.50	15.0	3.420	10
303	10050602	46915	1463	1.50	15.0	3.558	2
304	10050701	48378	10	1.50	15.0	3.559	10
305	10050702	48388	1519	1.50	15.0	3.703	2
306	10051001	49907	10	1.50	15.0	3.704	10
307	10051002	49917	1600	1.50	15.0	3.856	2
308	10051101	51517	10	1.50	15.0	3.857	10
309	10051102	51527	1600	1.50	15.0	4.008	2
310	10051201	53127	10	1.50	15.0	4.009	10
311	10051202	53137	1600	1.50	15.0	4.161	2
312	10051203	54737	567	1.50	20.0	4.214	2
313	10051301	55304	10	1.50	20.0	4.215	10
315	10051303	55315	1200	1.50	20.0	4.329	2
316	10051304	56515	10	1.50	20.0	4.330	10
317	10051305	56525	817	1.50	20.0	4.407	2
318	10051401	57342	10	1.50	20.0	4.408	10
319	10051402	57352	1200	1.50	20.0	4.522	2
320	10051403	58552	10	1.50	20.0	4.523	10
321	10051404	58562	469	1.50	20.0	4.567	2
324	10051701	60241	10	1.50	20.0	4.683	10
325	10051702	60251	1200	1.50	20.0	4.796	2
326	10051801	61451	10	1.50	20.0	4.797	10
327	10051802	61461	29	1.50	20.0	4.800	2
328	10051803	61490	139	1.50	20.0	4.813	2
329	10051901	61629	10	1.50	20.0	4.814	10
330	10051902	61639	1200	1.50	20.0	4.928	2
331	10052001	62839	10	1.50	20.0	4.929	10
332	10052002	62849	1200	1.50	20.0	5.042	2
333	10052101	64049	10	1.50	20.0	5.043	10
334	10052102	64059	1100	1.50	20.0	5.148	2
335	10052103	65159	10	1.50	20.0	5.148	10
336	10052104	65169	690	1.50	20.0	5.214	2
337	10052201	65859	10	1.50	20.0	5.215	10
338	10052202	65869	1200	1.50	20.0	5.328	2
339	10052501	67069	10	1.50	20.0	5.329	10
340	10052502	67079	1200	1.50	20.0	5.443	2
341	10052503	68279	10	1.50	16.7	5.444	10
342	10052504	68289	715	1.50	16.7	5.512	2

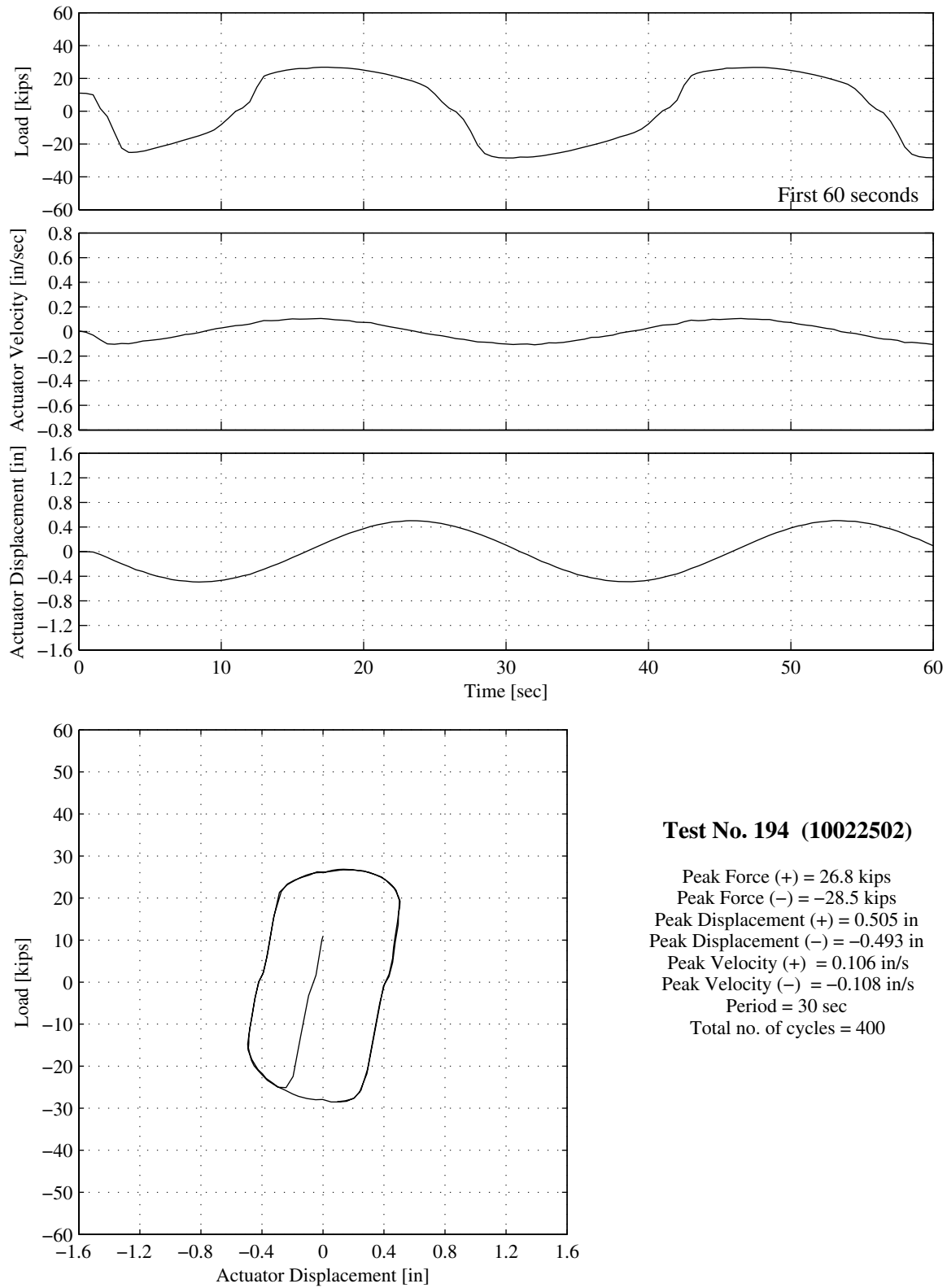
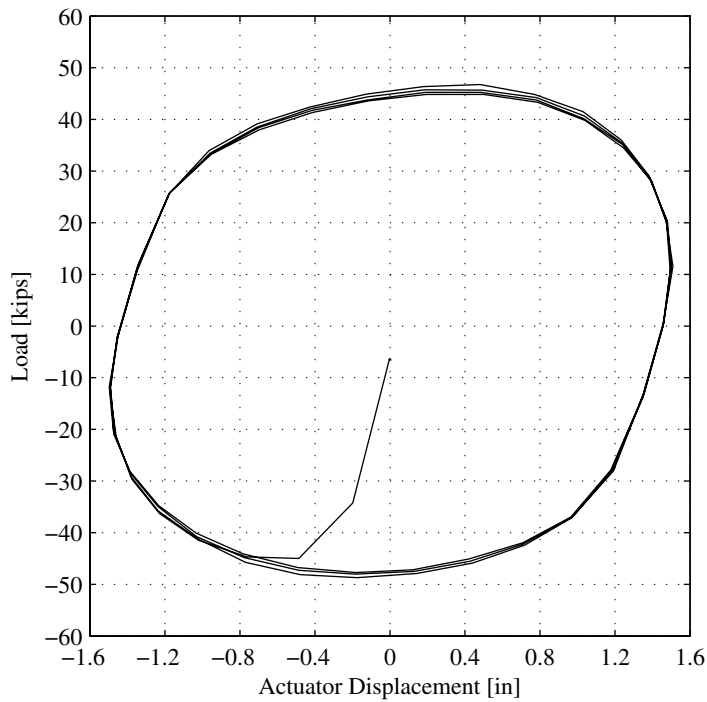
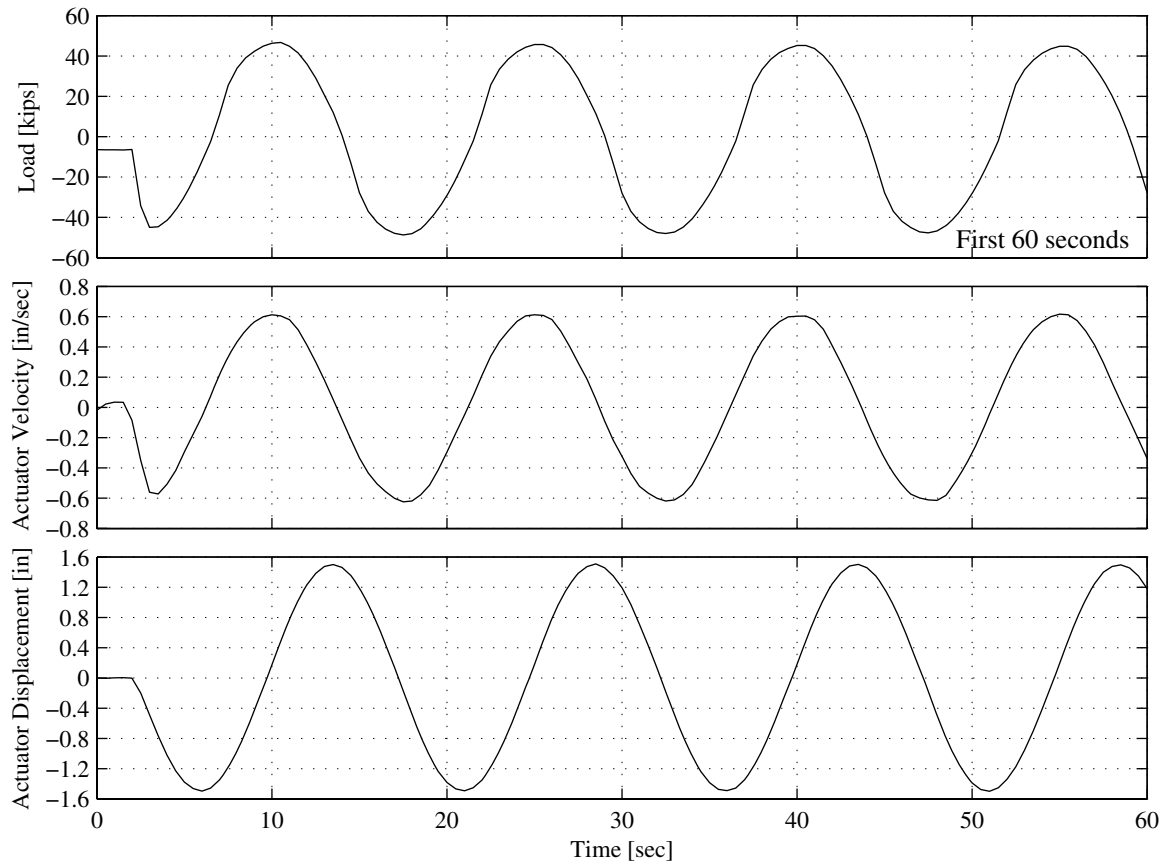


Fig. 3.7 Results of a slow outdoor test with low-displacement amplitude.



Test No. 272 (10033102)

Peak Force (+) = 46.7 kips
 Peak Force (-) = -48.7 kips
 Peak Displacement (+) = 1.51 in
 Peak Displacement (-) = -1.5 in
 Peak Velocity (+) = 0.616 in/s
 Peak Velocity (-) = -0.624 in/s
 Period = 15 sec
 Total no. of cycles = 1600

Fig. 3.8 Results of a fast outdoor test with large-displacement amplitude.

that these two figures plot the force output of the damper as recorded with the load cell, and the discussion that follows in the next section uses the readings obtained from the load cell. Discussion on the force obtained from the strain gauges is presented at a later section.

3.2.1 Results of Daily First Cycle Tests with Damper Force Obtained from Load Cell

In an effort to separate the effects of temperature rise due to self-heating from the effect of cumulative travel, we examined the response of the outside damper at the first three cycles per day when the temperature was the ambient temperature and it is assumed that the effect of variation of temperature is negligible by virtue of the internal temperature compensation system within the damper. The force values reported in this section were those obtained directly from the load cell. We have a large number of sequences at the lowest velocity (0.114 in/sec) and at the highest velocity (0.616 in/sec).

At the lowest velocity, the peak forces never varied by more than $\pm 5\%$ from the average over ten days of tests, and within any one day they showed no systematic variation over that day's set of sequences. The conclusion is that there appears to be no change in the peak damper force over the distance travelled by the damper. Of course, the low velocity is achieved by using small displacements (± 0.5 in.) and long periods so that the distance is not large even over ten days of tests, from Test No. 168 to No. 233, over a complete set of cycles from 7487 to 17331 (or 0.404 to 0.717 miles).

At the highest velocity (0.63 in/sec) used on the outside damper test program, the peak force steadily diminished from a maximum peak force of ± 50.1 kips at the initial test (Test No. 275) at this velocity to a minimum of ± 42.8 kips at the final test (Test No. 310) at this velocity, over a set of cycles from 28894 to 53137 (or 1.714 to 4.009 miles). This is approximately a 15% loss in force. Figure 3.9 shows the results of the first two cycles of these tests side-by-side. It should be emphasized that these forces are measured for the first tests each day so that self-heating should not be an issue, although it is also clear that the temperature rise over a day of testing also steadily increases and the peak force diminishes steadily during each with the rise in temperature. With this and the observation that the temperature increase at the lowest velocity is negligible, it can be concluded that it is the combination of temperature rise and distance travelled that influences the change in the response of the damper. The importance of this for a damper on a bridge is that if a

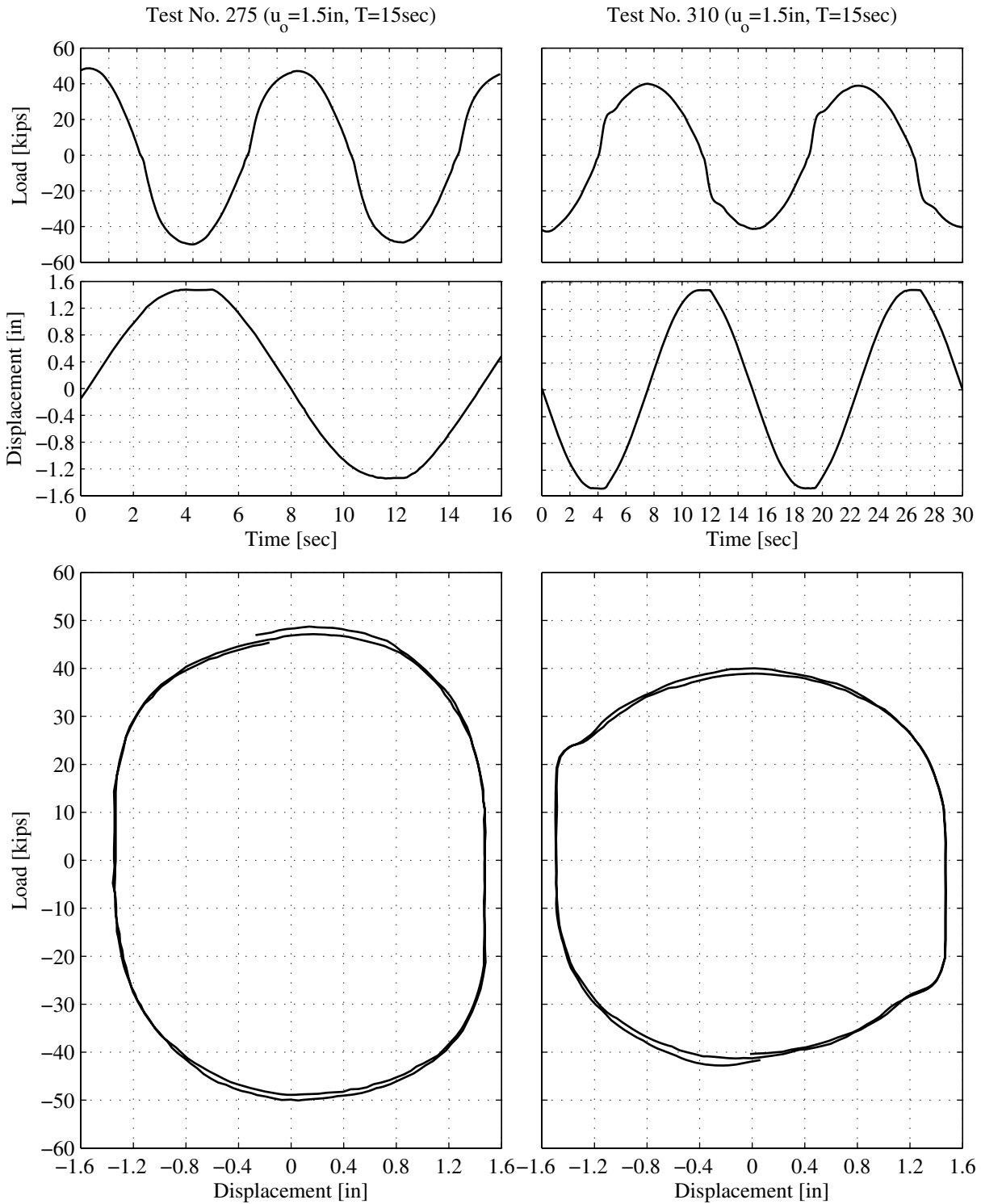


Fig. 3.9 Comparison of the results from the first two cycles of a fast test (0.63 in/sec). Test No. 310 (right), which was conducted 2.295 miles (cumulative travel) after Test 275 (left), shows a 15% drop in peak recorded force.

damper is located at a position on the bridge that causes a steady state velocity of the order of the highest velocity of these tests, then a loss in peak force must be anticipated. The question of whether this loss in force at service level input translates into a loss at seismic levels of input cannot be answered by the current test program but should be an urgent objective of future tests.

3.2.2 Effect of Temperature on Peak Damper Force Obtained from Load Cell

Figures 3.10 to 3.13 show the effect of temperature on the peak force. The solid line and left axis of the figures show the peak force, while the dashed line and the right axis show the difference in temperature between the thermocouple located on the barrel of the damper, 5.0 in. away from the mid-stroke position of the piston, and the thermocouple attached on the reaction frame, measure ambient temperature. The graphs show the change in these two quantities over the course of the day. Figure 3.10 shows results for tests 257 and 258, which had displacement amplitude 1.0 in. and period 30 sec and ran for a total of 610 cycles (approximately five hours). These quantities correspond to a velocity of 0.21 in/sec. The two tests were run one after the other with no interruption. The graphs show that while the temperature increases steadily over the course of the two tests, rising by about 23 degrees F, the peak force is nearly constant at 30 kips. On the other hand, Fig. 3.11, which shows the results of tests 329 and 330 (with ± 1.5 -in stroke and 20-sec period, corresponding to velocity of 0.47 in/sec) shows a drop of approximately 11 kips in force and a rise in temperature of about 50 degrees F. Figures 3.12 and 3.13, which plot results of tests 298/299 and 295/296/297, respectively (all at 0.63 in/sec), show the same phenomenon of rise in temperature followed by drop in peak force. The sudden drop in temperature and rise in force at cycle 1610 in Fig. 3.13 occurs because there was a delay before the start of Test No. 297 which allowed the damper to cool down.

Figures 3.10 to 3.13 show that while the force in the damper, for the ranges plotted, appears to asymptotically reach a steady value, the temperature of the damper does not reach a steady state. For faster tests, the temperature increased without bound. In several tests, the temperature exceeded 160 degrees F. This temperature, again, was recorded at a distance of 5 in. from the mid-stroke position of the damper since the cover of the damper did not allow from placing any instruments closer to the mid-stroke position. The temperature is, of course, anticipated to be higher at that position. This finding raises the question of how these dampers would behave in a

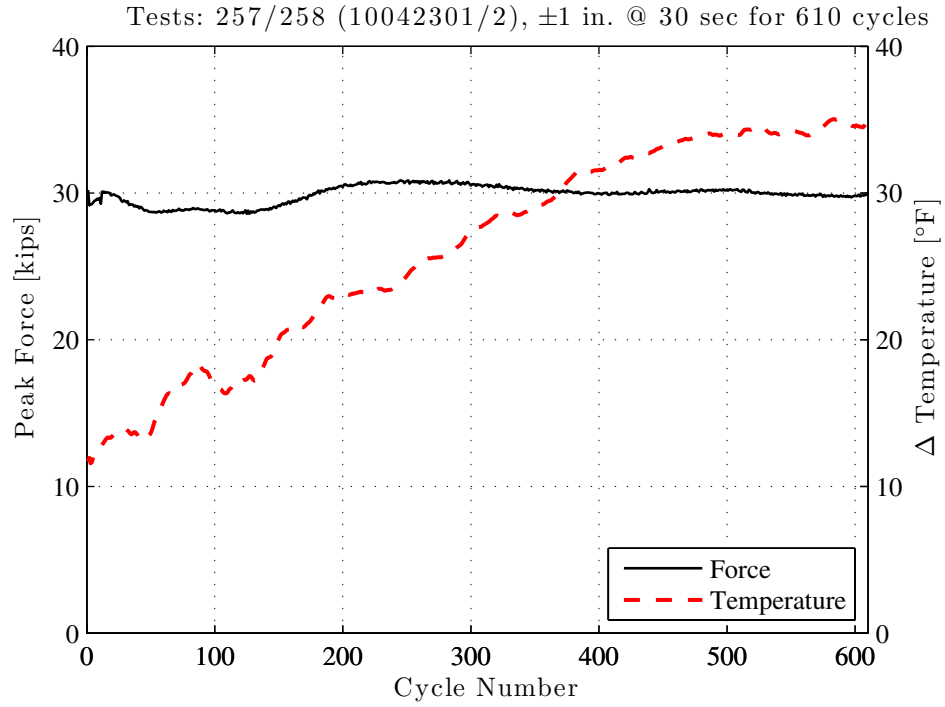


Fig. 3.10 Peak force and temperature rise over the course of Tests 257 and 258.

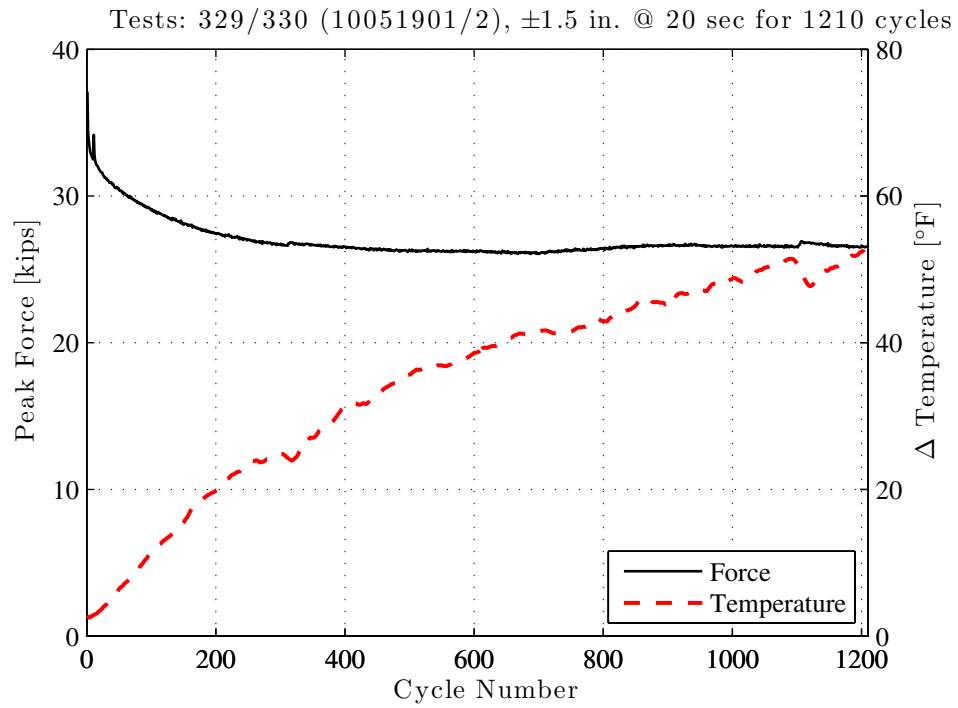


Fig. 3.11 Peak force and temperature rise over the course of Tests 329 and 330.

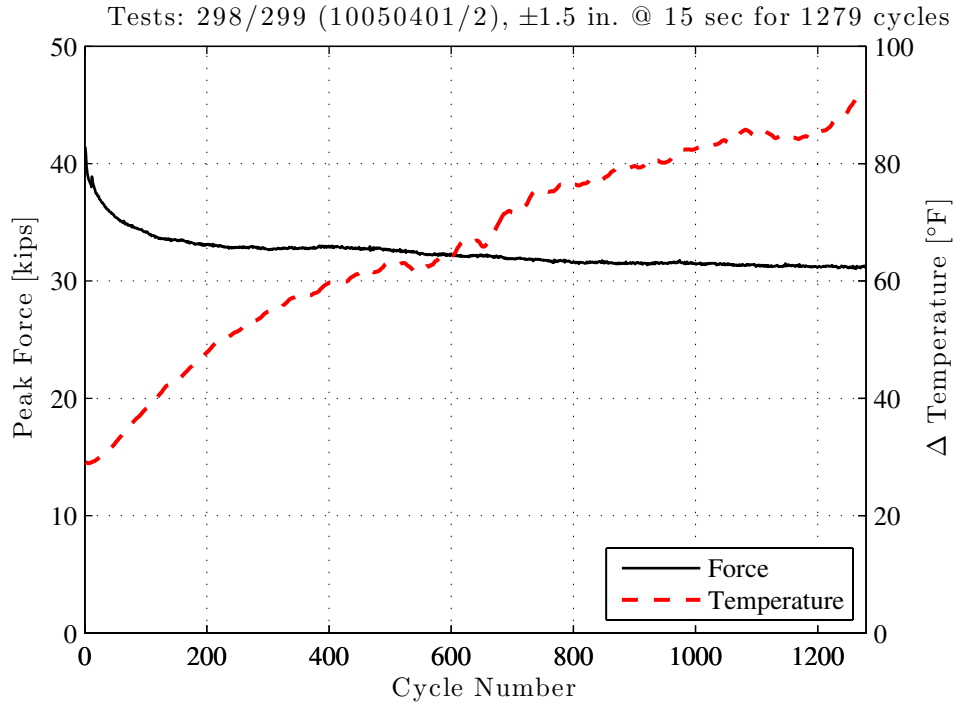


Fig. 3.12 Peak force and temperature rise over the course of Tests 298 and 299.

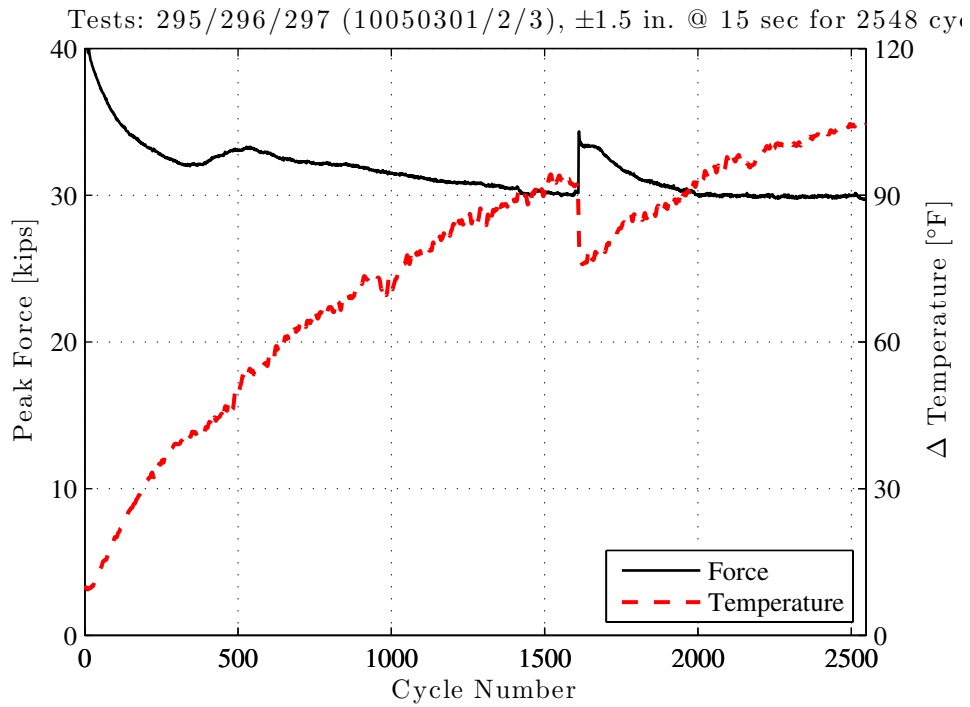


Fig. 3.13 Peak force and temperature rise over the course of Tests 295, 296 and 297.

bridge when they are cycled repeatedly at a fast rate and with a large displacement, as in the case of a wind storm. If the power input is high enough and the duration of loading long enough, such a storm may cause damage to the dampers.

3.2.3 Damper Force Estimated from the Strain Gauges

The top graph of Fig. 3.14 shows with a heavy black line the damper force as recorded by the load cell during Test No. 298 (displacement amplitude 1.5 in., period 15 sec). The thin line shows the damper force as computed using the recorded values of strain. We observe that the force signal computed from the strain gauges exhibits a pronounced drift, probably because of interference in the cables and in the circuits of the data acquisition system. The drift is easy to eliminate by subtracting from its drifting baseline (the drifting baseline can be easily computed using a moving average with very wide span) or by considering the peak-to-peak of the signal. Moreover, the signal can be filtered to reduce noise. The bottom graph of Fig. 3.14 shows with a heavy black line the force recorded by the load cell and with a thin line the drifted force computed from the strain gauges after it has been filtered to reduce noise. The heavy grey line is the force that is obtained after the filtered signal has been treated to eliminate drift. It is very important to note here that the drifting of the zero is not an issue because in a bridge application, where the bridge is constantly moving, the concept of such a zero does not exist, anyway. Thus, it is necessary to consider the peak-to-peak of the recorded or computed quantities. We note that the force computed from the strain gauges does not match well the force recorded by the load cell; the peaks are on average 85 to 90% of the load cell readings. Figure 3.15 shows the first 500 seconds of Test No. 299. Again the computed force from the strain gauges exhibits drift and does not capture the force from the load cell accurately. We believe that this happened because of losses in the cables. The cables used were 120 ft. long, going from the strain gauges attached on the damper outside of the laboratory to the data acquisition system inside the laboratory. The drift in the response was not something that developed over time. Figure 3.16, which shows results of Test No. 242 (which was conducted on March 18, 2010 and was one of the earlier tests for which strain gauges had been attached on the damper, as opposed to Test No. 298 in Fig. 3.14, which was conducted on May 04, 2010), indicates that the drift and losses were present from the beginning.

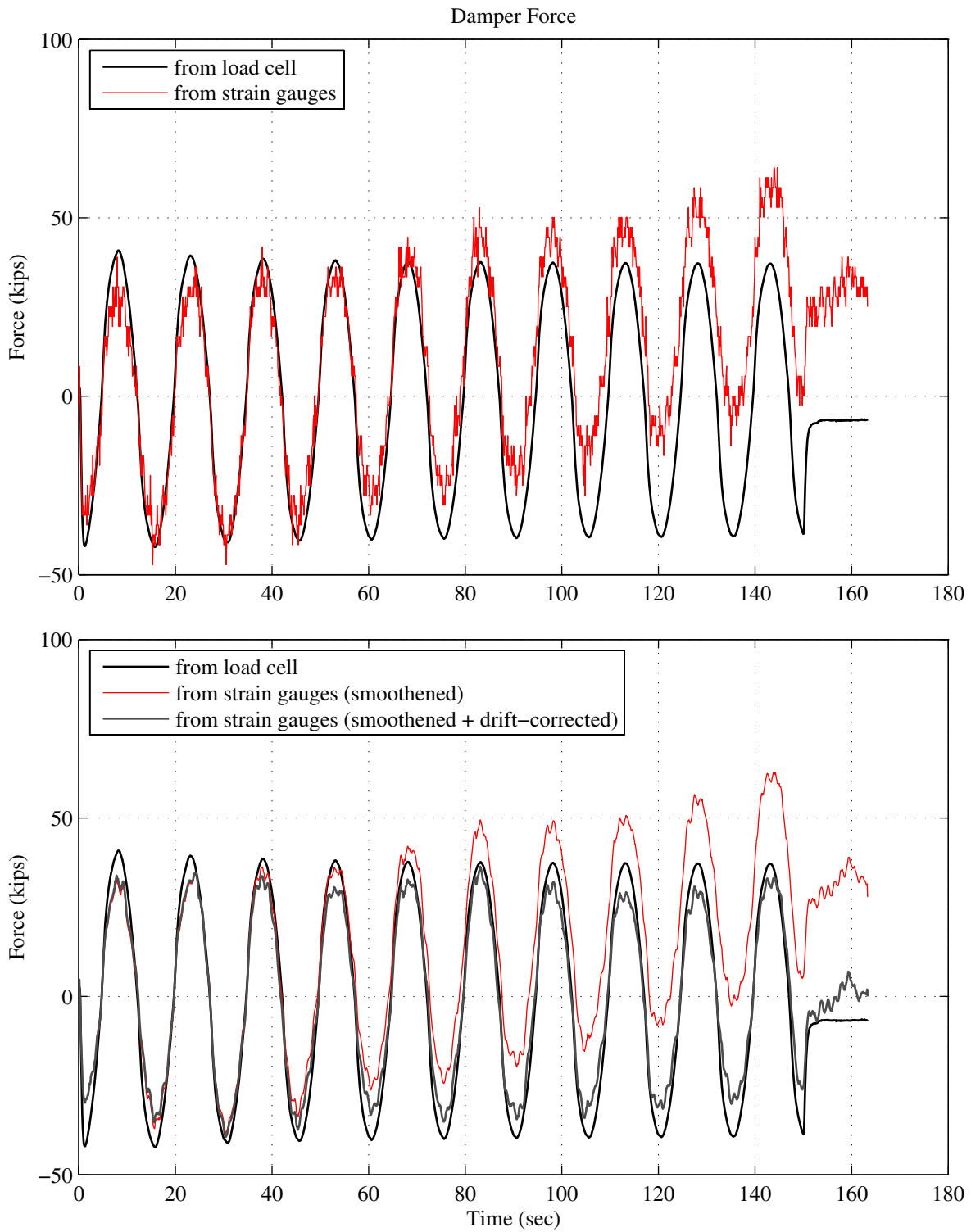


Fig. 3.14 Damper force for Test No. 298 as obtained from the load cell and as computed from the strain gauges attached on the damper extender.

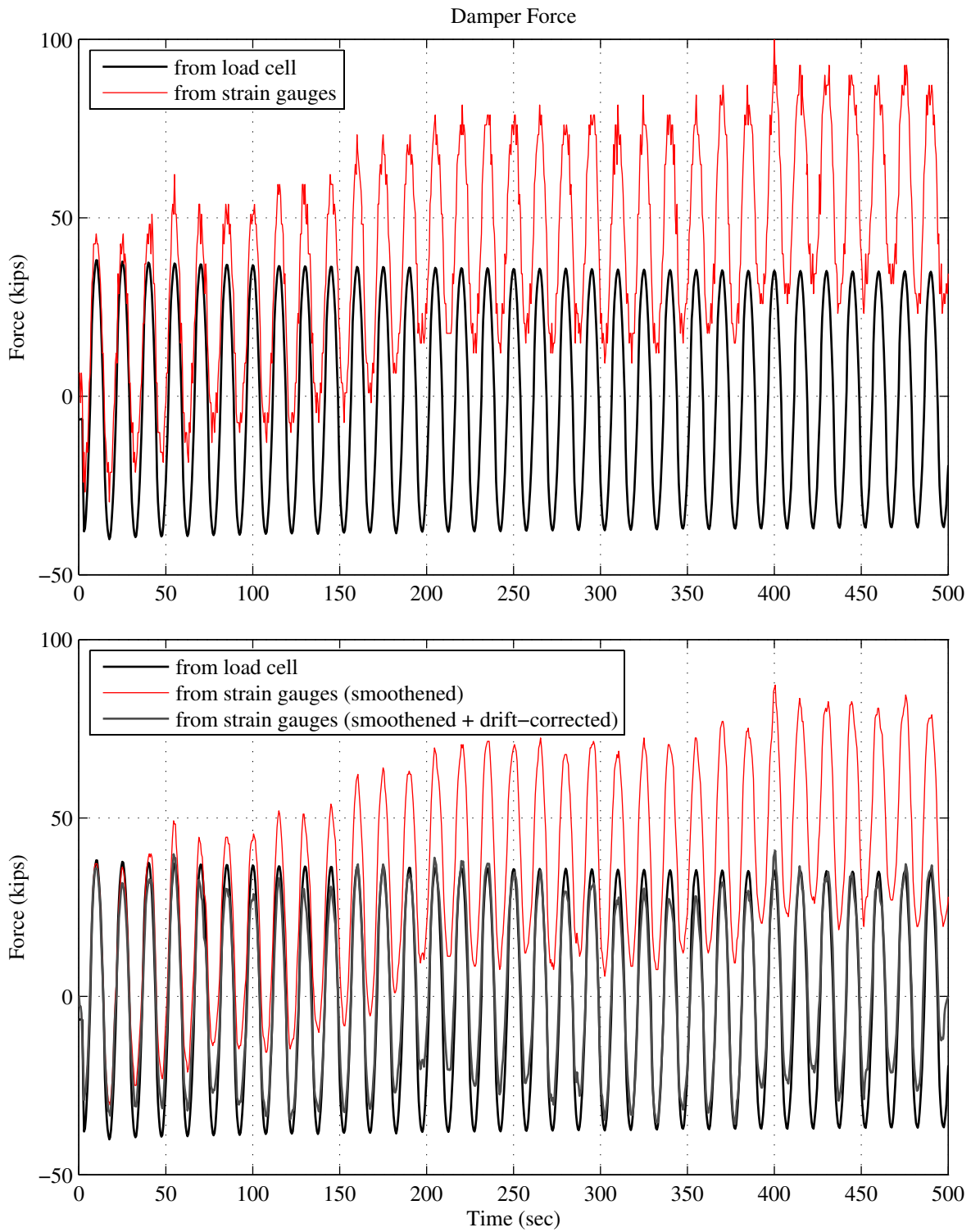


Fig. 3.15 Damper force for the first 500 seconds of Test No. 299 as obtained from the load cell and as computed from the strain gauges attached on the damper extender.

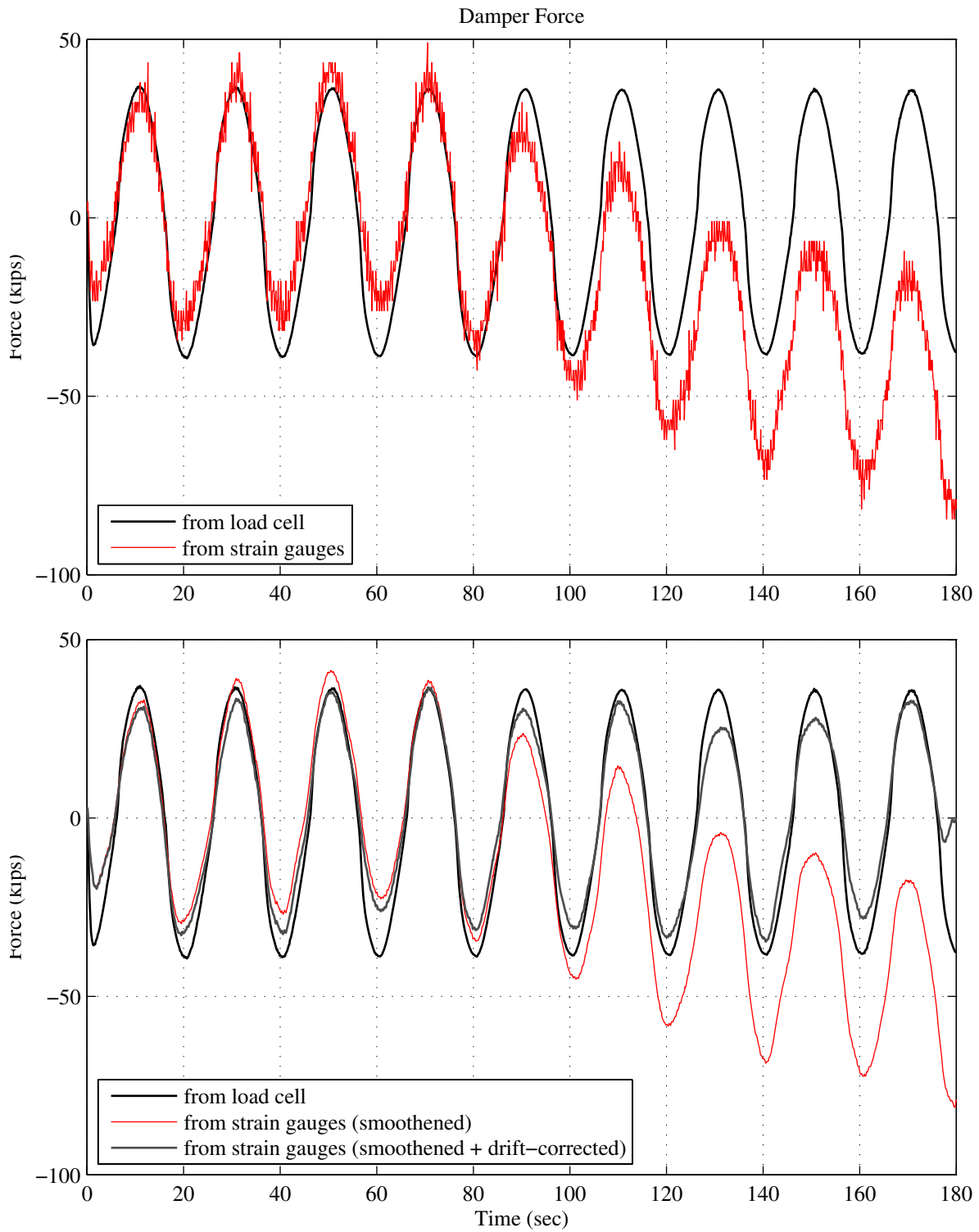


Fig. 3.16 Damper force for Test No. 242 as obtained from the load cell and as computed from the strain gauges attached on the damper extender.

More evidence that shows that the problematic behavior with the strain gauge readings did not develop over time is presented in Figs. 3.17 to 3.22. These figures show results of a test with ± 1.5 in. stroke and 15 sec period conducted in the beginning of the day on

- March 31 (Test No. 271),
- April 14 (Test No. 283),
- April 21 (Test No. 289),
- May 3 (Test No. 295),
- May 6 (Test No. 302), and
- May 10 (Test No. 306).

The graphs show that the readings from the strain gauges provide a force estimate (SG) that is consistently different from the force measured with the load cell (LC), yet the amount by which the SG force deviates from the LC force does not change over time. This is also clearly evident in Fig. 3.23, which plots only the hysteretic loops of these tests next to one another.

Figures 3.24 to 3.27 show results of a test with ± 1.5 -in. stroke and 20-sec period conducted in the beginning of the day on

- May 14 (Test No. 318),
- May 17 (Test No. 324),
- May 21 (Test No. 333),
- May 25 (Test No. 339),

Again, the deviation of the SG force from the LC force is always present, but the amount does not change, which can also be seen in Fig. 3.28, which shows only the hysteretic loops for these four tests.

In the indoor tests presented in Chapter 2, where we were able to capture the force very well using the strain gauge readings, everything was the same as the outdoor tests except for the length of the cables, which in that case were short (less than 20 ft.). Figure 3.29 shows side-by-side the results of two tests, both with ± 1.5 in. stroke and 15-sec period. Test No. 101 on the left column was conducted indoors, where short cables were used, while Test No. 271 on the right column was conducted outdoors, where long cables were used. We can see that, all other things being equal, the test where short cables were used provides a very good SG force estimate compared to the test where long cables were used. Therefore, we believe that the cause of the problem in the

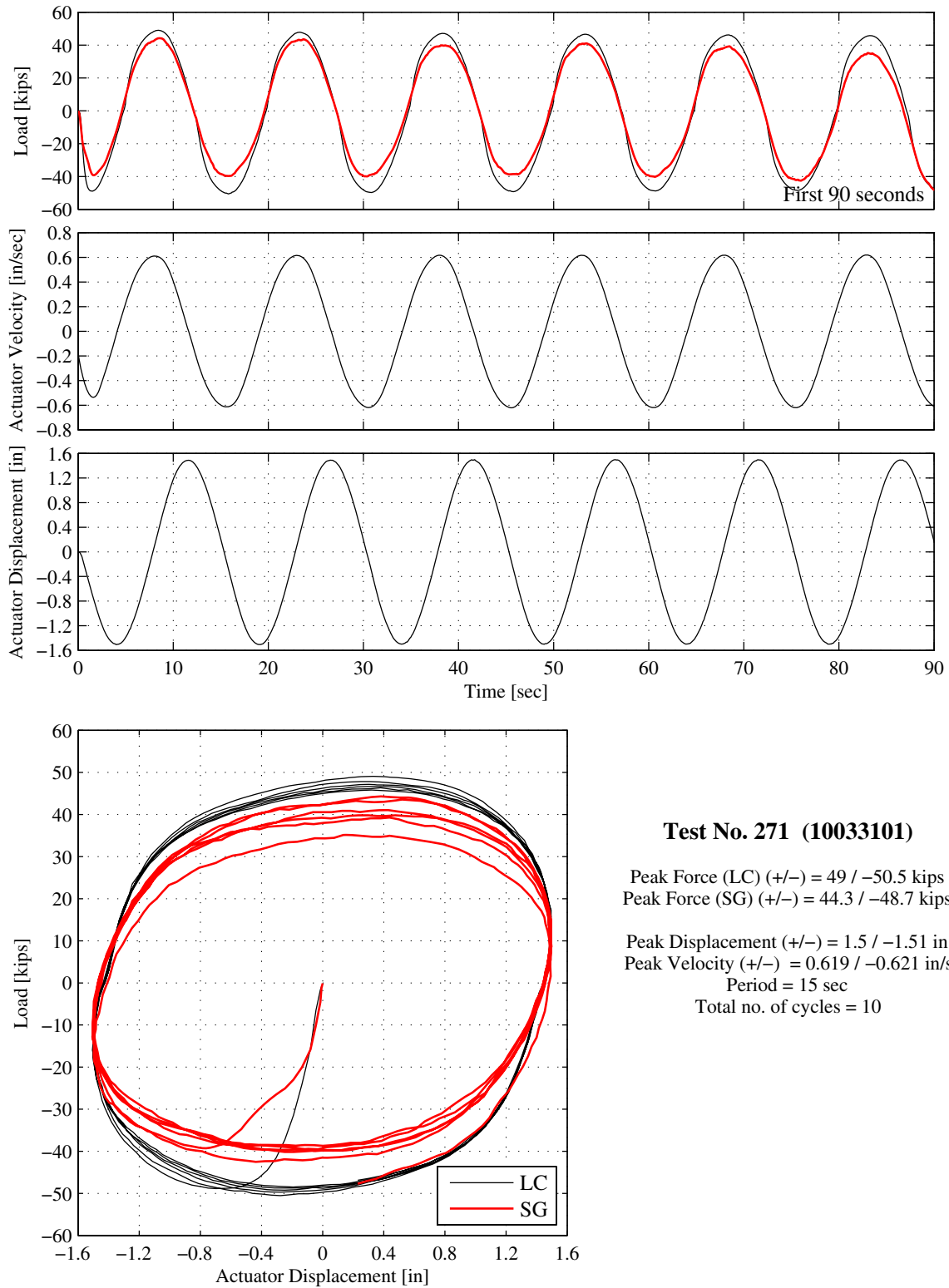


Fig. 3.17 Results of Test 271 (conducted on March 31, 2010). LC: force obtained from the load cell; SG: force computed from the strain gauges.

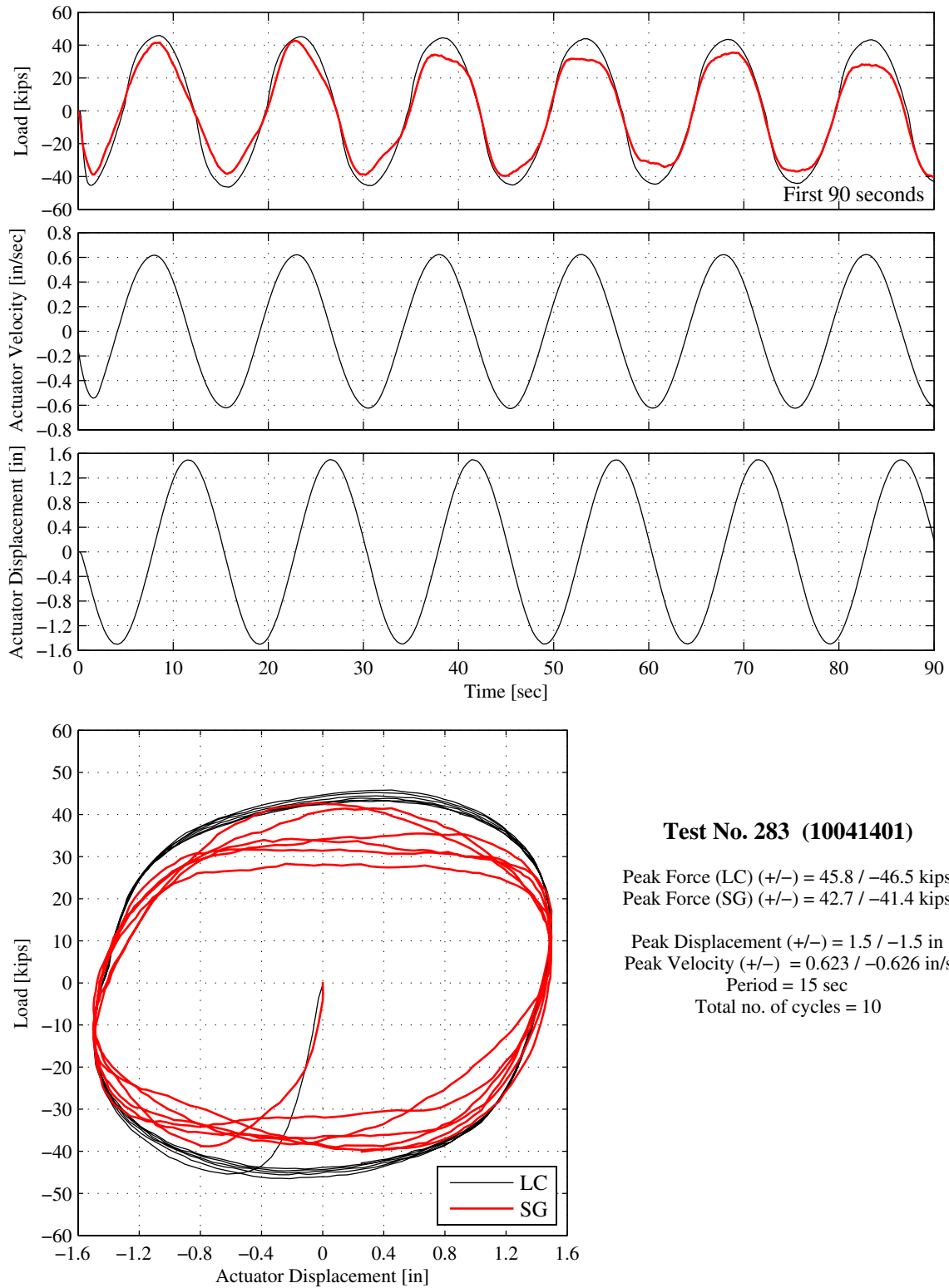


Fig. 3.18 Results of Test 283 (conducted on April 14, 2010). LC: force obtained from the load cell; SG: force computed from the strain gauges.

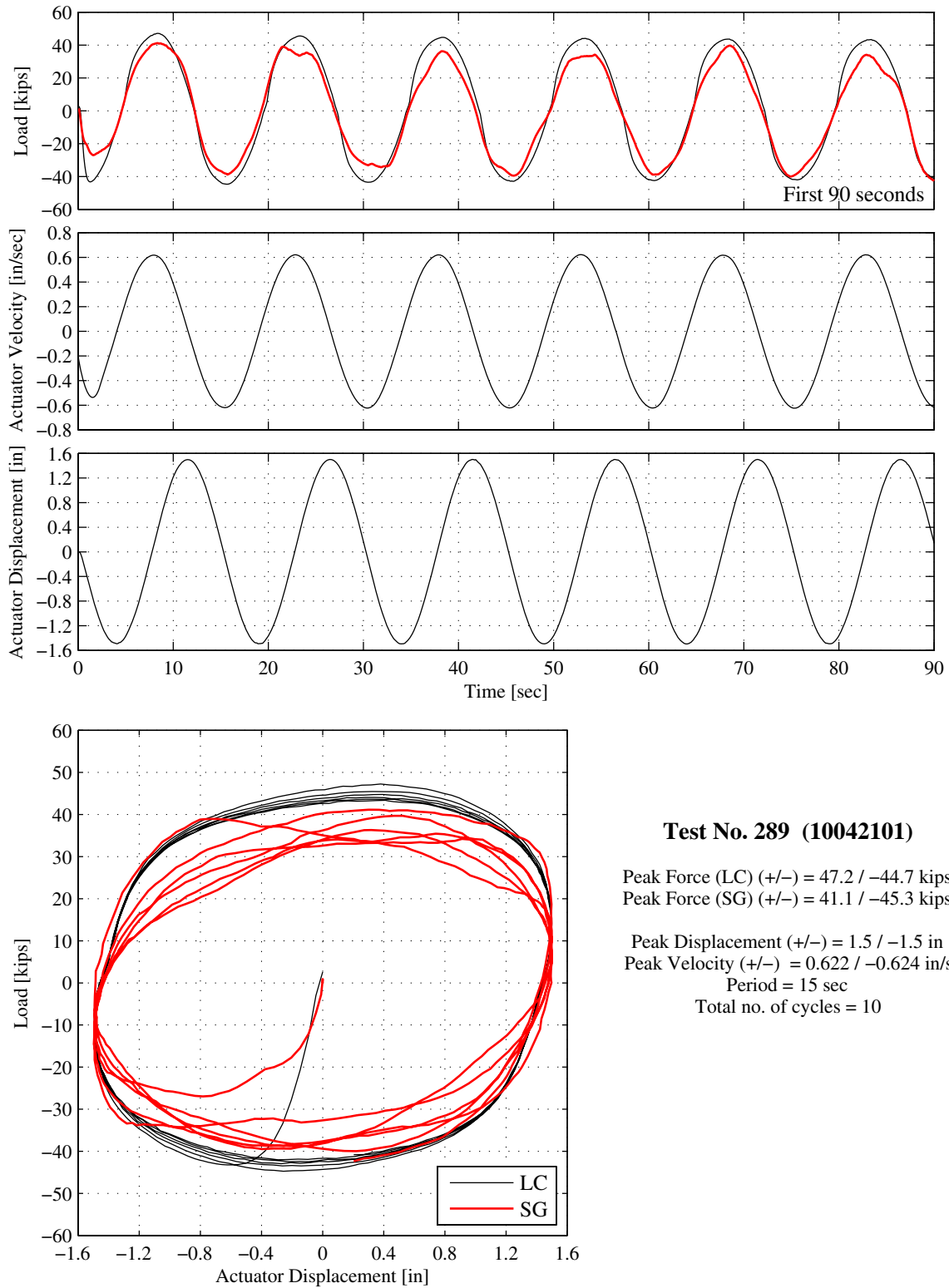


Fig. 3.19 Results of Test 289 (conducted on April 21, 2010). LC: force obtained from the load cell; SG: force computed from the strain gauges.

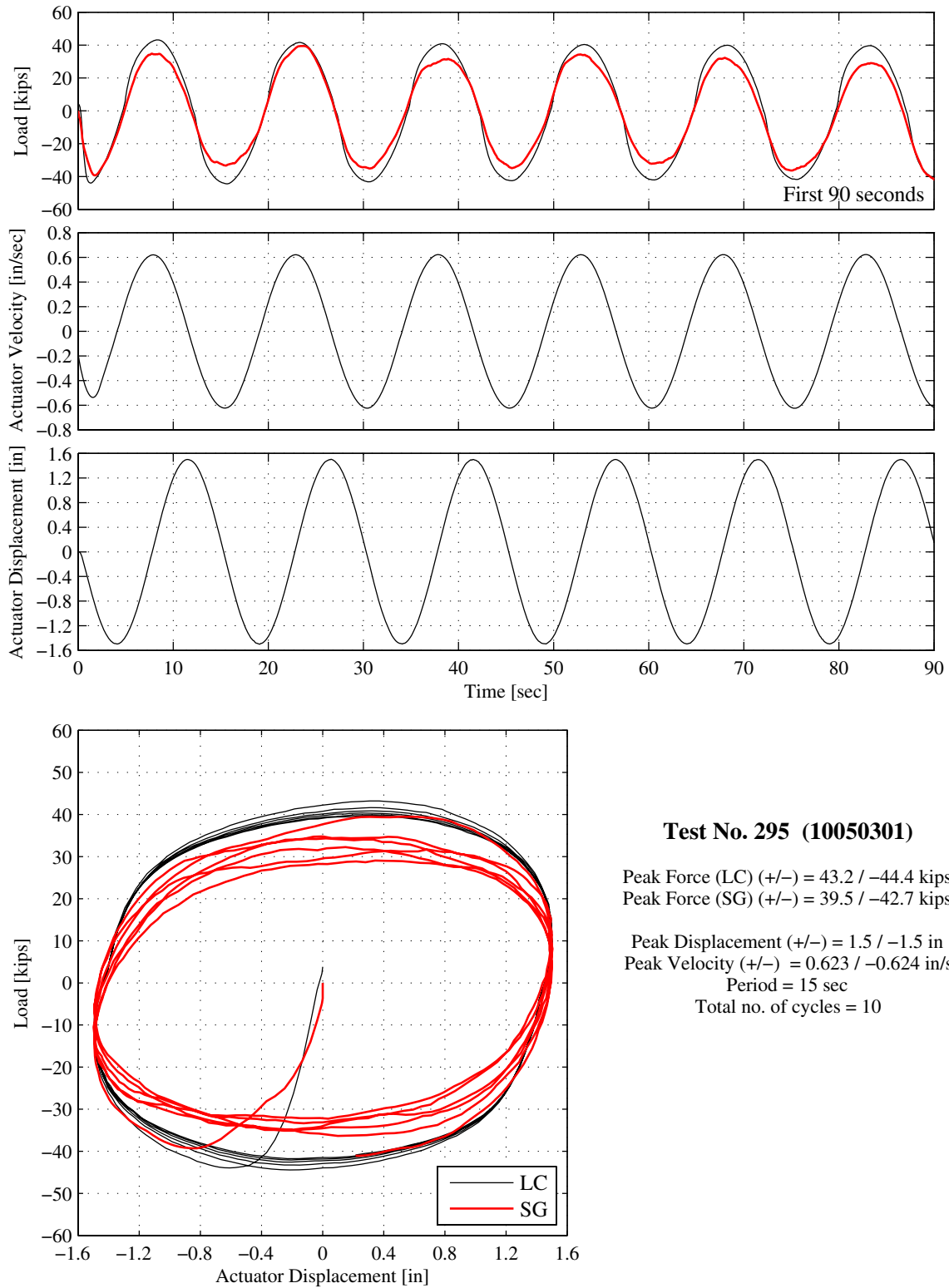


Fig. 3.20 Results of Test 295 (conducted on May 03, 2010). LC: force obtained from the load cell; SG: force computed from the strain gauges.

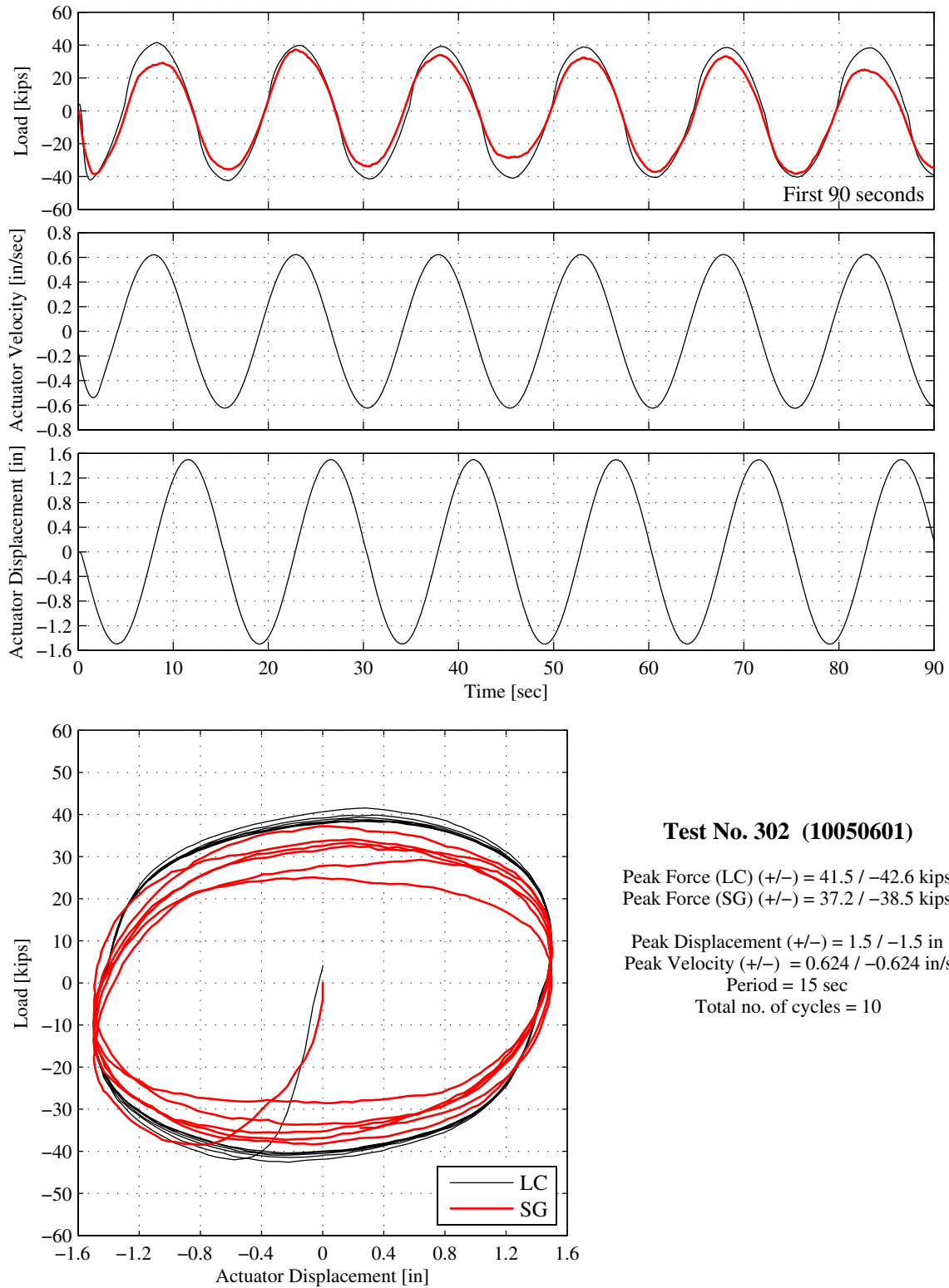


Fig. 3.21 Results of Test 302 (conducted on May 06, 2010). LC: force obtained from the load cell; SG: force computed from the strain gauges.

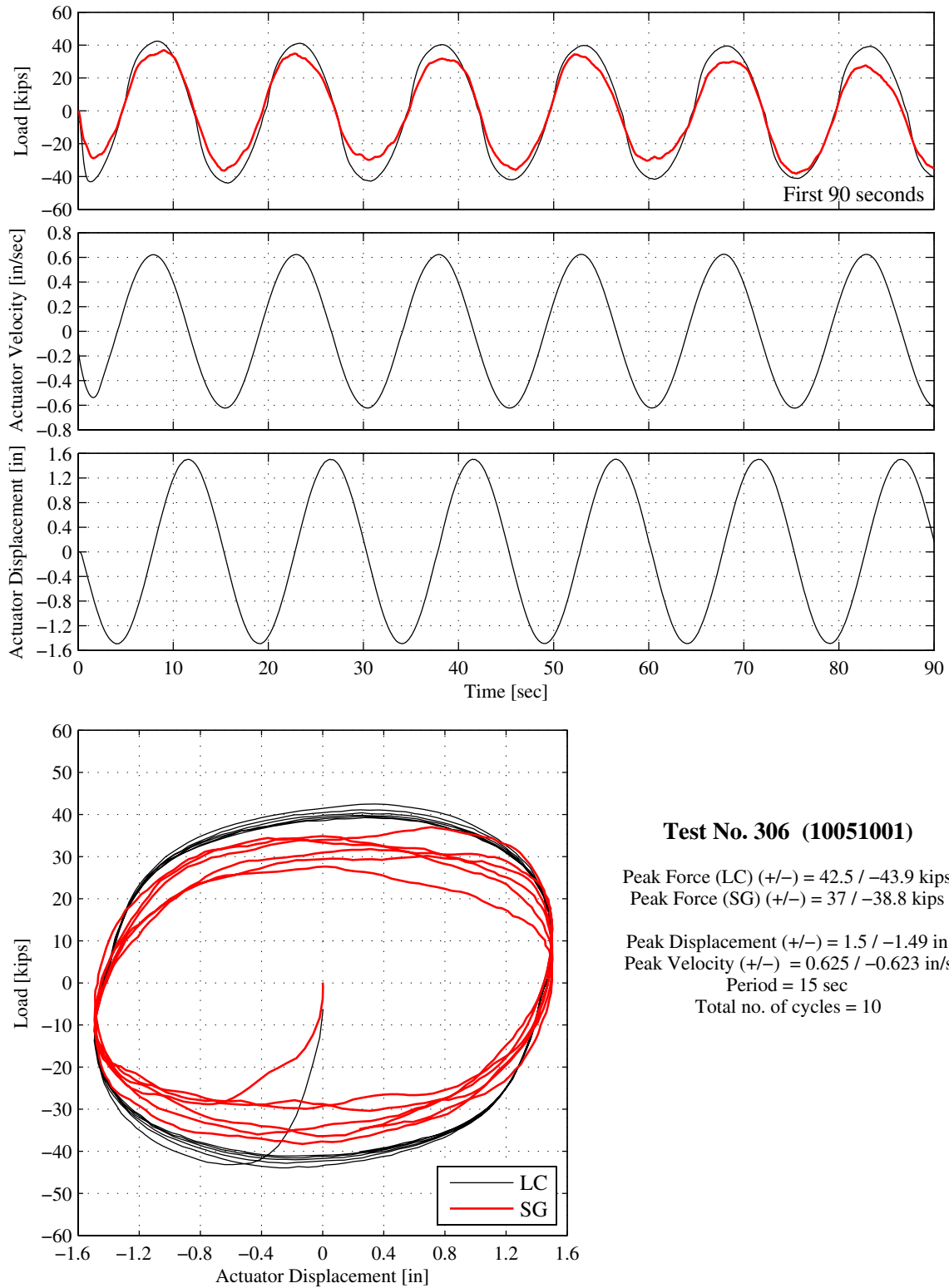


Fig. 3.22 Results of Test 306 (conducted on May 10, 2010). LC: force obtained from the load cell; SG: force computed from the strain gauges.

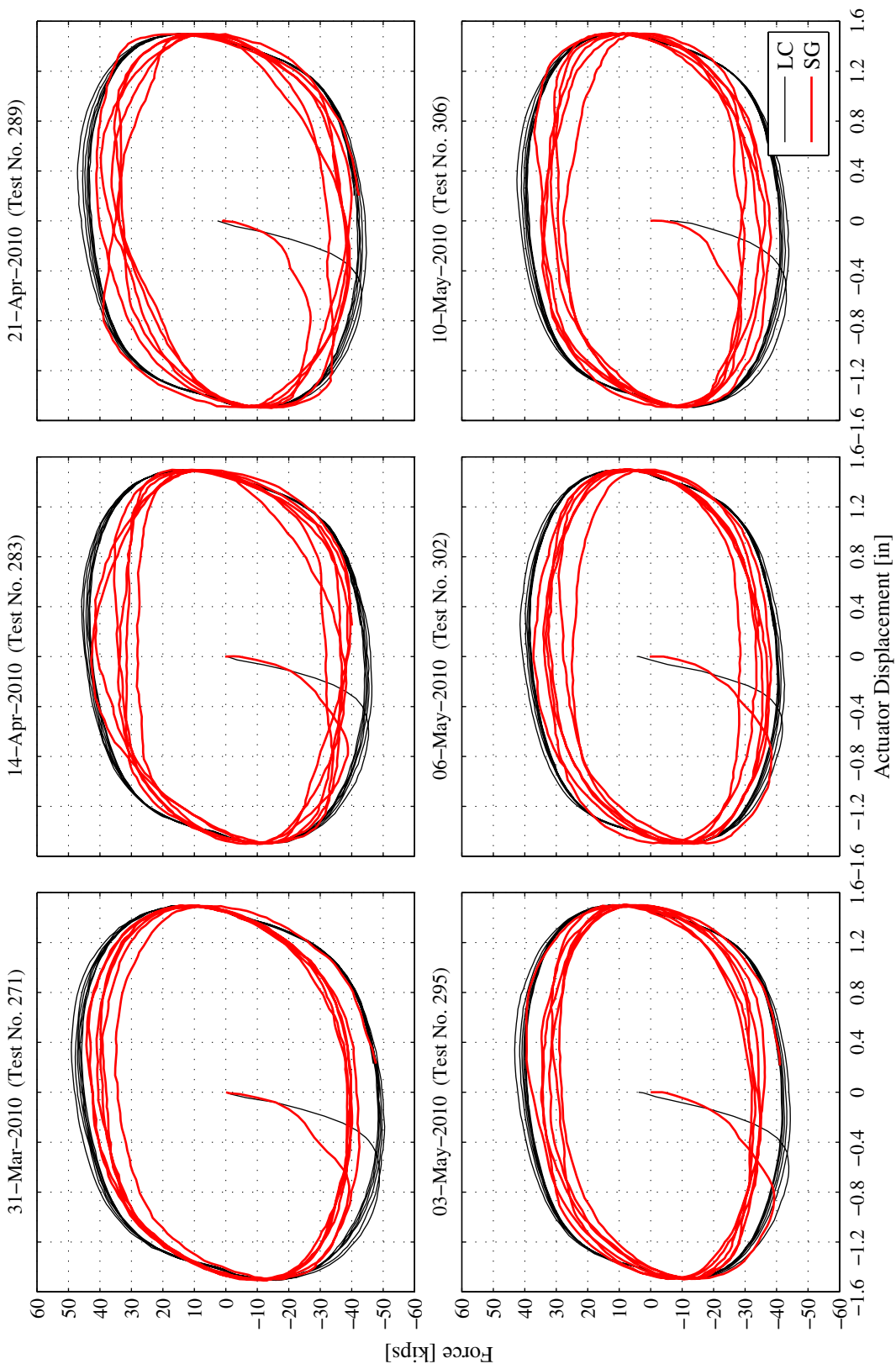


Fig. 3.23 Hystereses loops of Figs. 3.17 to 3.22.

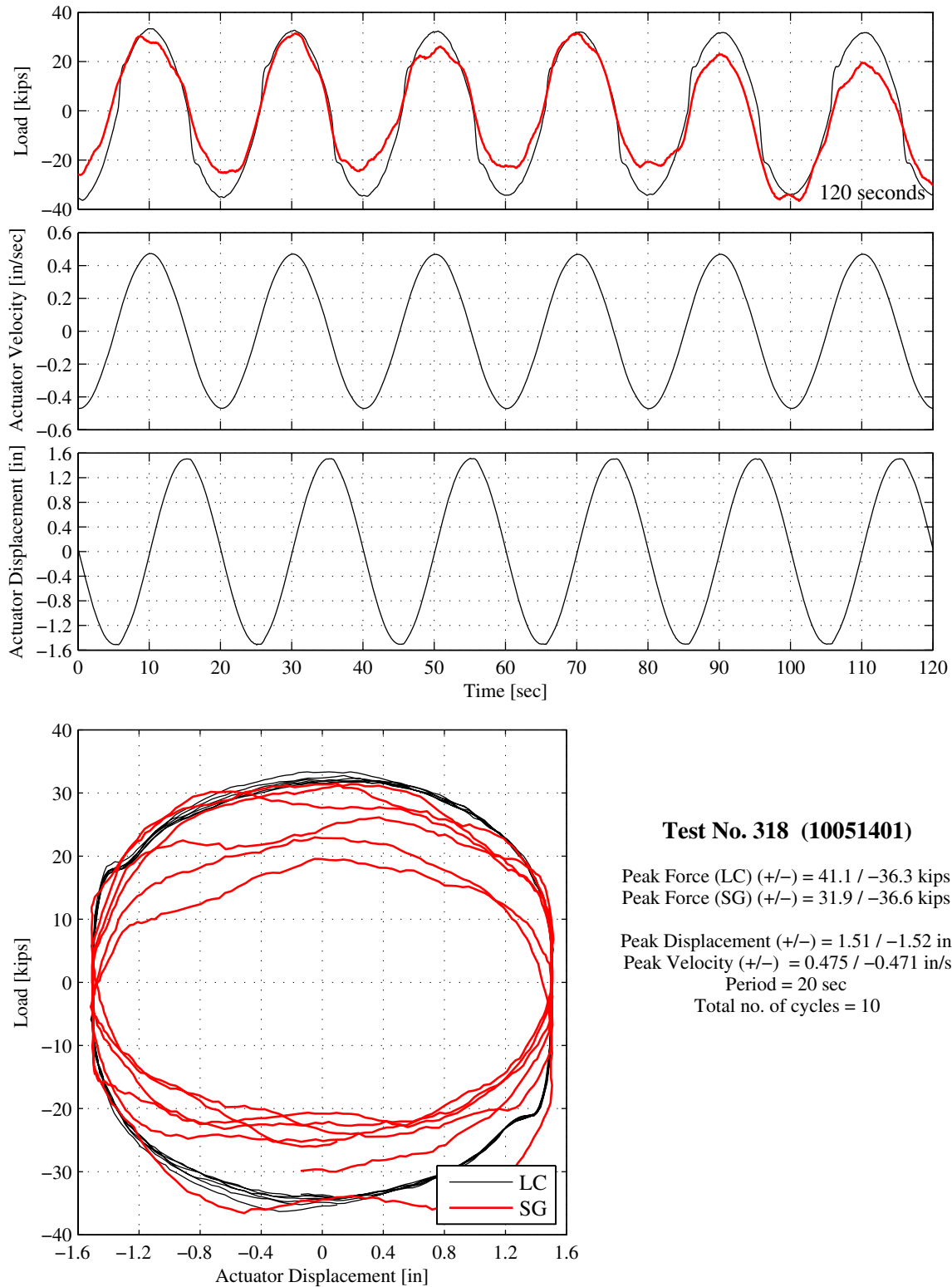


Fig. 3.24 Results of Test 318 (conducted on May 14, 2010). LC: force obtained from the load cell; SG: force computed from the strain gauges.

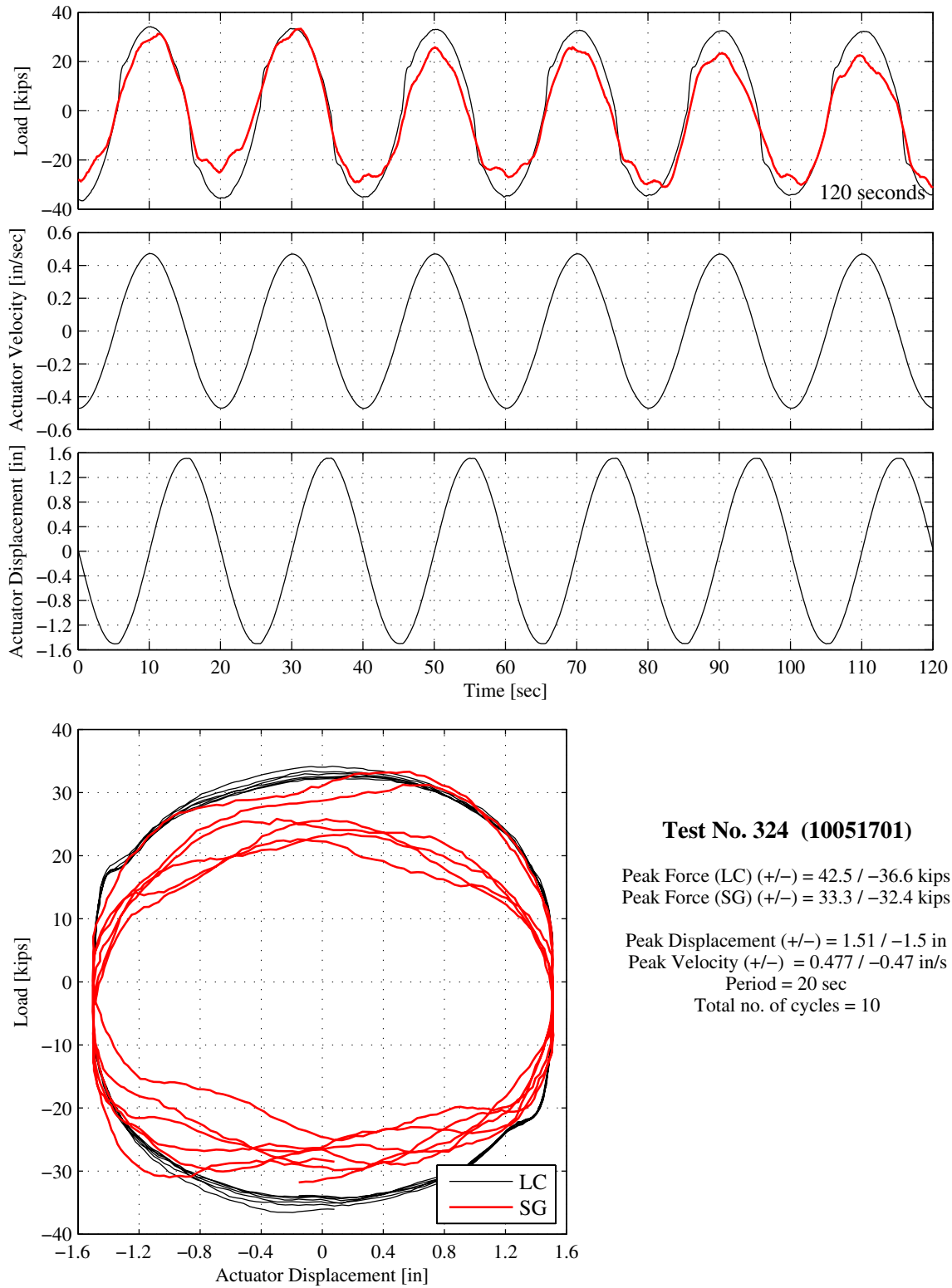


Fig. 3.25 Results of Test 324 (conducted on May 17, 2010). LC: force obtained from the load cell; SG: force computed from the strain gauges.

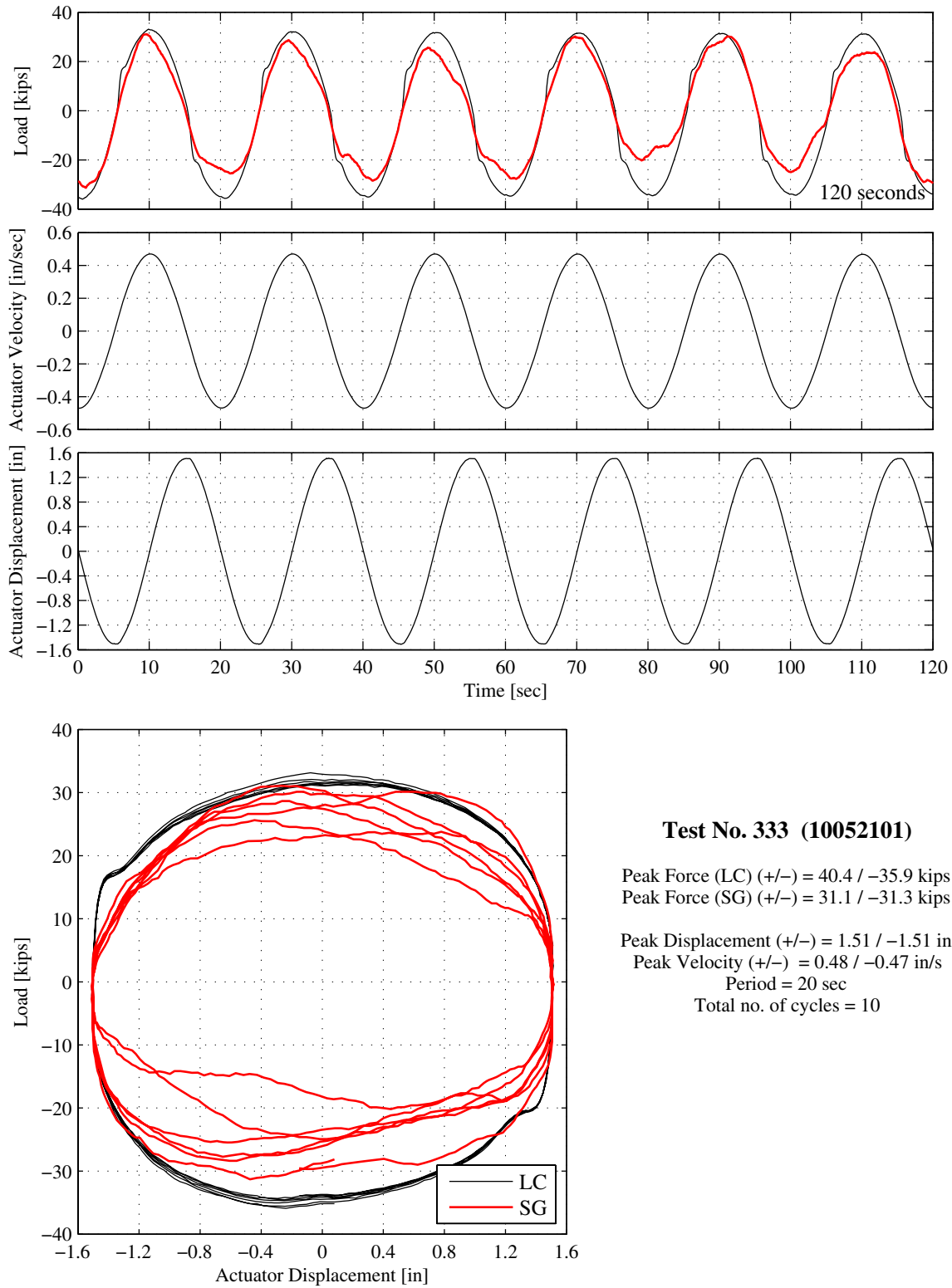


Fig. 3.26 Results of Test 333 (conducted on May 21, 2010). LC: force obtained from the load cell; SG: force computed from the strain gauges.

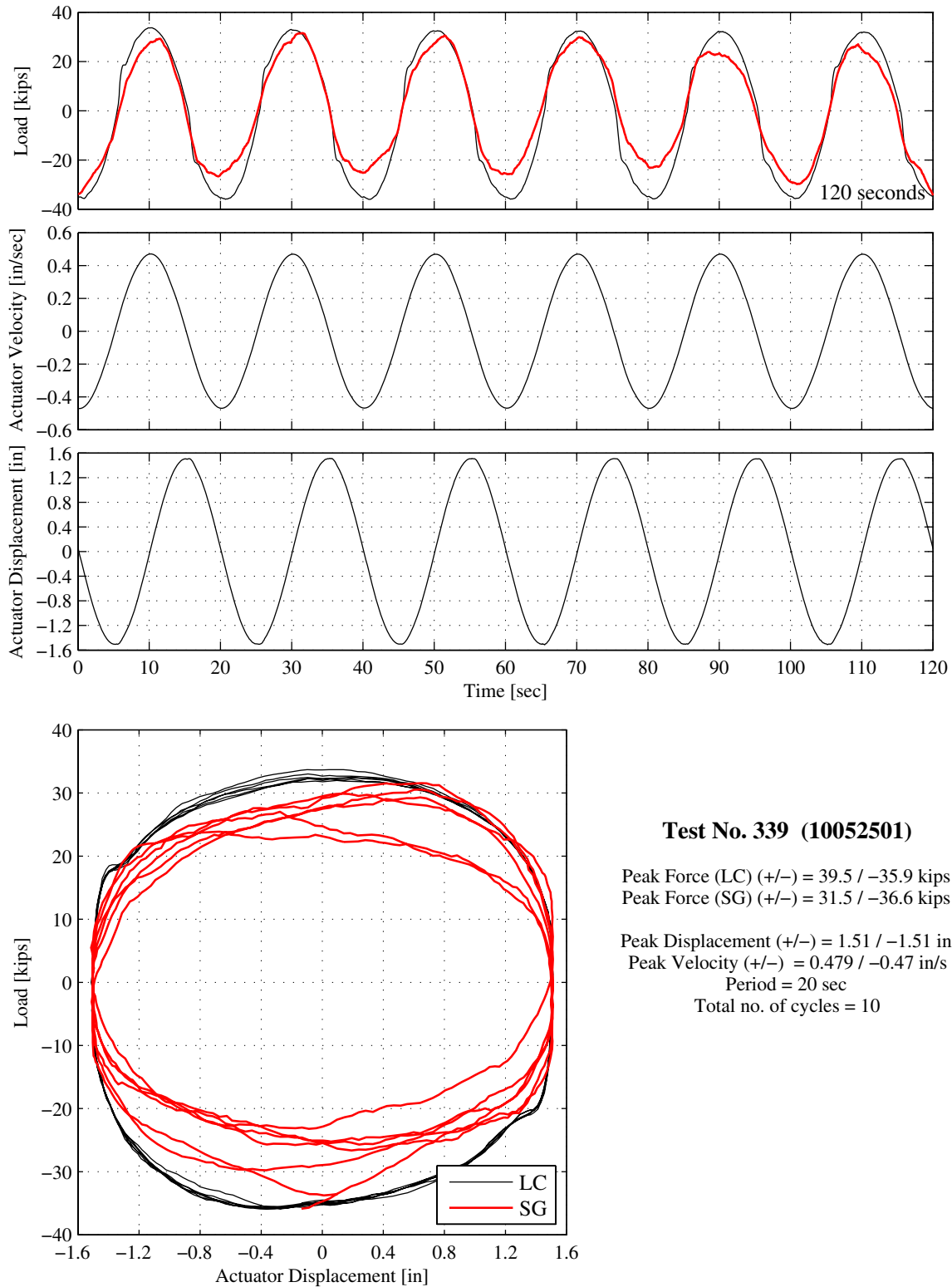


Fig. 3.27 Results of Test 339 (conducted on May 25, 2010). LC: force obtained from the load cell; SG: force computed from the strain gauges.

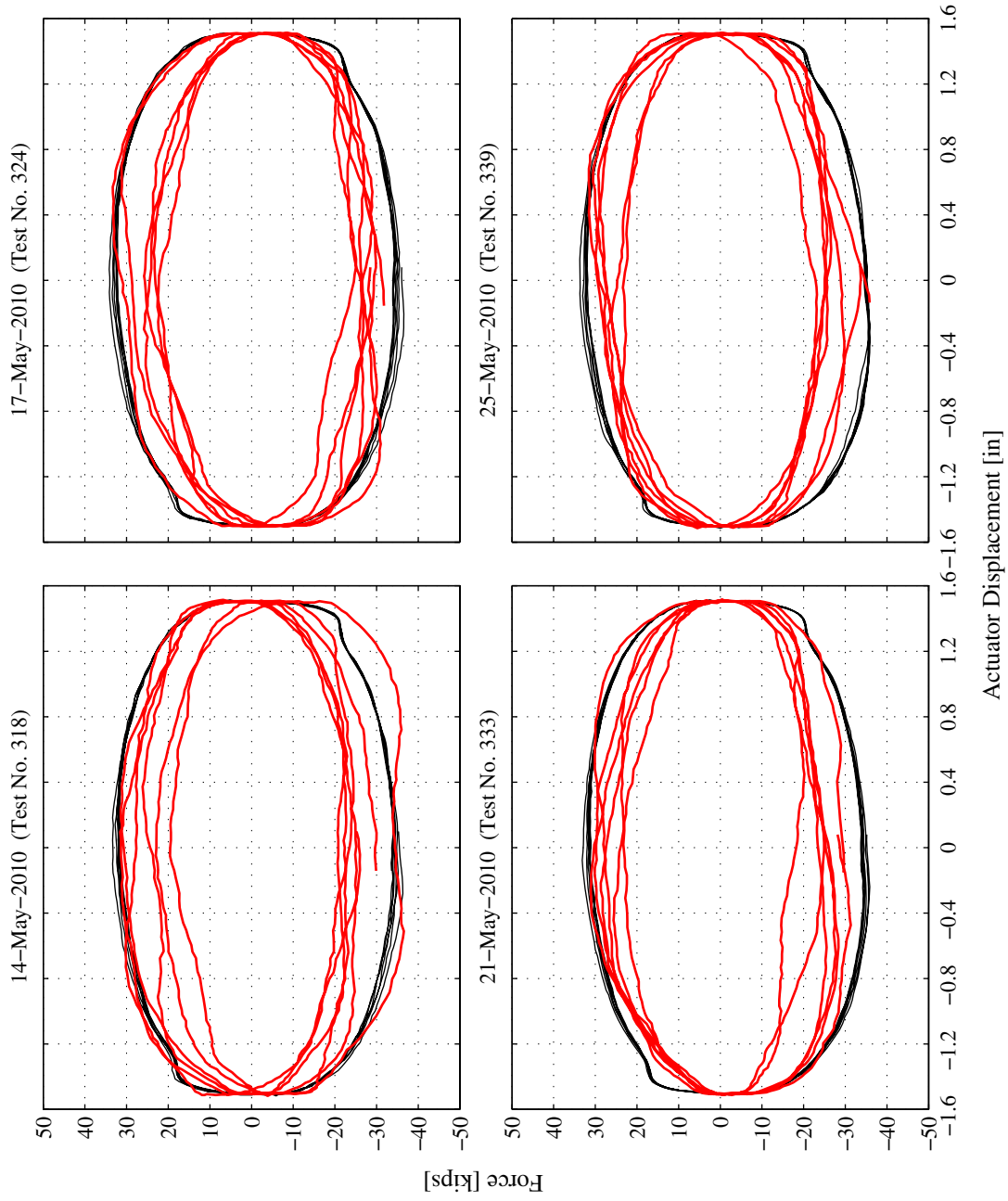


Fig. 3.28 Hystereses loops of Figs. 3.24 to 3.27.

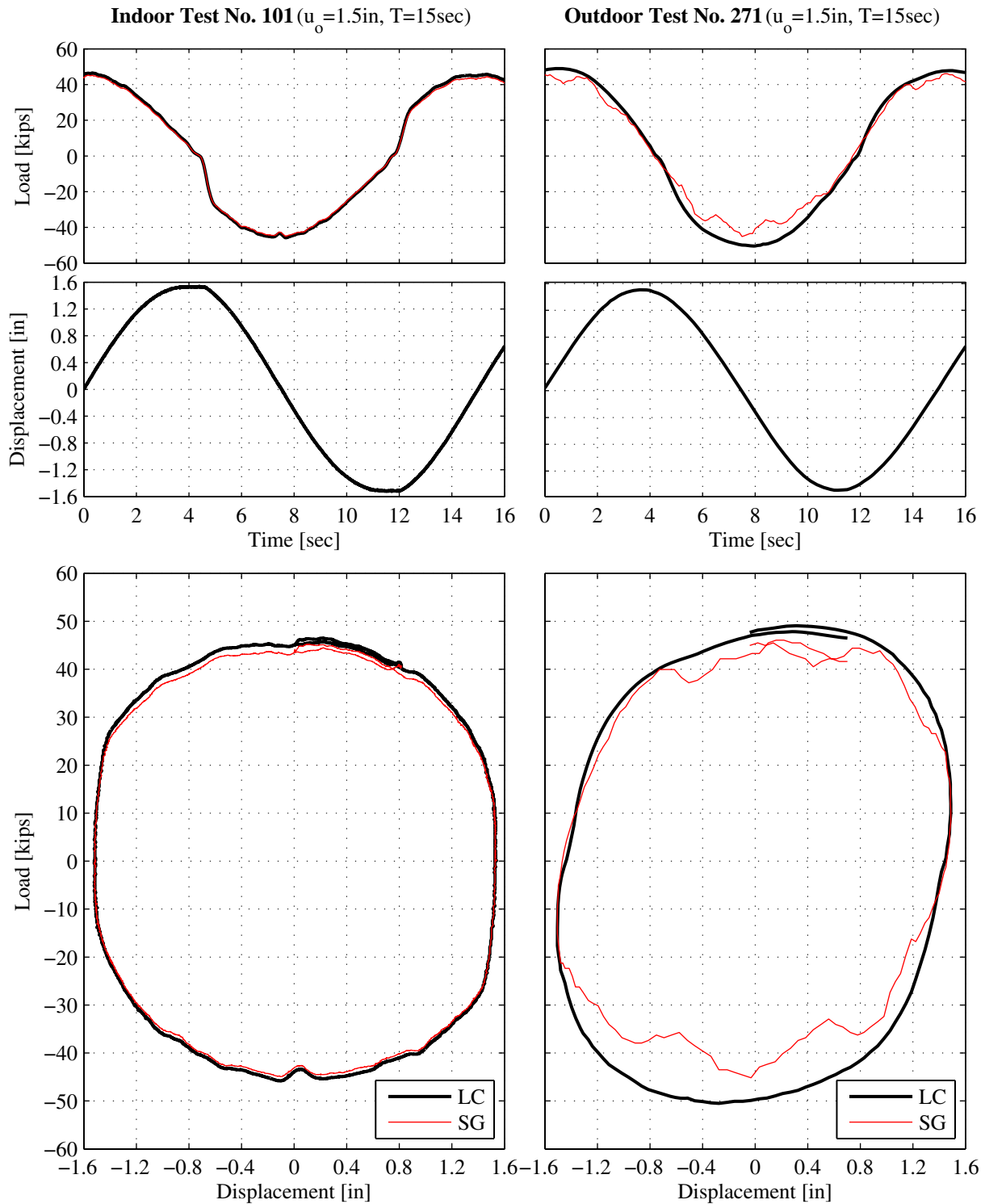


Fig. 3.29 Comparison of the results from a test with ± 1.5 in stroke and 15 sec period conducted indoors with short cables (left) and outdoors with long cables (right).

outdoor tests was losses in the cables. Thus, we recommend in a bridge application to use cables that are as short as possible. Furthermore, the cables should not be coiled up.

3.2.4 Sampling Rate

For some outdoor tests, the sampling rate for recording data was 10 Hz, while for others it was 2 Hz (see Table 3.2). Typically the first test of the day was ten cycles long, and the sampling rate was 10 Hz to ensure that the response was captured well, followed by longer tests (each up to 1600-cycles long) for which data were recorded at a lower sampling rate of 2 Hz in order to keep the data files manageable. In many cases, shorter tests with a 10 Hz sampling rate were ran in-between long tests. We found that for the cycling period of 15 to 30 seconds used in the outdoor tests in this study, the sampling rate of 2 Hz proved sufficient to capture the response adequately while at the same time maintaining small data files. Figure 3.30, for example, shows response quantities for two consecutive tests, one of which was recorded with a sampling rate of 10 Hz (Test No. 318), while the other was recorded with a sampling rate of 2 Hz (Test No. 319). Both of these tests have the same displacement amplitude of 1.5 in. and period of 20 sec. We note that in the test with the 2 Hz sampling rate, the recorded signal captures adequately the response.

The sampling rate depends on the specific monitoring application, and if the vibration period is much smaller, a higher sampling may be necessary to capture the response.

3.2.5 Force at Low Velocity

Figure 3.31 shows the peak force as a function of peak velocity from the first test of each day of outdoor tests on the 450-kip damper. The graph shows the experimental data (positive and negative peak force) and a least-squares power-law fit, shown with a heavy grey line and given by

$$\hat{P} = 56.06v_0^{0.3215}, \quad 0.1 < v_0 < 0.7 \quad (3.1)$$

where v_0 is in in/sec and \hat{P} is in kips. Together with these data and fit is shown the “target” value (provided by the manufacturer) characterize the behavior at seismic design velocities. As described in the previous chapter, if the input signal is $u(t) = u_0 \sin(2\pi ft)$, then the velocity amplitude is $v_0 = 2\pi fu_0$, and the target peak force for the particular damper is

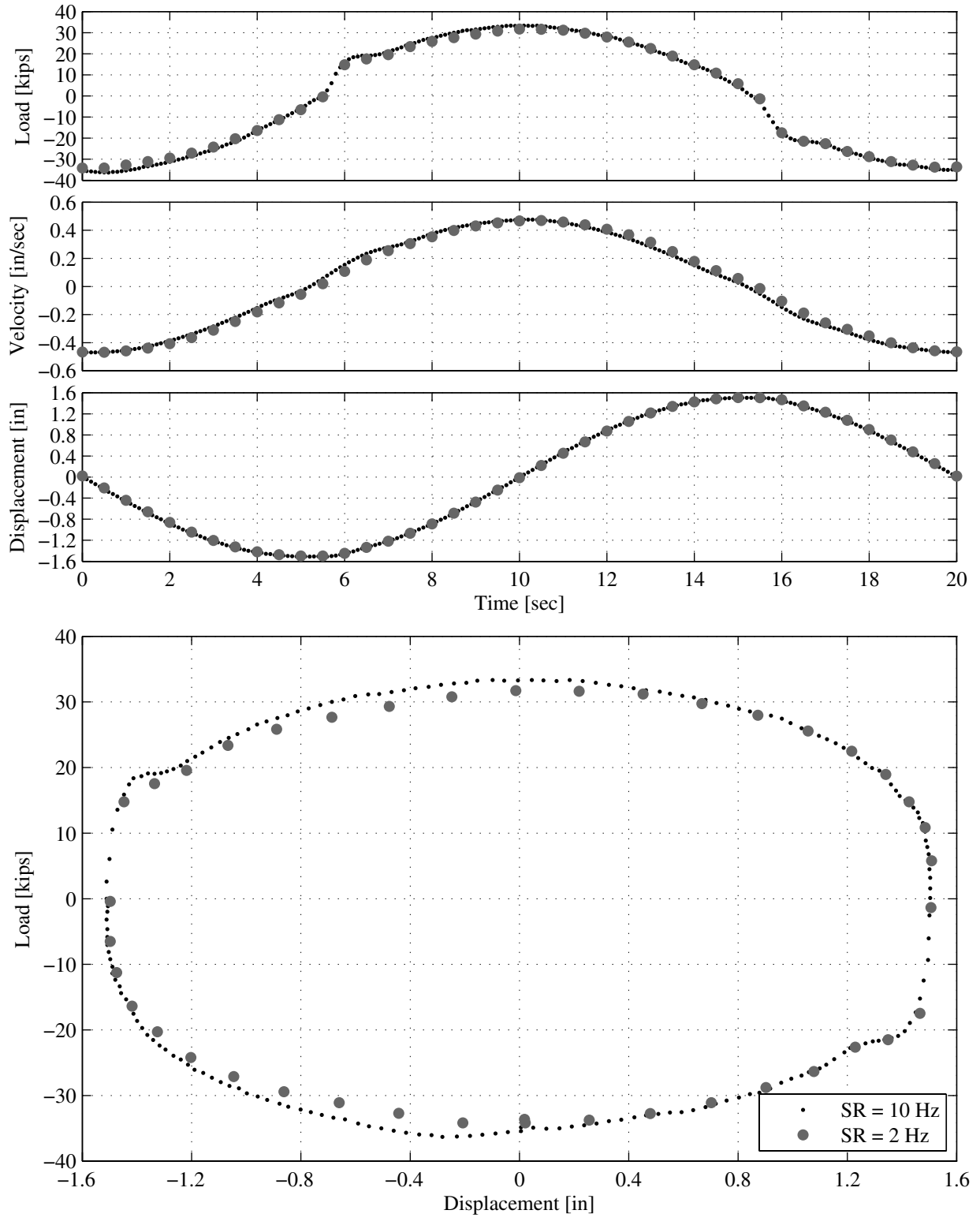


Fig. 3.30 Response quantities for Test No. 318 recorded with a sampling rate of 10 Hz and for Test No. 319 recorded with a sampling rate of 2 Hz.

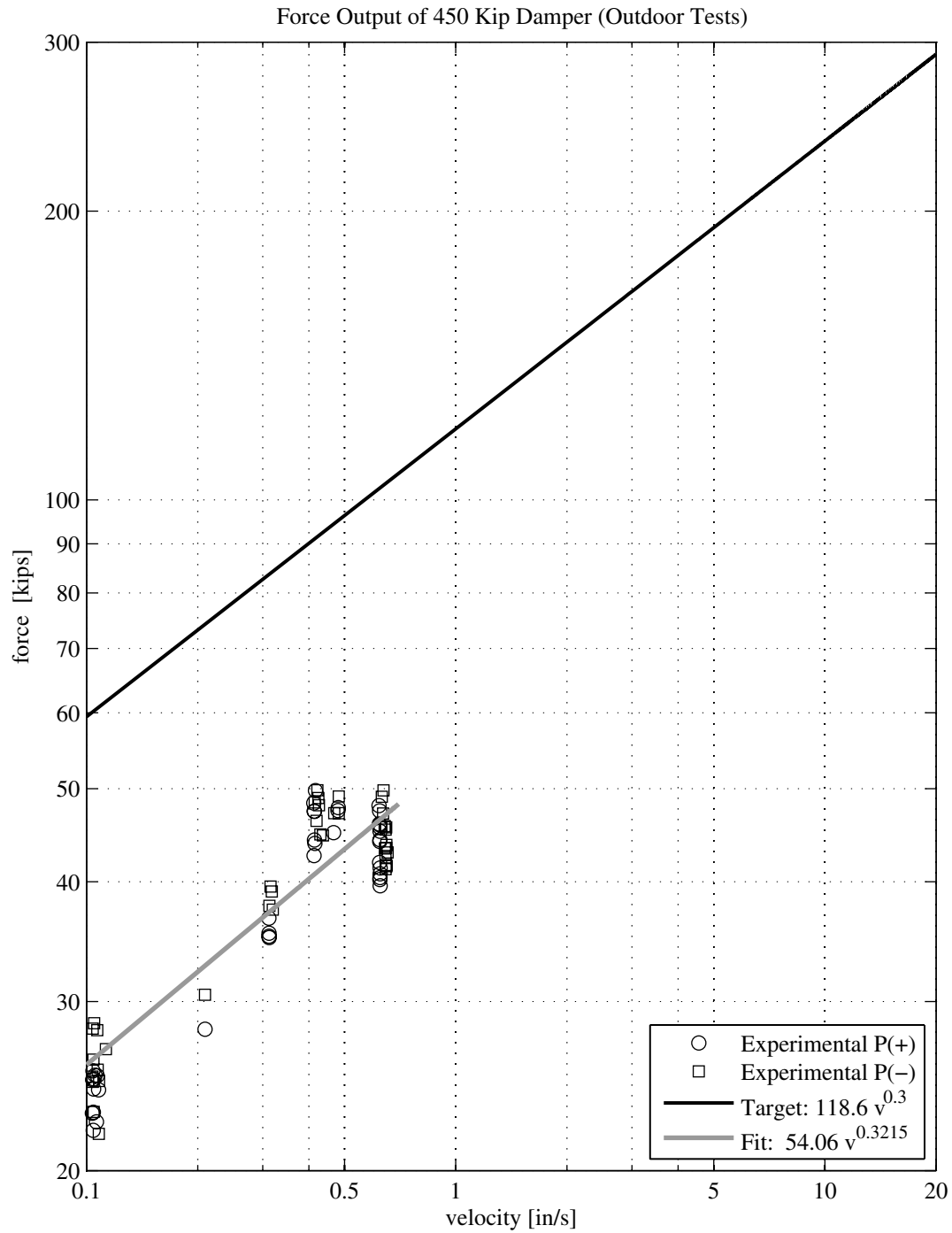


Fig. 3.31 Velocity-dependence of damper force output at low velocities. The bold black line shows the force of the manufacturer’s specification at design velocity, while the heavy grey line shows a fit of the experimental data in the 0.1–0.7 in/s velocity range.

$\bar{P} = 118.6 \text{ kips (sec / in)}^{0.3} v_0^{0.3}$, which is shown in Fig. 3.31 with a heavy black line. We note that in the low-velocity range the actual behavior of the damper is dramatically different than the specification provided by the manufacturer for the design velocity range. This confirms the finding in the previous chapter that the formula for force output of a fluid damper in the service-level velocity range is different than that in the seismic-design velocity range, and therefore it is necessary to conduct tests at low velocities in order to characterize the behavior.

3.3 CONCLUSIONS

The implications of the test results for the use of this technology to monitor the performance of in-situ dampers on a bridge are several and are outlined below:

- Weldable strain gages are easy to install and can be protected from environmental hazards produced by severe weather, salt-laden atmosphere, and corrosive liquids such as fuel oil.
- The preferable location of the strain gages on the damper is on the extender element, which experiences the full cycle of tension and compression. It is recommended to install strain gauges in the middle of the extender piece to avoid end effects. Although it is theoretically possible to measure the force using a single longitudinal strain gauge, it is highly recommended to install two strain-gauge rosettes (e.g., one on the top and one on the side of the damper) to provide redundancy but also to be able to capture any undesired shears and moments that may develop in the damper.
- The dampers are installed with an internal pressure of 3000 psi, which is set at the factory. If the pressure is lost the change in the hoop strain can be detected by strain gages in the circumferential direction on the barrel of the damper. This was verified only by calculation as it was not possible to depressurize any one of the four dampers in the laboratory. The question of the nature of the force output of a damper with zero internal pressure is thus unresolved. Specialized equipment from the manufacturer of the damper is needed to safely release the pressure.
- It will be essential before installing a monitoring system on one or more dampers on a bridge to have an estimate of the service-level input that the particular damper will experience. It will be necessary to estimate the damper displacement, velocity (or frequency), and any daily or seasonal variation in these quantities.

- The tests have shown that the service-level response of a damper must be modelled differently from the specified seismic response. The test results (Chapter 2) have shown that although the response to seismic-level input accurately conformed to the target formula, at low-level input the response cannot be predicted by the same formula. This means that in addition to production tests to demonstrate conformance with seismic specifications, it will be necessary to test all dampers to be monitored at a range of low-level input as identified under the previous section.
- In the low-level tests of the outside damper it was fitted with three thermocouples at three locations on the barrel. In many tests there was an unexpected degree of temperature increase. It will be essential in the implementation of this technology for in-situ monitoring to include one or more thermocouples on the monitored damper. They proved to be very stable unaffected by weather including heavy winter rain. The importance of monitoring the temperature rise is especially evident for bridges such as suspension bridges that are sensitive to wind. The response of the damper is affected by self-induced heating more than by ambient temperature or by wear.
- The tests were usually run continuously for approximately ten hours a day for a period of four months for a cumulative wear of 5.5 miles. To attempt to separate temperature effects from wear effects, the first three cycles of the first test each day was reviewed separately. The results of these daily first tests indicated that wear may not be a significant issue in the response of the damper provided the damper does not leak.
- The strain gage signals transmitted are noisy and without processing do not allow us to capture the damper forces well. It will be necessary to use a simple filtering algorithm to clean up the signals before computing the damper forces.
- In many cases the recorded strain values exhibited a drift, which we think is caused by the length of the cables from the strain gages to the data acquisition system (DAS), necessary in our test setup since the damper was outside and the DAS inside the laboratory. Our recommendation is to use good shielded cables of the shortest possible length and kept from touching one another.
- The drift in the zero of the gages will not be a problem in the field since it will not be possible to set a zero position under the random motion of the damper due to service-level input. The

assessment of the performance will be based on the peak-to-peak measurement of any particular strain or displacement measurement.

3.4 RESEARCH IDEAS ARISING FROM PROJECT

3.4.1 Prediction of Damper Temperature Rise during Wind Storms.

Dampers designed specifically for seismic loading generally have exponents in the range of 0.3 to 0.4, as is the case of the current San Francisco–Oakland Bay Bridge dampers. When subjected to strong seismic input, the dampers experience a great deal of energy dissipation and a consequent rate of temperature rise. The increasing temperature is not expected to compromise the damper performance as the duration of strong motion is short, and this will limit the total increase in temperature.

However, a damper with an exponent in the above range will still dissipate a great deal of energy at a lower velocity. For example, if the exponent is $1/3$ and the velocity is reduced by a factor of 27, the force is only reduced by a factor of three. This means that a long duration wind storm could be a more critical event for the damper than a seismic event since the wind storm could be several hours in duration, as opposed to a minute at most in a seismic event.

To determine the behavior of a damper under external loading by wind cannot be done by scale model tests, as the thermal response to power input does not scale. The test will have to be done at full-scale. It will be straightforward with the existing damper test facility to subject the full-size Bay Bridge damper to a simulated wind storm motion and to estimate the wear on the seals and to measure directly the temperature increase during a large storm to verify or not if a steady state temperature can be achieved or if the damper can be damaged and rendered unusable by a storm.

A research program to address this issue would include the formulation of a peak storm size and duration during the possible lifetime of specific dampers on the bridge.

3.4.2 Health Monitoring of In-Situ Bay-Bridge Dampers

The current test program at the PEER laboratory has shown that it is possible using welded strain

gages to obtain good strain-gage output data on full-size dampers under ambient (i.e., traffic-induced) vibrations. Testing both within the laboratory and outside, in a variety of weather conditions, including severe rain storms, has shown that the gages can be protected against severe environmental situations and continue to function properly. Not yet demonstrated, but highly likely on the basis of computations, is the additional test possibility that loss of internal pressure can be detected by hoop strain gages on the barrel of the damper.

Using this technology, it will be possible to monitor in real time the state of any or all of the dampers on the bridge and provide indications to maintenance crews to changes in the response of the selected dampers with a view to assessing whether the dampers need to be inspected or even removed for further testing to verify if they should be replaced.

4 Wireless System for Monitoring of Dampers

An in-house system that utilizes a commercially available portable data acquisition system manufactured by Opto 22 (Fig. 4.1) with very flexible capability has been chosen to collect and transmit data. The Opto 22 system can transmit data both wirelessly and with wired connections. The device is highly scalable to accommodate a number of channels with a variety of different sensor types. There is large flexibility on sampling rates and the device can be equipped with a buffer memory that will save data before an event is triggered. For example, if the trigger is a velocity threshold, once the velocity threshold is reached the device starts recording data from that point on but also appends data from a specified duration before the threshold was exceeded, the backwards duration being controlled by the size of the buffer memory.

The system shown in Fig. 4.1 consists of a integrated board with several slots for data channel modules. The one shown on the photograph presently features six channels: one for a position sensor, one for a velocity sensor, and four for strain gauges. The central processing unit Opto 22 SNAP PAC R1-W has a 10/100 Mbps wired Ethernet network interface and a wireless LAN interface (802.11a, b, and g network standards) to transmit/receive data to/from a remote computer. The SNAP PAC can be used wirelessly, on a wired network, or both at once. This rack-mounted programmable automation controller provides control, communication, and I/O processing in a compact package. The SNAP-PAC-R1-W is fully integrated with PAC Project software, SNAP PAC brains, and SNAP I/O modules made by Opto 22. Used with the PAC Project Basic software suite (included with the SNAP PAC controller unit) or PAC Project Professional (purchased separately), the Ethernet-based SNAP-PAC-R1-W can handle a very wide variety of remote monitoring, data acquisition, and even control applications. Other options are also available, including the capability to attach an external powerful wi-fi antenna with range up to three or more miles. More data channels can be easily accommodated on the same board or an expansion board. Two high-end power supplies are included to power the different components of the

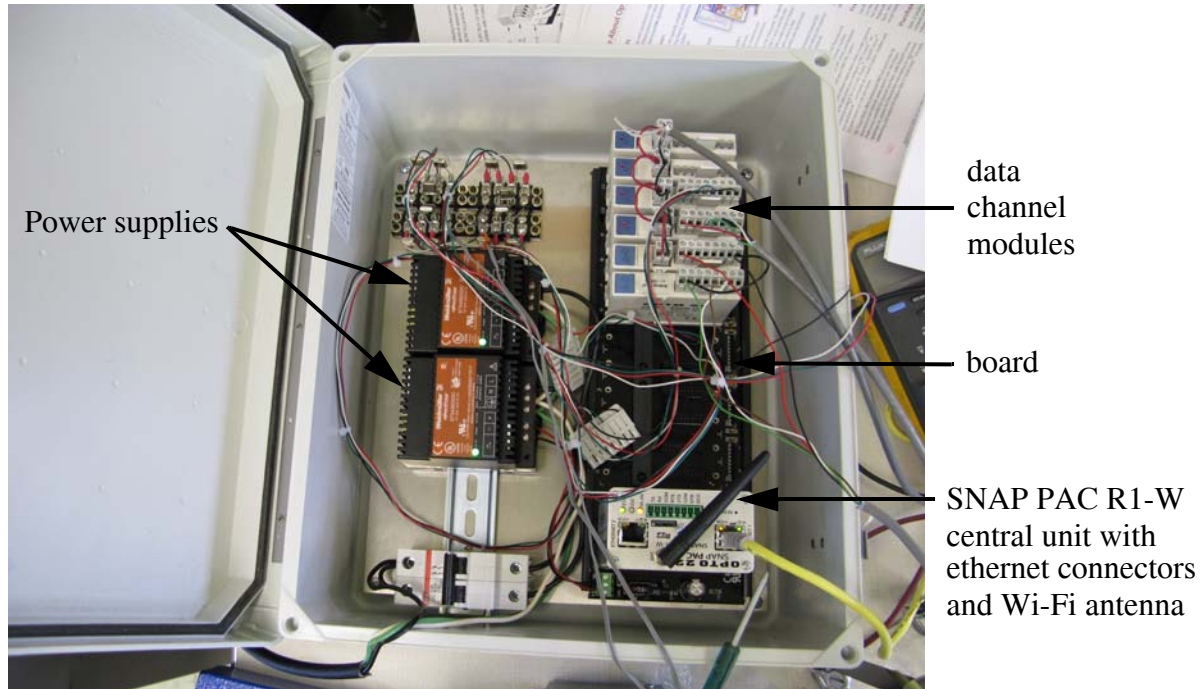


Fig. 4.1 Opto22 system featuring board with central unit with wireless antenna, six channel modules (one displacement, one velocity, and four strain gauge) and two power supplies. The system is protected by a hermetically sealed plastic enclosure box.

system. The components of the system are contained within a heavy-duty plastic, hermetically sealed enclosure box, as shown in Fig. 4.2. Special sealed fittings can be installed on the box in order for wires (e.g, for power) to enter the enclosure.

Figure 4.2 shows the Opto22 system connected to a laptop computer. The Opto 22 can be connected to a computer by a variety of ways, such as wi-fi, wired ethernet and RS-232 serial port connection. The computer can be used to program and control the Opto 22 and to store data on its hard-drive or to transmit the data in-turn to a storage unit elsewhere.

The Opto22 was tested on the outdoor 450-kip damper test setup in parallel with a conventional ATS data acquisition system used commonly at the PEER center test facility at Richmond Field Station, University of California, Berkeley. The Opto22 system featured one Celesco PT5AV position and velocity transducer, and four 120Ω weldable strain gauges (identical to the ones described in Chapters 2 and 3). The results of an early test were excellent, with the system

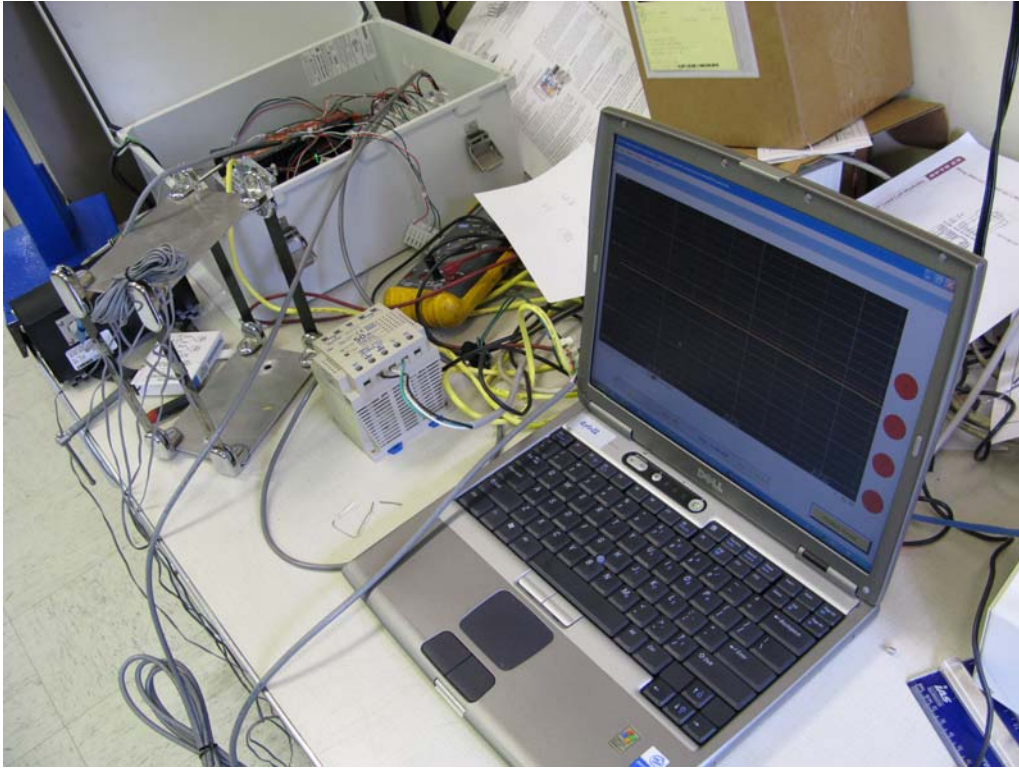


Fig. 4.2 Opto 22 connected to a laptop computer with ethernet LAN line.

being able to reliably acquire and transmit to a remote laptop clean displacement, velocity, and strain-gauge history signals.

In a bridge, several monitoring boxes will be installed, and all of them will connect to a central computer at a remote location, e.g., the maintenance station. The monitoring box can attain different configurations. The configuration that is favorable for a particular application will depend on various factors, such as the number of dampers, how far apart the dampers are from each other, and how far the central computer that controls the different boxes is. Figure 4.3 shows a configuration in which a single box corresponds to a single damper. Each of the boxes powers and receives data from the sensors attached on its damper. The box communicates wirelessly or via wired ethernet to a remote central computer, which in turn can communicate with other computer or data storage devices. Considering that the retail price of each SNAP PAC wireless controller is approximately \$1400 and that each data module is approximately \$200, the cost of a

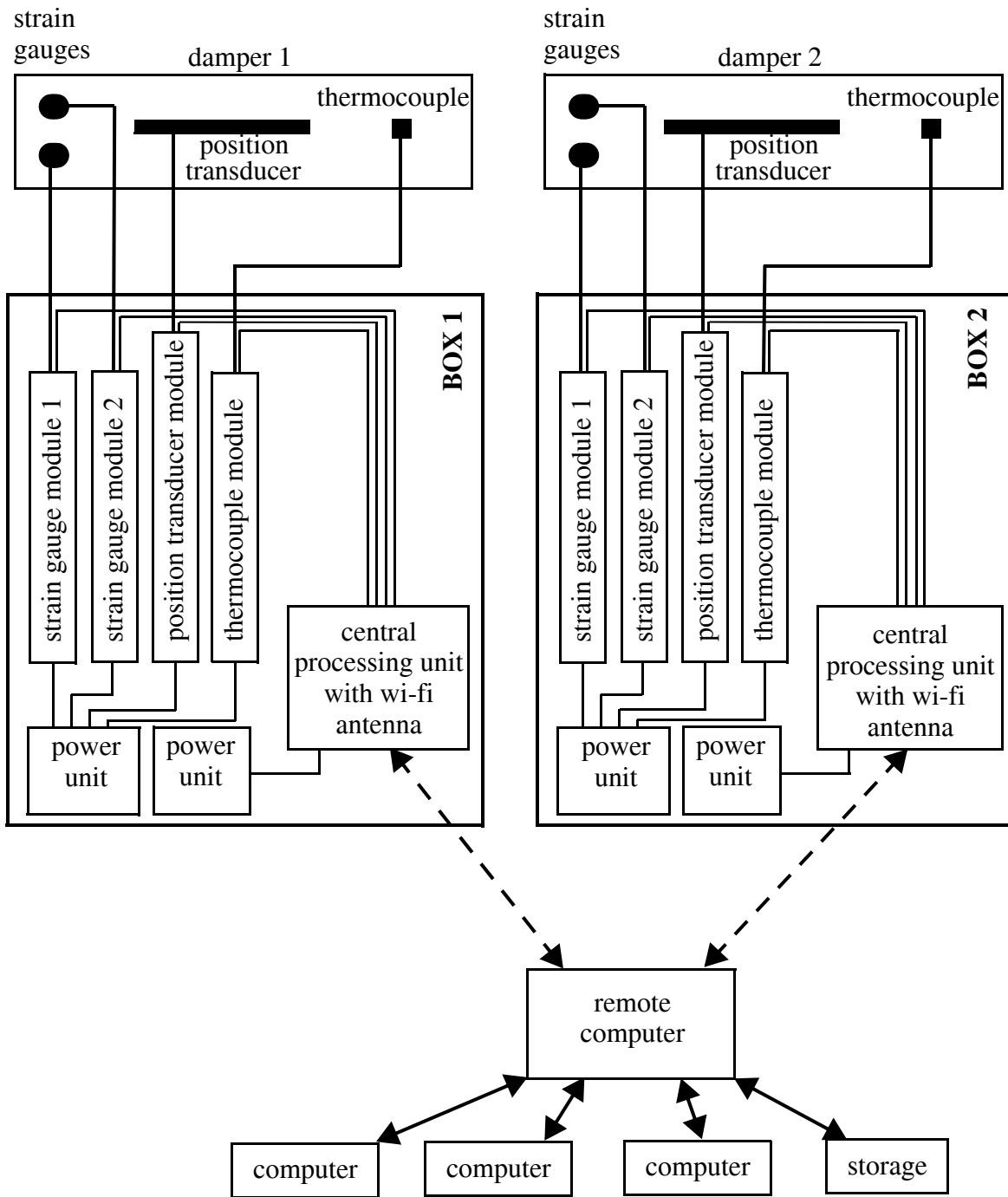


Fig. 4.3 Schematic diagram of wireless monitoring system in which each damper is configured with its own Opto22 enclosure box (as the one shown in Fig. 4.1) communicating with a remote computer.

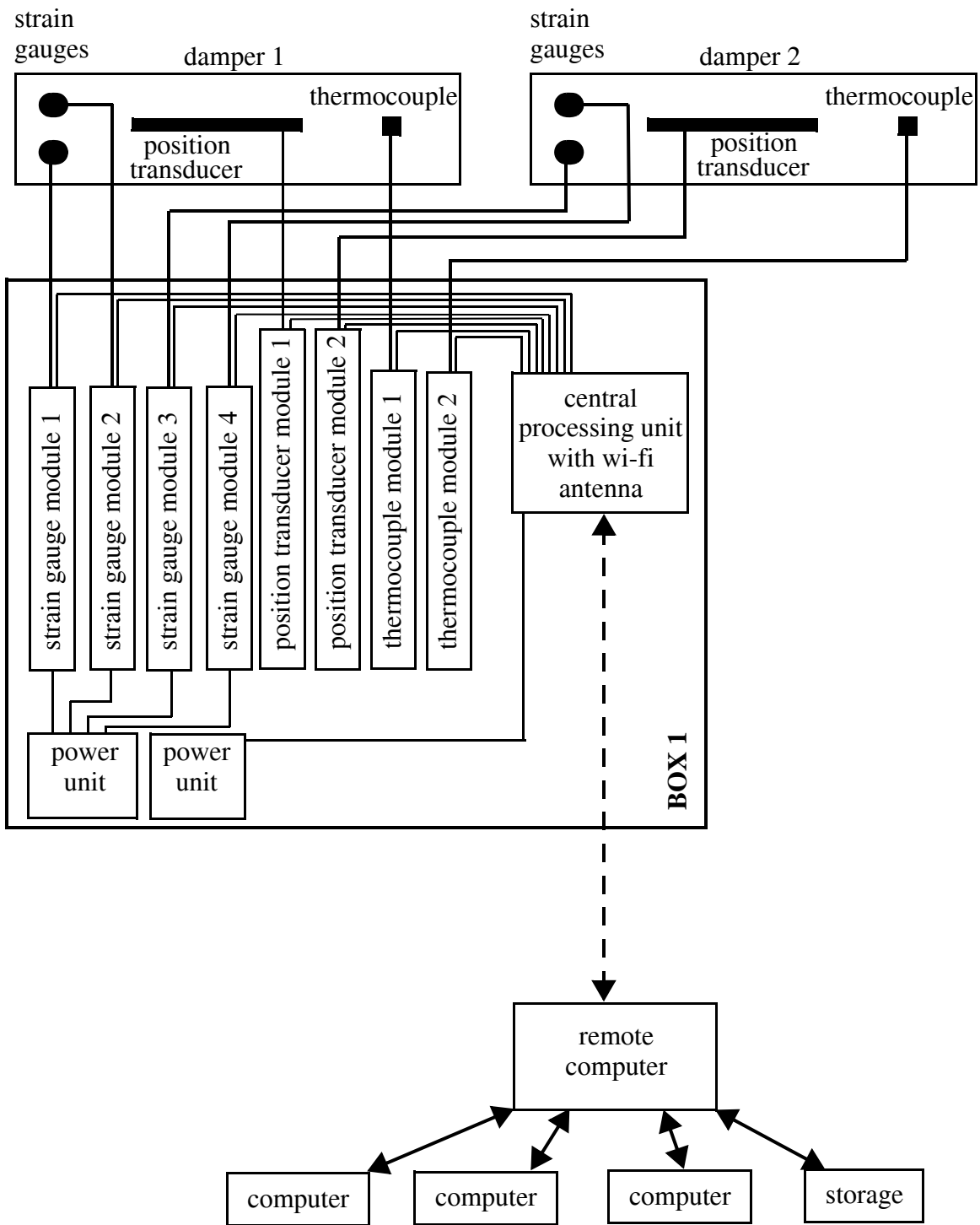


Fig. 4.4 Schematic diagram of wireless monitoring system in which two dampers share an Opto22 enclosure box communicating with a remote computer.

monitoring box can be relatively high. Cases where damper are far apart from each other may necessitate the use of this configuration.

Figure 4.4 shows the schematic diagram of a damper health monitoring configuration in which two dampers are connected to a single box. The flexibility of the Opto 22 system allows for multiple dampers to be connected to a single box. Caution must, of course, be taken that the cables from the sensors attached on the dampers are not long, thus avoiding the signal-loss problems discussed in Chapter 3. Bigger boxes with large rails can be used to mount many sensor modules. A single SNAP PAC R1 controller can be used to collect data from multiple dampers.

The success of the Opto 22 wireless monitoring system in this preliminary phase at the lab opens very promising opportunities for the system to be tested and adapted to wide applications of health monitoring of fluid dampers in bridges.

REFERENCES

- Black, C. J. and Makris, N. (2005). Viscous Heating of Fluid Dampers under Wind and Seismic Loading: Experimental Studies, Mathematical Modeling and Design Formulae. *Report No. EERC 2006-01*, Earthquake Engineering Research Center, University of California, Berkeley.
- Black, C. J. and Makris, N. (2007). “Viscous Heating of Fluid Dampers under Small and Large Amplitude Motions: Experimental Studies and Parametric Modeling,” *Journal of Engineering Mechanics, ASCE*, Vol. 133, No. 5, pp. 566–577.
- Delis, E. A, Malla, R. B., Madani, M., and Thompson, K. J. (1996). “Energy Dissipation Devices in Bridges Using Hydraulic Dampers,” *Building to Last, Proceedings of the Structures Congress XIV, IL, 2*, pp. 1188–1196, Chicago, IL, April 15-18, 1996.
- Howell, D.A. and Shenton, H.W. III (2006). “System for In-Service Strain Monitoring of Ordinary Bridges.” *Journal of Bridge Engineering. Journal of Bridge Engineering*, Vol. 11, No. 6, pp. 673–680.
- Makris, N. and Zhang, J. (2004). “Seismic Response Analysis of Highway Overcrossings Equipped with Elastomeric Bearings and Fluid Dampers”, *Journal of Structural Engineering (ASCE)*, Vol.130, No. 6, pp. 830–845.
- Mathworks (2007). MATLAB, Version 7.5 (computer software). The MathWorks, Inc., Natick, MA.
- Papanikolas, P. K. (2002). “Deck Superstructure and Cable Stays of the Rion-Antirion Bridge,” *Proceedings of the 4th National Conference on Steel Structures*, Patras, Greece, May 24–25, 2002.
- Timoshenko, S. P. and Goodier, J. N. (1970). *Theory of Elasticity*. 3rd ed. McGraw-Hill, New York.
- Transtek Inc. (2009). *Series 100 Linear Velocity Transducers*. Ellington, CT.

Appendix A: Installation and Protection of Weldable Strain Gauges

In this Appendix, we offer general information that we have collected from Vishay Micro-Measurements. This information can be used to aid in the installation and protection of weldable strain gauges. We urge the installation technician to obtain recommendations and updated information by the Vishay Micro-Measurements Engineers for the specific application at hand. This Appendix includes the following Vishay Micro-Measurements product literature:

- “Special Use Sensors - Weldable Strain Gauges.” The weldable strain gauge model used in the tests in this report was the CEA-06-W250A-120.
- “Model 700: Portable Strain Gage Welding and Soldering Unit.”
- “Attachment Techniques for Weldable Strain Gages and Temperature Sensors.”
- “M-Coat A Protective Coating.”
- “M-Coat B Protective Coating.”
- “M-Coat C Protective Coating.”
- “M-Coat J Protective Coating.”

Standard Weldable Patterns



Micro-Measurements



Special Use Sensors - Weldable Strain Gages

Micro-Measurements Standard Weldable Strain Gages and Temperature Sensors are specially designed for spot welding to structures and components. They are ideal for applications where test or environmental conditions preclude clamping and curing an adhesively bonded gage installation. These gages are equally advantageous when strain measurements must be made at an elevated temperature, but the nature of the test object does not permit the use of an elevated-temperature-curing adhesive.

Surface preparation requirements are minimal; only an appropriate solvent cleaning and abrasion of the test part surface with silicon-carbide paper or a small, hand-held grinder is needed. Spot welding is accomplished with a portable stored-energy hand-probe spot welder, such as the Model 700. Environmental protection is as easily applied to a welded gage installation as to an adhesively bonded gage.

Refer to Instruction Bulletin B-131 and Catalog A-110 for further information on installation and protective coatings, and to Bulletin 302 for specifications on the Model 700 Welding/Soldering Unit.

DESCRIPTION AND PERFORMANCE

General — All sensors are laboratory-prebonded, with a high-performance adhesive, to thin (0.005 in [0.13 mm]) metal carriers. Sensor grids are fully encapsulated for protection against handling and installation damage. Standard weldable strain gages are offered in two series to meet differing performance requirements. Both series are available in either 06 or 09 self-temperature compensation. Strain gages with 06 S-T-C have Inconel carriers, while S-T-C 09 gages and temperature sensors are mounted on 300-series stainless steel.

CEA-Series Weldable Strain Gage — Polyimide-encapsulated constantan foil grid, with large, rugged, copper-coated tabs. In most cases, the carrier can be contoured to a radius as small as 1/2in [13mm]. The CEA

Series is ideal for direct leadwire attachment, before or after installation.

Strain range is $\pm 5000\mu\text{in/in}$ [$\pm 5000\mu\text{m/m}$], and normal operating temperature range is -100° to $+200^\circ\text{F}$ [-75° to $+95^\circ\text{C}$]. Short-term maximum temperature is $+300^\circ\text{F}$ [$+150^\circ\text{C}$].

LWK-Series Weldable Strain Gage — Nickel-chromium alloy grid, encapsulated in fiberglass-reinforced epoxy phenolic. The LWK gage is provided with a three-wire lead system with 10 in [250 mm] of Teflon®-insulated leadwire.

This construction simplifies leadwire temperature compensation and provides for easy connection of the lead system to the instrumentation cable. Minimum installation radius is generally limited to 2in [50 mm].

Strain range is $\pm 5000\mu\text{in/in}$ [$\pm 5000\mu\text{m/m}$], and normal operating temperature range is -320° to $+500^\circ\text{F}$ [-195° to $+260^\circ\text{C}$]. Short-term maximum temperature is $+550^\circ\text{F}$ [$+290^\circ\text{C}$].

WWT-Series Temperature Sensor — High-purity nickel foil grid encapsulated in fiberglass-reinforced epoxy-phenolic, and equipped with integral three-tab terminal to facilitate leadwire attachment. The temperature sensor is normally installed on a flat surface of the workpiece, but, in any case, should always be oriented with the gridlines in the direction of minimum strain to avoid strain-induced errors (see Micro-Measurements Tech Note TN-506, Bondable Resistance Temperature Sensors and Associated Circuitry). With an appropriate LST Matching Network, the temperature response characteristic of the nickel can be linearized and scaled for direct readout (in degrees) with any strain indicator.

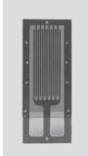
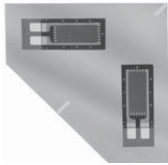
Teflon is a Registered Trademark of DuPont.

MEASUREMENT CONSIDERATIONS

It is important to note that operating characteristics of weldable strain gages (gage factor, transverse sensitivity, and thermal output) are specified for the basic strain gage itself — without the metal carrier. Thus, the properties are measured by bonding a conventional strain gage directly to an appropriate calibration specimen, following standard methods specified for all Micro-Measurements strain gages. This procedure assures the most accurate results, independent of the variables introduced by welding. In particular, the user should be aware that the gage factor specified on the engineering data sheet accompanying the gage applies only to the basic strain gage, without the shim. The effective gage factor of the weldable assembly (after welding to the test member) is commonly 5 to 10%

lower than this, due primarily to the stiffness of the shim. The reduction in gage factor is not subject to quantitative generalization, because it depends on the cross-sectional properties of the test specimen, and on the mode of loading (e.g., bending versus direct stress). It has been demonstrated, however, that for a group of like specimens, loaded in the same manner, the weldable gages exhibit very good repeatability and uniformity of response. Therefore, when test requirements dictate greatest accuracy, the weldable gages should be calibrated on a specimen of the same material and cross section as the test part, and under the same mode of loading.

Special Use Sensors - Weldable Strain Gages

GAGE PATTERN AND DESIGNATION Insert Desired S-T-C No. in Spaces Marked XX. See Note 1	RES. IN OHMS.	DIMENSIONS						
		CARRIER			ACTIVE GRID		MATRIX	
		Length	Width	Thick	Length	Width	Length	Width
CEA-XX-W250A-120 CEA-XX-W250A-350 	120 ± 0.4% 350 ± 0.4%	0.63	0.34	0.005	0.230	0.125	0.44	0.17
		16.0	8.6	0.13	5.84	3.18	11.2	4.3
		Most flexible and conformable pattern. Type 326-DFV and 330-DFV flat three-conductor cable typically used to solder directly to copper-coated tabs.						
CEA-XX-W250C-120 CEA-XX-W250C-350 	120 ± 0.4% 350 ± 0.4%	0.90	0.90	0.005	0.230	0.125	0.44	0.17
		22.9	22.9	0.13	5.84	3.18	11.2	4.3
		Tee rosette, used in biaxial stress states where directions of principal stresses are known. See W250A pattern for typical leadwire recommendations.						
LWK-XX-W250B-350 	350 ± 0.4%	0.88	0.32	0.005	0.250	0.125	0.62	0.17
		22.4	8.1	0.13	6.35	3.18	15.7	4.3
		Wide-temperature-range linear pattern with 10 in [250 mm] pre-attached leads. Teflon insulation is pretreated for best bond to protective coatings.						
LWK-XX-W250D-350 	350 ± 0.4%	1.15	1.15	0.005	0.250	0.125	0.62	0.17
		29.2	29.2	0.13	6.35	3.18	15.7	4.3
		Tee rosette, used in biaxial stress states where directions of principal stresses are known and a wide operating temperature range is required.						
WWT-TG-W200B-050 	50 ± 0.4% @ +75°F [+24°C]	0.71	0.43	0.005	0.200	0.200	0.52	0.26
		18.0	10.9	0.13	5.08	5.08	13.1	6.6
		Easy-to-use temperature sensor that can be welded or adhesively bonded to the test structure. For standard bondable temperature sensors, see Document Number 11522, "Temperature Sensors and LST Networks."						

Note 1: Products with designations and options shown in bold are not RoHS compliant.

Model 700

MEME Micro-Measurements



Portable Strain Gage Welding and Soldering Unit



FEATURES

- Separate visual and audible indicators monitor welder status - Weld energy is continuously adjustable from 3 to 50 joules, making the Model 700 an excellent choice for installing weldable strain gages and temperature sensors, as well as small thermocouples and light-gauge metal.
- Supplied with a lightweight soldering pencil - A front-panel control adjusts soldering tip temperature for a wide range of soldering applications in the field or in the laboratory.
- “Low-battery” light to warn the user when the internal, sealed lead-acid battery requires charging - A battery charger is included to provide for full battery charge with no danger of overcharging. Indicator lights monitor battery charge rate.
- Convenient storage space for cables, battery charger and instruction manual.

GENERAL SPECIFICATIONS

Overall Size:

9 L x 9 W x 9-3/4 H-in [230 x 230 x 250mm].

Weight:

21lb [9.5kg].

Power for Recharging:

115Vac or 230Vac, 50-60Hz. Uses external AC transformer (provided).

Operating and Storage Temperature Range:

0° to +120°F [-20° to +50°C].

WELDING SPECIFICATIONS

Weld Energy Range:

3 to 50 joules, continuously adjustable by front-panel control. Maximum open-circuit voltage less than 25Vdc.

Maximum Weld Repetition Rate:

20 per minute at 30 joules, typical.

Number of Welds per Battery Charge:

Approximately 2000 at weld energy setting of 30 joules. This is equivalent to 40 Micro-Measurements weldable gage installations.

Battery Charge Time: (from full discharge)

12 hours to 75% full charge; 18 hours to full charge.

Battery:

One sealed, rechargeable lead-acid (non-liquid) type, 12 volt, 5 ampere-hour.

Welding Probe:

Manually fired with trigger control and “steady-rest.”

Welding Cables:

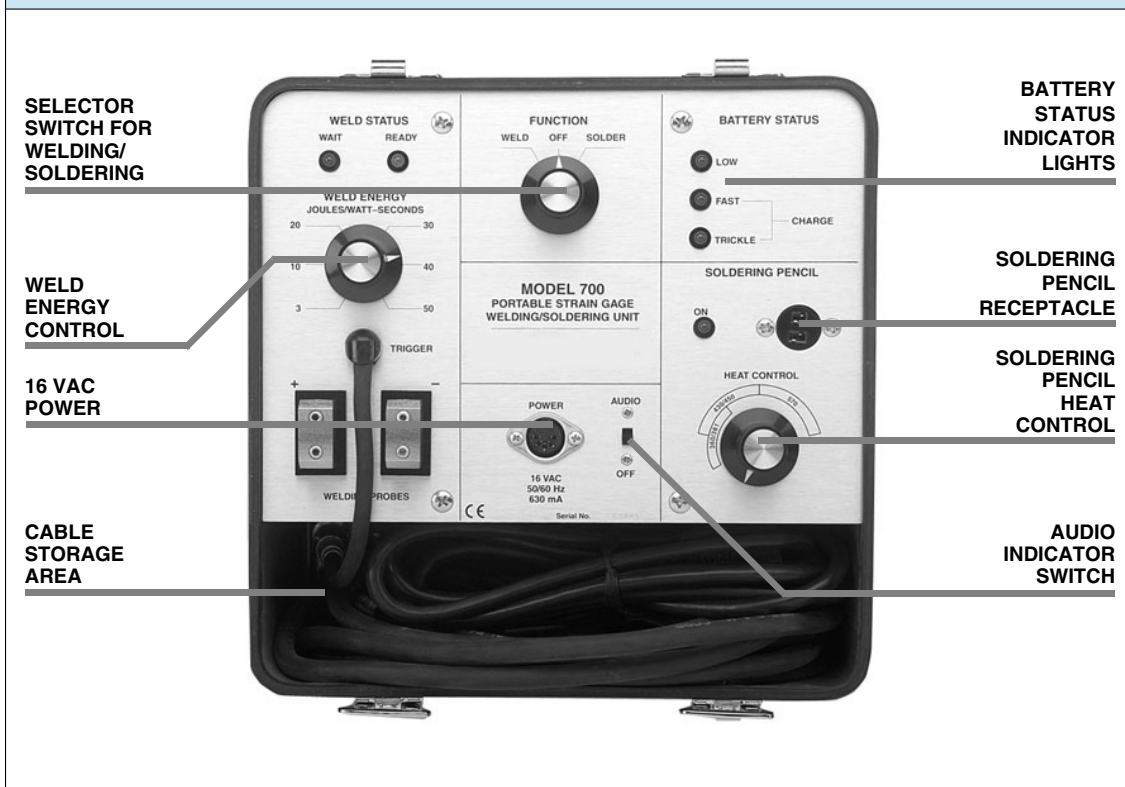
Two 5 ft [1.5m], fully flexible.

Weld Energy Monitor:

Calibrated front-panel control with READY and WAIT indicators; audible indication selectable.

Portable Strain Gage Welding and Soldering Unit

PANEL CONTROL FEATURES



SOLDERING SPECIFICATIONS

Temperature Control:

Continuously variable with bands indicating melting range of solders.

Soldering Pencil:

1.1 oz [31 gm], rated at 25 watts, 12 volt operation. Tip temperature adjustable from +200° to +900°F [+90° to +480°C].

Soldering Duration:

4 hours using +361°F [+183°C] melting point solders (with initial full charge).

Accessory:

Model 700-A103 Spot Welding Probe Set:

Recommended for spot welding instrument leadwires to ZC-Series high-temperature gage ribbons.

All specifications are nominal or typical at +23°C unless noted.



Instruction Bulletin B-131-5

Micro-Measurements



Attachment Techniques for Weldable Strain Gages and Temperature Sensors

INTRODUCTION

The Weldable Gage is a precision foil sensor bonded to a metal carrier for spot welding to structures and components. Spot welding is often more convenient than adhesively bonding a gage, particularly in field testing applications where bonding conditions are not ideal. This type of gage is also well-suited to laboratory test programs requiring elevated-temperature testing and minimum installation time.

After minimal surface preparation, spot welding is easily accomplished with a stored-energy handprobe spot welder. The gage is useful immediately after welding and leadwire attachment. Environmental protection is as easily applied to or installed over a welded gage as an adhesively bonded gage.

CEA-Series Weldable Strain Gage

This gage combines a fully encapsulated self-temperature-compensated constantan foil grid with large, rugged copper-coated tabs for direct leadwire attachment.

LWK-Series Weldable Strain Gage

Fully encapsulated self-temperature-compensated modified Karma (K-alloy) grid, with an integral three-wire lead system, and wide temperature capability.

WWT-Series Weldable Temperature Sensor

The WWT temperature sensor is manufactured from high-purity nickel foil and incorporates an integral three-tab terminal for leadwire attachment. This sensor complements the weldable strain gage by monitoring the temperature at the gage location for thermal output correction. With the appropriate matching network, a strain indicator will serve as a direct-readout instrument. For additional information on the Weldable Gage product line, and the general operating characteristics of Micro-Measurements strain gages, refer to the Precision Strain Gages databook.

Welding Unit

Best results are obtained with a 20 watt-second (minimum) capacitive-discharge spot welder, with a repetition capability of at least 15 welds per minute. It is recommended that the welder employ a spring-type ground clamp to ensure a low-resistance connection between the welder "common" terminal and specimen. Use a welding electrode with a spherical tip approximately 0.03in [0.8mm] in diameter. The Model 700 Portable Strain Gage Welding and Soldering Unit was specially

designed for installing weldable sensors. Refer to Bulletin 302 for specifications.

Surface Preparation

Although surface preparation for welding is less critical than for adhesive bonding, the surface must be free of grease, rust, scale, oxides and surface irregularities for efficient welding.

Step 1

Degrease the specimen with an appropriate solvent such as CSM Degreaser.

Step 2

Hand grind, abrade with silicon-carbide paper, or file the surface until smooth.

Step 3

Thoroughly wash with an appropriate solvent to remove all residue.

Safety Note

Safety goggles should always be worn during all installation processes. Serious and permanent eye injury could otherwise occur. In case of accident, secure immediate medical attention. For additional health and safety information concerning the products discussed in this Application Note, consult the specific Material Safety Data Sheets, which are available upon request.

Gage Handling and Welding Procedure

A sample metal carrier is supplied with each package of gages for practice welding. It is essential to first determine the proper weld-energy setting and electrode force. A setting of approximately 10 watt-seconds, with firm electrode force, will generally produce satisfactory welds. After a practice weld, pull the metal carrier from the specimen surface; with a satisfactory weld, a small slug of metal will break away from either the carrier or the specimen at the weld.

Attachment Techniques for Weldable Strain Gages and Temperature Sensors

Document No: 11131
Micro-Measurements

1 of 2
micro-measurements@vishaypg.com

Revision 13-Apr-10
www.micro-measurements.com

Step 1

Align the gage on the specimen surface by placing a short piece of drafting tape across the lower portion of the gage assembly.

Step 2

Tack the metal carrier in place with a single weld adjacent to the alignment triangles on each side of the gage, close to but not touching the gage backing (Figure 1).

Step 3

Remove the drafting tape by peeling it back directly over itself (Figure 2), being particularly careful not to distort the metal carrier during tape removal.

Step 4

Continue spot welding, close to the gage backing, welding from the center tacks to the ends of the carrier, completing one side at a time and spacing the welds on approximately 1/16in [1.6mm] centers. Weld across the top and bottom of the carrier (Figure 3).

Note: For the LWK Series, follow the same welding sequence shown in Figure 3, omitting sequence No. 6 (the area over which the integral leads extend). Sequences 1 and 3 must extend to the end of the metal carrier.

Step 5

Complete the welding procedure by welding a second row approximately 1/32in [0.8mm] outside the first row, spacing the welds as shown in Figure 4.

Note: Leadwires may be preattached to the CEA and WWT Series using the technique shown in Figure 5. Special care must then be taken to prevent the leads from peeling up the gage tab area or otherwise damaging the gage.

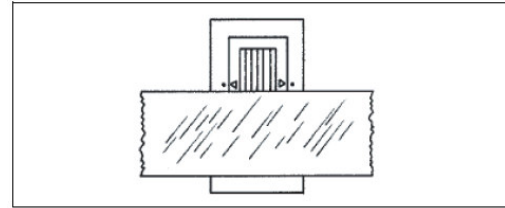


Fig. 1

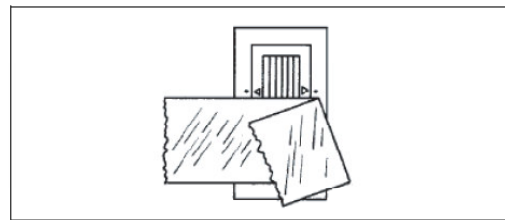


Fig. 2

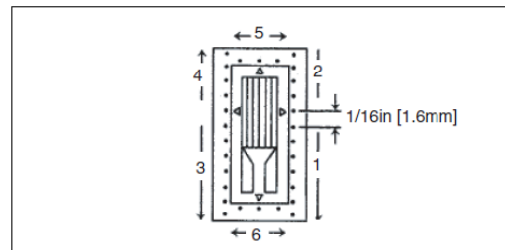


Fig. 3

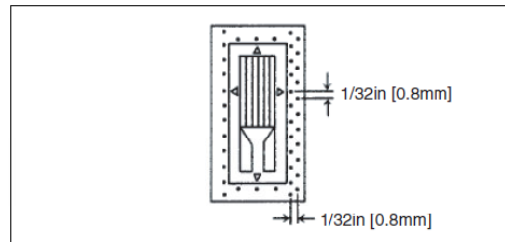


Fig. 4

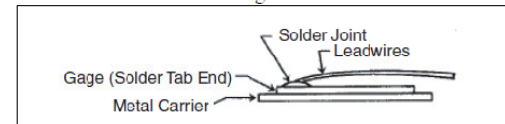


Fig. 5

COMMON WELDING PROBLEMS

PROBLEM	PROBABLE CAUSE
Expulsion of metal at the weld, or deformation of carrier or specimen material	Excessive weld-energy setting or electrode force
Reduced electrode life	Excessive weld-energy setting or insufficient electrode force
Poor weld strength	Insufficient weld-energy setting or electrode force
Sparking	Insufficient electrode force, pitted welding electrode, or insufficient surface preparation; welding electrode partially on gage backing
Welding requires excessive electrode force or a high weld-energy setting	Poor connection to welder "common" cable or poorly prepared specimen surface

Attachment Techniques for Weldable Strain Gages and Temperature Sensors

M-Coat A

Vishay Micro-Measurements



Protective Coating



FEATURES

- Easy to use
- Transparent
- Good general-purpose coating for laboratory use

DESCRIPTION

Air-drying solvent-thinned (xylene) polyurethane. Transparent. Moderate hardness; good flexibility. Can be removed with *M-LINE* Rosin Solvent or toluene. Film thickness 0.005-0.01 in [0.1-0.25 mm] per coat.

General-purpose coating for lab use, and as base coating for field applications. Must be fully cured before addition of other coatings. Fair moisture resistance. Not readily attacked by many solvents. Convenient to use.

CHARACTERISTICS

Cure Requirements:

Dries tack-free at room temperature in 20 minutes. Completely dry in 2 hours.

Normal cure 24 hours at room temperature. Chemical resistance and coating hardness increase for 6 to 7 days.

Operating Temperature Range:

Short Term: -100° to +300°F [-75° to +150°C].

Long Term: -100° to +250°F [-75° to +120°C].

Shelf Life:

1 year at +75°F [+24°C].

PACKAGING OPTIONS

Kit:

4 brush-cap bottles (1 oz [30 ml] ea)

Bulk:

Quart container

Protective Coating



FEATURES

- Good resistance to chemicals
- Air drying
- Also used for priming leadwires

DESCRIPTION

Air-drying solvent-thinned (MEK) nitrile rubber. Forms flexible rubbery coating. Do not use directly on exposed foil or bare leads. Often used to prime vinyl-insulated wire to improve bondability to other coatings. If used as primer on

leads, thin 50:50 with MEK. Flexible at cryogenic temperatures. Excellent resistance to gasoline, kerosene, commercial oils. Electrical properties poorer than other M-Coats, particularly at elevated temperatures.

CHARACTERISTICS

Cure Requirements:

Air-dries in 1 hour at +75°F [+24°C]. Do not apply subsequent protective coatings for at least 2 hours from time of application. Normal cure 24 hours at room temperature.

Further improve chemical resistance with 1 hour bake at +200°F [+95°C].

Operating Temperature Range:

Short Term: -320° to +300°F [-195° to +150°C].

Long Term: -320° to +200°F [-195° to +95°C].

Shelf Life:

1 year at +75°F [+24°C].

PACKAGING OPTIONS

Kit:

4 brush-cap bottles (1 oz [30 ml] ea)

Bulk:

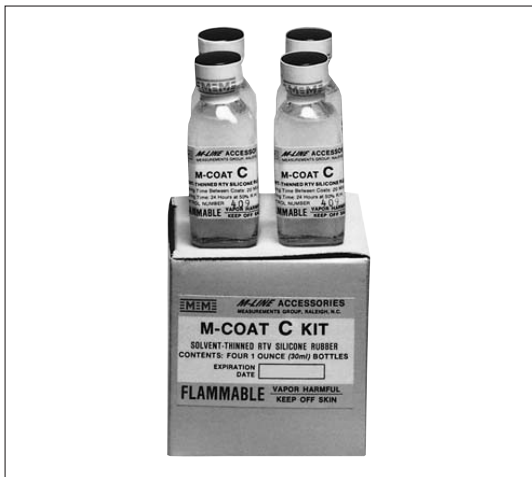
Quart container

M-Coat C

Vishay Micro-Measurements



Protective Coating



FEATURES

- Air drying
- Low reinforcement
- Transparent

DESCRIPTION

Solvent-thinned (naphtha) RTV silicone rubber. Cures to tough, rubbery transparent film. Good all-around mechanical and electrical properties. Completely noncorrosive. Film thickness 0.015-0.02 in [0.4-0.5 mm] per coat.

Recommended for lab and field installations that require a high degree of protection in thin coatings. Good water-splash protection. Good chemical resistance.

CHARACTERISTICS

Cure Requirements:

Solvents evaporate in about 60 minutes at room temperature. Allow 20 minutes drying time between coats.

Cures in 24 hours at +75°F [+24°C] and 50% RH. Longer cure at lower humidity.

Operating Temperature Range:

Short Term: -75° to +550°F [-60° to +290°C].

Long Term: -75° to +500°F [-60° to +260°C].

Shelf Life:

9 months at +75°F [+24°C] kept tightly sealed.

PACKAGING OPTIONS

Kit:

4 brush-cap bottles (1 oz [30 ml] ea)

Bulk:

Quart container

M-Coat J

Vishay Micro-Measurements



Protective Coating



FEATURES

- Excellent resistance to moisture
- Good resistance to chemicals
- Good protection against mechanical damage
- Room-temperature cure

DESCRIPTION

Two-part polysulfide liquid polymer compound. Can be applied in coating thickness of 1/8 in [3 mm] without flowing on vertical surfaces. Tough, flexible coating. No weighing required. Uncured coating can be removed with CSM Degreaser, Rosin Solvent, or MEK.

General-purpose coating. Good protection against oil, grease, most acids and alkalis, and most solvents. Strong solvents may cause swelling and softening with time. Concentrated acids eventually break down coating. Good salt-water immersion coating.

CHARACTERISTICS

Cure Requirements:

Mixed pot life 30 minutes at +75°F [+24°C].

Normal cure in 24 hours at +75°F [+24°C].

To accelerate cure and improve properties, cure 2 hours at +130°F [+55°C].

Operating Temperature Range:

Short Term: -50° to +250°F [-45° to +120°C].

Long Term: -50° to +200°F [-45° to +95°C].

Shelf Life:

6 months at +75°F [+24°C].

PACKAGING OPTIONS

M-Coat J-1:

- 1 mixing dispenser [70 g]
- 1 piece M-Coat FT Teflon® Tape
1 x 20 x 0.003in [25 x 500 x 0.08mm]

M-Coat J-3:

- 3 mixing dispensers [70 g ea]
- 3 pieces M-Coat FT Teflon Tape
1 x 20 x 0.003in [25 x 500 x 0.08mm]

Teflon is a Registered Trademark of DuPont.



Legal Disclaimer Notice

Vishay Precision Group

Disclaimer

All product specifications and data are subject to change without notice.

Vishay Precision Group, Inc., its affiliates, agents, and employees, and all persons acting on its or their behalf (collectively, "Vishay Precision Group"), disclaim any and all liability for any errors, inaccuracies or incompleteness contained herein or in any other disclosure relating to any product.

Vishay Precision Group disclaims any and all liability arising out of the use or application of any product described herein or of any information provided herein to the maximum extent permitted by law. The product specifications do not expand or otherwise modify Vishay Precision Group's terms and conditions of purchase, including but not limited to the warranty expressed therein, which apply to these products.

No license, express or implied, by estoppel or otherwise, to any intellectual property rights is granted by this document or by any conduct of Vishay Precision Group.

The products shown herein are not designed for use in medical, life-saving, or life-sustaining applications unless otherwise expressly indicated. Customers using or selling Vishay Precision Group products not expressly indicated for use in such applications do so entirely at their own risk and agree to fully indemnify Vishay Precision Group for any damages arising or resulting from such use or sale. Please contact authorized Vishay Precision Group personnel to obtain written terms and conditions regarding products designed for such applications.

Product names and markings noted herein may be trademarks of their respective owners.

PEER REPORTS

PEER reports are available individually or by yearly subscription. PEER reports can be ordered at http://peer.berkeley.edu/publications/peer_reports.html or by contacting the Pacific Earthquake Engineering Research Center, 325 Davis Hall mail code 1792, Berkeley, CA 94720. Tel.: (510) 642-3437; Fax: (510) 665-1655; Email: peer_editor@berkeley.edu

- PEER 2011/03** *New Ground Motion Selection Procedures and Selected Motions for the PEER Transportation Research Program.* Jack W. Baker, Ting Lin, Shrey K. Shahi, and Nirmal Jayaram. March 2011.
- PEER 2011/02** *A Bayesian Network Methodology for Infrastructure Seismic Risk Assessment and Decision Support.* Michelle T. Bensi, Armen Der Kiureghian, and Daniel Straub. March 2011.
- PEER 2011/01** *Demand Fragility Surfaces for Bridges in Liquefied and Laterally Spreading Ground.* Scott J. Brandenberg, Jian Zhang, Pirooz Kashighandi, Yili Huo, and Minxing Zhao. March 2011.
- PEER 2010/05** *Guidelines for Performance-Based Seismic Design of Tall Buildings.* Developed by the Tall Buildings Initiative. November 2010.
- PEER 2010/04** *Application Guide for the Design of Flexible and Rigid Bus Connections between Substation Equipment Subjected to Earthquakes.* Jean-Bernard Dastous and Armen Der Kiureghian. September 2010.
- PEER 2010/03** *Shear Wave Velocity as a Statistical Function of Standard Penetration Test Resistance and Vertical Effective Stress at Caltrans Bridge Sites.* Scott J. Brandenberg, Naresh Bellana, and Thomas Shantz. June 2010.
- PEER 2010/02** *Stochastic Modeling and Simulation of Ground Motions for Performance-Based Earthquake Engineering.* Sanaz Rezaeian and Armen Der Kiureghian. June 2010.
- PEER 2010/01** *Structural Response and Cost Characterization of Bridge Construction Using Seismic Performance Enhancement Strategies.* Ady Aviram, Božidar Stojadinović, Gustavo J. Parra-Montesinos, and Kevin R. Mackie. March 2010.
- PEER 2009/03** *The Integration of Experimental and Simulation Data in the Study of Reinforced Concrete Bridge Systems Including Soil-Foundation-Structure Interaction.* Matthew Dryden and Gregory L. Fenves. November 2009.
- PEER 2009/02** *Improving Earthquake Mitigation through Innovations and Applications in Seismic Science, Engineering, Communication, and Response. Proceedings of a U.S.-Iran Seismic Workshop.* October 2009.
- PEER 2009/01** *Evaluation of Ground Motion Selection and Modification Methods: Predicting Median Interstory Drift Response of Buildings.* Curt B. Haselton, Ed. June 2009.
- PEER 2008/10** *Technical Manual for Strata.* Albert R. Kottke and Ellen M. Rathje. February 2009.
- PEER 2008/09** *NGA Model for Average Horizontal Component of Peak Ground Motion and Response Spectra.* Brian S.-J. Chiou and Robert R. Youngs. November 2008.
- PEER 2008/08** *Toward Earthquake-Resistant Design of Concentrically Braced Steel Structures.* Patxi Uriz and Stephen A. Mahin. November 2008.
- PEER 2008/07** *Using OpenSees for Performance-Based Evaluation of Bridges on Liquefiable Soils.* Stephen L. Kramer, Pedro Arduino, and HyungSuk Shin. November 2008.
- PEER 2008/06** *Shaking Table Tests and Numerical Investigation of Self-Centering Reinforced Concrete Bridge Columns.* Hyung IL Jeong, Junichi Sakai, and Stephen A. Mahin. September 2008.
- PEER 2008/05** *Performance-Based Earthquake Engineering Design Evaluation Procedure for Bridge Foundations Undergoing Liquefaction-Induced Lateral Ground Displacement.* Christian A. Ledezma and Jonathan D. Bray. August 2008.
- PEER 2008/04** *Benchmarking of Nonlinear Geotechnical Ground Response Analysis Procedures.* Jonathan P. Stewart, Annie On-Lei Kwok, Youssef M. A. Hashash, Neven Matasovic, Robert Pyke, Zhiliang Wang, and Zhaohui Yang. August 2008.
- PEER 2008/03** *Guidelines for Nonlinear Analysis of Bridge Structures in California.* Ady Aviram, Kevin R. Mackie, and Božidar Stojadinović. August 2008.
- PEER 2008/02** *Treatment of Uncertainties in Seismic-Risk Analysis of Transportation Systems.* Evangelos Stergiou and Anne S. Kiremidjian. July 2008.
- PEER 2008/01** *Seismic Performance Objectives for Tall Buildings.* William T. Holmes, Charles Kircher, William Petak, and Nabih Youssef. August 2008.
- PEER 2007/12** *An Assessment to Benchmark the Seismic Performance of a Code-Conforming Reinforced Concrete Moment-Frame Building.* Curt Haselton, Christine A. Goulet, Judith Mitrani-Reiser, James L. Beck, Gregory G. Deierlein, Keith A. Porter, Jonathan P. Stewart, and Ertugrul Taciroglu. August 2008.

- PEER 2007/11** *Bar Buckling in Reinforced Concrete Bridge Columns.* Wayne A. Brown, Dawn E. Lehman, and John F. Stanton. February 2008.
- PEER 2007/10** *Computational Modeling of Progressive Collapse in Reinforced Concrete Frame Structures.* Mohamed M. Talaat and Khalid M. Mosalam. May 2008.
- PEER 2007/09** *Integrated Probabilistic Performance-Based Evaluation of Benchmark Reinforced Concrete Bridges.* Kevin R. Mackie, John-Michael Wong, and Božidar Stojadinović. January 2008.
- PEER 2007/08** *Assessing Seismic Collapse Safety of Modern Reinforced Concrete Moment-Frame Buildings.* Curt B. Haselton and Gregory G. Deierlein. February 2008.
- PEER 2007/07** *Performance Modeling Strategies for Modern Reinforced Concrete Bridge Columns.* Michael P. Berry and Marc O. Eberhard. April 2008.
- PEER 2007/06** *Development of Improved Procedures for Seismic Design of Buried and Partially Buried Structures.* Linda Al Atik and Nicholas Sitar. June 2007.
- PEER 2007/05** *Uncertainty and Correlation in Seismic Risk Assessment of Transportation Systems.* Renee G. Lee and Anne S. Kiremidjian. July 2007.
- PEER 2007/04** *Numerical Models for Analysis and Performance-Based Design of Shallow Foundations Subjected to Seismic Loading.* Sivapalan Gajan, Tara C. Hutchinson, Bruce L. Kutter, Prishati Raychowdhury, José A. Ugalde, and Jonathan P. Stewart. May 2008.
- PEER 2007/03** *Beam-Column Element Model Calibrated for Predicting Flexural Response Leading to Global Collapse of RC Frame Buildings.* Curt B. Haselton, Abbie B. Liel, Sarah Taylor Lange, and Gregory G. Deierlein. May 2008.
- PEER 2007/02** *Campbell-Bozorgnia NGA Ground Motion Relations for the Geometric Mean Horizontal Component of Peak and Spectral Ground Motion Parameters.* Kenneth W. Campbell and Yousef Bozorgnia. May 2007.
- PEER 2007/01** *Boore-Atkinson NGA Ground Motion Relations for the Geometric Mean Horizontal Component of Peak and Spectral Ground Motion Parameters.* David M. Boore and Gail M. Atkinson. May 2007.
- PEER 2006/12** *Societal Implications of Performance-Based Earthquake Engineering.* Peter J. May. May 2007.
- PEER 2006/11** *Probabilistic Seismic Demand Analysis Using Advanced Ground Motion Intensity Measures, Attenuation Relationships, and Near-Fault Effects.* Polsak Tothong and C. Allin Cornell. March 2007.
- PEER 2006/10** *Application of the PEER PBEE Methodology to the I-880 Viaduct.* Sashi Kunnath. February 2007.
- PEER 2006/09** *Quantifying Economic Losses from Travel Forgone Following a Large Metropolitan Earthquake.* James Moore, Sungbin Cho, Yue Yue Fan, and Stuart Werner. November 2006.
- PEER 2006/08** *Vector-Valued Ground Motion Intensity Measures for Probabilistic Seismic Demand Analysis.* Jack W. Baker and C. Allin Cornell. October 2006.
- PEER 2006/07** *Analytical Modeling of Reinforced Concrete Walls for Predicting Flexural and Coupled-Shear-Flexural Responses.* Kutay Orakcal, Leonardo M. Massone, and John W. Wallace. October 2006.
- PEER 2006/06** *Nonlinear Analysis of a Soil-Drilled Pier System under Static and Dynamic Axial Loading.* Gang Wang and Nicholas Sitar. November 2006.
- PEER 2006/05** *Advanced Seismic Assessment Guidelines.* Paolo Bazzurro, C. Allin Cornell, Charles Menun, Maziar Motahari, and Nicolas Luco. September 2006.
- PEER 2006/04** *Probabilistic Seismic Evaluation of Reinforced Concrete Structural Components and Systems.* Tae Hyung Lee and Khalid M. Mosalam. August 2006.
- PEER 2006/03** *Performance of Lifelines Subjected to Lateral Spreading.* Scott A. Ashford and Teerawut Juirnarongrit. July 2006.
- PEER 2006/02** *Pacific Earthquake Engineering Research Center Highway Demonstration Project.* Anne Kiremidjian, James Moore, Yue Yue Fan, Nesrin Basoz, Ozgur Yazali, and Meredith Williams. April 2006.
- PEER 2006/01** *Bracing Berkeley. A Guide to Seismic Safety on the UC Berkeley Campus.* Mary C. Comerio, Stephen Tobriner, and Ariane Fehrenkamp. January 2006.
- PEER 2005/16** *Seismic Response and Reliability of Electrical Substation Equipment and Systems.* Junho Song, Armen Der Kiureghian, and Jerome L. Sackman. April 2006.
- PEER 2005/15** *CPT-Based Probabilistic Assessment of Seismic Soil Liquefaction Initiation.* R. E. S. Moss, R. B. Seed, R. E. Kayen, J. P. Stewart, and A. Der Kiureghian. April 2006.
- PEER 2005/14** *Workshop on Modeling of Nonlinear Cyclic Load-Deformation Behavior of Shallow Foundations.* Bruce L. Kutter, Geoffrey Martin, Tara Hutchinson, Chad Harden, Sivapalan Gajan, and Justin Phalen. March 2006.

- PEER 2005/13** *Stochastic Characterization and Decision Bases under Time-Dependent Aftershock Risk in Performance-Based Earthquake Engineering.* Gee Liek Yeo and C. Allin Cornell. July 2005.
- PEER 2005/12** *PEER Testbed Study on a Laboratory Building: Exercising Seismic Performance Assessment.* Mary C. Comerio, editor. November 2005.
- PEER 2005/11** *Van Nuys Hotel Building Testbed Report: Exercising Seismic Performance Assessment.* Helmut Krawinkler, editor. October 2005.
- PEER 2005/10** *First NEES/E-Defense Workshop on Collapse Simulation of Reinforced Concrete Building Structures.* September 2005.
- PEER 2005/09** *Test Applications of Advanced Seismic Assessment Guidelines.* Joe Maffei, Karl Telleen, Danya Mohr, William Holmes, and Yuki Nakayama. August 2006.
- PEER 2005/08** *Damage Accumulation in Lightly Confined Reinforced Concrete Bridge Columns.* R. Tyler Rant, Jared M. Nelson, Zach Price, Marc O. Eberhard, and John F. Stanton. April 2006.
- PEER 2005/07** *Experimental and Analytical Studies on the Seismic Response of Freestanding and Anchored Laboratory Equipment.* Dimitrios Konstantinidis and Nicos Makris. January 2005.
- PEER 2005/06** *Global Collapse of Frame Structures under Seismic Excitations.* Luis F. Ibarra and Helmut Krawinkler. September 2005.
- PEER 2005/05** *Performance Characterization of Bench- and Shelf-Mounted Equipment.* Samit Ray Chaudhuri and Tara C. Hutchinson. May 2006.
- PEER 2005/04** *Numerical Modeling of the Nonlinear Cyclic Response of Shallow Foundations.* Chad Harden, Tara Hutchinson, Geoffrey R. Martin, and Bruce L. Kutter. August 2005.
- PEER 2005/03** *A Taxonomy of Building Components for Performance-Based Earthquake Engineering.* Keith A. Porter. September 2005.
- PEER 2005/02** *Fragility Basis for California Highway Overpass Bridge Seismic Decision Making.* Kevin R. Mackie and Božidar Stojadinović. June 2005.
- PEER 2005/01** *Empirical Characterization of Site Conditions on Strong Ground Motion.* Jonathan P. Stewart, Yoojoong Choi, and Robert W. Graves. June 2005.
- PEER 2004/09** *Electrical Substation Equipment Interaction: Experimental Rigid Conductor Studies.* Christopher Stearns and André Filiatrault. February 2005.
- PEER 2004/08** *Seismic Qualification and Fragility Testing of Line Break 550-kV Disconnect Switches.* Shakhzod M. Takhirov, Gregory L. Fenves, and Eric Fujisaki. January 2005.
- PEER 2004/07** *Ground Motions for Earthquake Simulator Qualification of Electrical Substation Equipment.* Shakhzod M. Takhirov, Gregory L. Fenves, Eric Fujisaki, and Don Clyde. January 2005.
- PEER 2004/06** *Performance-Based Regulation and Regulatory Regimes.* Peter J. May and Chris Koski. September 2004.
- PEER 2004/05** *Performance-Based Seismic Design Concepts and Implementation: Proceedings of an International Workshop.* Peter Fajfar and Helmut Krawinkler, editors. September 2004.
- PEER 2004/04** *Seismic Performance of an Instrumented Tilt-up Wall Building.* James C. Anderson and Vitelmo V. Bertero. July 2004.
- PEER 2004/03** *Evaluation and Application of Concrete Tilt-up Assessment Methodologies.* Timothy Graf and James O. Malley. October 2004.
- PEER 2004/02** *Analytical Investigations of New Methods for Reducing Residual Displacements of Reinforced Concrete Bridge Columns.* Junichi Sakai and Stephen A. Mahin. August 2004.
- PEER 2004/01** *Seismic Performance of Masonry Buildings and Design Implications.* Kerri Anne Taeko Tokoro, James C. Anderson, and Vitelmo V. Bertero. February 2004.
- PEER 2003/18** *Performance Models for Flexural Damage in Reinforced Concrete Columns.* Michael Berry and Marc Eberhard. August 2003.
- PEER 2003/17** *Predicting Earthquake Damage in Older Reinforced Concrete Beam-Column Joints.* Catherine Pagni and Laura Lowes. October 2004.
- PEER 2003/16** *Seismic Demands for Performance-Based Design of Bridges.* Kevin Mackie and Božidar Stojadinović. August 2003.
- PEER 2003/15** *Seismic Demands for Nondeteriorating Frame Structures and Their Dependence on Ground Motions.* Ricardo Antonio Medina and Helmut Krawinkler. May 2004.

- PEER 2003/14** *Finite Element Reliability and Sensitivity Methods for Performance-Based Earthquake Engineering.* Terje Haukaas and Armen Der Kiureghian. April 2004.
- PEER 2003/13** *Effects of Connection Hysteretic Degradation on the Seismic Behavior of Steel Moment-Resisting Frames.* Janise E. Rodgers and Stephen A. Mahin. March 2004.
- PEER 2003/12** *Implementation Manual for the Seismic Protection of Laboratory Contents: Format and Case Studies.* William T. Holmes and Mary C. Comerio. October 2003.
- PEER 2003/11** *Fifth U.S.-Japan Workshop on Performance-Based Earthquake Engineering Methodology for Reinforced Concrete Building Structures.* February 2004.
- PEER 2003/10** *A Beam-Column Joint Model for Simulating the Earthquake Response of Reinforced Concrete Frames.* Laura N. Lowes, Nilanjan Mitra, and Arash Altoontash. February 2004.
- PEER 2003/09** *Sequencing Repairs after an Earthquake: An Economic Approach.* Marco Casari and Simon J. Wilkie. April 2004.
- PEER 2003/08** *A Technical Framework for Probability-Based Demand and Capacity Factor Design (DCFD) Seismic Formats.* Fatemeh Jalayer and C. Allin Cornell. November 2003.
- PEER 2003/07** *Uncertainty Specification and Propagation for Loss Estimation Using FOSM Methods.* Jack W. Baker and C. Allin Cornell. September 2003.
- PEER 2003/06** *Performance of Circular Reinforced Concrete Bridge Columns under Bidirectional Earthquake Loading.* Mahmoud M. Hachem, Stephen A. Mahin, and Jack P. Moehle. February 2003.
- PEER 2003/05** *Response Assessment for Building-Specific Loss Estimation.* Eduardo Miranda and Shahram Taghavi. September 2003.
- PEER 2003/04** *Experimental Assessment of Columns with Short Lap Splices Subjected to Cyclic Loads.* Murat Melek, John W. Wallace, and Joel Conte. April 2003.
- PEER 2003/03** *Probabilistic Response Assessment for Building-Specific Loss Estimation.* Eduardo Miranda and Hesameddin Aslani. September 2003.
- PEER 2003/02** *Software Framework for Collaborative Development of Nonlinear Dynamic Analysis Program.* Jun Peng and Kincho H. Law. September 2003.
- PEER 2003/01** *Shake Table Tests and Analytical Studies on the Gravity Load Collapse of Reinforced Concrete Frames.* Kenneth John Elwood and Jack P. Moehle. November 2003.
- PEER 2002/24** *Performance of Beam to Column Bridge Joints Subjected to a Large Velocity Pulse.* Natalie Gibson, André Filiatrault, and Scott A. Ashford. April 2002.
- PEER 2002/23** *Effects of Large Velocity Pulses on Reinforced Concrete Bridge Columns.* Greg L. Orozco and Scott A. Ashford. April 2002.
- PEER 2002/22** *Characterization of Large Velocity Pulses for Laboratory Testing.* Kenneth E. Cox and Scott A. Ashford. April 2002.
- PEER 2002/21** *Fourth U.S.-Japan Workshop on Performance-Based Earthquake Engineering Methodology for Reinforced Concrete Building Structures.* December 2002.
- PEER 2002/20** *Barriers to Adoption and Implementation of PBEE Innovations.* Peter J. May. August 2002.
- PEER 2002/19** *Economic-Engineered Integrated Models for Earthquakes: Socioeconomic Impacts.* Peter Gordon, James E. Moore II, and Harry W. Richardson. July 2002.
- PEER 2002/18** *Assessment of Reinforced Concrete Building Exterior Joints with Substandard Details.* Chris P. Pantelides, Jon Hansen, Justin Nadauld, and Lawrence D. Reaveley. May 2002.
- PEER 2002/17** *Structural Characterization and Seismic Response Analysis of a Highway Overcrossing Equipped with Elastomeric Bearings and Fluid Dampers: A Case Study.* Nicos Makris and Jian Zhang. November 2002.
- PEER 2002/16** *Estimation of Uncertainty in Geotechnical Properties for Performance-Based Earthquake Engineering.* Allen L. Jones, Steven L. Kramer, and Pedro Arduino. December 2002.
- PEER 2002/15** *Seismic Behavior of Bridge Columns Subjected to Various Loading Patterns.* Asadollah Esmaeili-Gh. and Yan Xiao. December 2002.
- PEER 2002/14** *Inelastic Seismic Response of Extended Pile Shaft Supported Bridge Structures.* T.C. Hutchinson, R.W. Boulanger, Y.H. Chai, and I.M. Idriss. December 2002.
- PEER 2002/13** *Probabilistic Models and Fragility Estimates for Bridge Components and Systems.* Paolo Gardoni, Armen Der Kiureghian, and Khalid M. Mosalam. June 2002.

- PEER 2002/12** *Effects of Fault Dip and Slip Rake on Near-Source Ground Motions: Why Chi-Chi Was a Relatively Mild M7.6 Earthquake.* Brad T. Aagaard, John F. Hall, and Thomas H. Heaton. December 2002.
- PEER 2002/11** *Analytical and Experimental Study of Fiber-Reinforced Strip Isolators.* James M. Kelly and Shakhzod M. Takhirov. September 2002.
- PEER 2002/10** *Centrifuge Modeling of Settlement and Lateral Spreading with Comparisons to Numerical Analyses.* Sivapalan Gajan and Bruce L. Kutter. January 2003.
- PEER 2002/09** *Documentation and Analysis of Field Case Histories of Seismic Compression during the 1994 Northridge, California, Earthquake.* Jonathan P. Stewart, Patrick M. Smith, Daniel H. Whang, and Jonathan D. Bray. October 2002.
- PEER 2002/08** *Component Testing, Stability Analysis and Characterization of Buckling-Restrained Unbonded Braces™.* Cameron Black, Nicos Makris, and Ian Aiken. September 2002.
- PEER 2002/07** *Seismic Performance of Pile-Wharf Connections.* Charles W. Roeder, Robert Graff, Jennifer Soderstrom, and Jun Han Yoo. December 2001.
- PEER 2002/06** *The Use of Benefit-Cost Analysis for Evaluation of Performance-Based Earthquake Engineering Decisions.* Richard O. Zerbe and Anthony Falit-Baiamonte. September 2001.
- PEER 2002/05** *Guidelines, Specifications, and Seismic Performance Characterization of Nonstructural Building Components and Equipment.* André Filiatrault, Constantin Christopoulos, and Christopher Stearns. September 2001.
- PEER 2002/04** *Consortium of Organizations for Strong-Motion Observation Systems and the Pacific Earthquake Engineering Research Center Lifelines Program: Invited Workshop on Archiving and Web Dissemination of Geotechnical Data, 4–5 October 2001.* September 2002.
- PEER 2002/03** *Investigation of Sensitivity of Building Loss Estimates to Major Uncertain Variables for the Van Nuys Testbed.* Keith A. Porter, James L. Beck, and Rustem V. Shaikhutdinov. August 2002.
- PEER 2002/02** *The Third U.S.-Japan Workshop on Performance-Based Earthquake Engineering Methodology for Reinforced Concrete Building Structures.* July 2002.
- PEER 2002/01** *Nonstructural Loss Estimation: The UC Berkeley Case Study.* Mary C. Comerio and John C. Stallmeyer. December 2001.
- PEER 2001/16** *Statistics of SDF-System Estimate of Roof Displacement for Pushover Analysis of Buildings.* Anil K. Chopra, Rakesh K. Goel, and Chatpan Chintanapakdee. December 2001.
- PEER 2001/15** *Damage to Bridges during the 2001 Nisqually Earthquake.* R. Tyler Ranf, Marc O. Eberhard, and Michael P. Berry. November 2001.
- PEER 2001/14** *Rocking Response of Equipment Anchored to a Base Foundation.* Nicos Makris and Cameron J. Black. September 2001.
- PEER 2001/13** *Modeling Soil Liquefaction Hazards for Performance-Based Earthquake Engineering.* Steven L. Kramer and Ahmed-W. Elgamal. February 2001.
- PEER 2001/12** *Development of Geotechnical Capabilities in OpenSees.* Boris Jeremić. September 2001.
- PEER 2001/11** *Analytical and Experimental Study of Fiber-Reinforced Elastomeric Isolators.* James M. Kelly and Shakhzod M. Takhirov. September 2001.
- PEER 2001/10** *Amplification Factors for Spectral Acceleration in Active Regions.* Jonathan P. Stewart, Andrew H. Liu, Yoojoong Choi, and Mehmet B. Baturay. December 2001.
- PEER 2001/09** *Ground Motion Evaluation Procedures for Performance-Based Design.* Jonathan P. Stewart, Shyh-Jeng Chiou, Jonathan D. Bray, Robert W. Graves, Paul G. Somerville, and Norman A. Abrahamson. September 2001.
- PEER 2001/08** *Experimental and Computational Evaluation of Reinforced Concrete Bridge Beam-Column Connections for Seismic Performance.* Clay J. Naito, Jack P. Moehle, and Khalid M. Mosalam. November 2001.
- PEER 2001/07** *The Rocking Spectrum and the Shortcomings of Design Guidelines.* Nicos Makris and Dimitrios Konstantinidis. August 2001.
- PEER 2001/06** *Development of an Electrical Substation Equipment Performance Database for Evaluation of Equipment Fragilities.* Thalia Agnanos. April 1999.
- PEER 2001/05** *Stiffness Analysis of Fiber-Reinforced Elastomeric Isolators.* Hsiang-Chuan Tsai and James M. Kelly. May 2001.
- PEER 2001/04** *Organizational and Societal Considerations for Performance-Based Earthquake Engineering.* Peter J. May. April 2001.

- PEER 2001/03** *A Modal Pushover Analysis Procedure to Estimate Seismic Demands for Buildings: Theory and Preliminary Evaluation.* Anil K. Chopra and Rakesh K. Goel. January 2001.
- PEER 2001/02** *Seismic Response Analysis of Highway Overcrossings Including Soil-Structure Interaction.* Jian Zhang and Nicos Makris. March 2001.
- PEER 2001/01** *Experimental Study of Large Seismic Steel Beam-to-Column Connections.* Egor P. Popov and Shakhzod M. Takhirov. November 2000.
- PEER 2000/10** *The Second U.S.-Japan Workshop on Performance-Based Earthquake Engineering Methodology for Reinforced Concrete Building Structures.* March 2000.
- PEER 2000/09** *Structural Engineering Reconnaissance of the August 17, 1999 Earthquake: Kocaeli (Izmit), Turkey.* Halil Sezen, Kenneth J. Elwood, Andrew S. Whittaker, Khalid Mosalam, John J. Wallace, and John F. Stanton. December 2000.
- PEER 2000/08** *Behavior of Reinforced Concrete Bridge Columns Having Varying Aspect Ratios and Varying Lengths of Confinement.* Anthony J. Calderone, Dawn E. Lehman, and Jack P. Moehle. January 2001.
- PEER 2000/07** *Cover-Plate and Flange-Plate Reinforced Steel Moment-Resisting Connections.* Taejin Kim, Andrew S. Whittaker, Amir S. Gilani, Vitelmo V. Bertero, and Shakhzod M. Takhirov. September 2000.
- PEER 2000/06** *Seismic Evaluation and Analysis of 230-kV Disconnect Switches.* Amir S. J. Gilani, Andrew S. Whittaker, Gregory L. Fenves, Chun-Hao Chen, Henry Ho, and Eric Fujisaki. July 2000.
- PEER 2000/05** *Performance-Based Evaluation of Exterior Reinforced Concrete Building Joints for Seismic Excitation.* Chandra Clyde, Chris P. Pantelides, and Lawrence D. Reaveley. July 2000.
- PEER 2000/04** *An Evaluation of Seismic Energy Demand: An Attenuation Approach.* Chung-Che Chou and Chia-Ming Uang. July 1999.
- PEER 2000/03** *Framing Earthquake Retrofitting Decisions: The Case of Hillside Homes in Los Angeles.* Detlof von Winterfeldt, Nels Roselund, and Alicia Kitsuse. March 2000.
- PEER 2000/02** *U.S.-Japan Workshop on the Effects of Near-Field Earthquake Shaking.* Andrew Whittaker, ed. July 2000.
- PEER 2000/01** *Further Studies on Seismic Interaction in Interconnected Electrical Substation Equipment.* Armen Der Kiureghian, Kee-Jeung Hong, and Jerome L. Sackman. November 1999.
- PEER 1999/14** *Seismic Evaluation and Retrofit of 230-kV Porcelain Transformer Bushings.* Amir S. Gilani, Andrew S. Whittaker, Gregory L. Fenves, and Eric Fujisaki. December 1999.
- PEER 1999/13** *Building Vulnerability Studies: Modeling and Evaluation of Tilt-up and Steel Reinforced Concrete Buildings.* John W. Wallace, Jonathan P. Stewart, and Andrew S. Whittaker, editors. December 1999.
- PEER 1999/12** *Rehabilitation of Nonductile RC Frame Building Using Encasement Plates and Energy-Dissipating Devices.* Mehrdad Sasani, Vitelmo V. Bertero, James C. Anderson. December 1999.
- PEER 1999/11** *Performance Evaluation Database for Concrete Bridge Components and Systems under Simulated Seismic Loads.* Yael D. Hose and Frieder Seible. November 1999.
- PEER 1999/10** *U.S.-Japan Workshop on Performance-Based Earthquake Engineering Methodology for Reinforced Concrete Building Structures.* December 1999.
- PEER 1999/09** *Performance Improvement of Long Period Building Structures Subjected to Severe Pulse-Type Ground Motions.* James C. Anderson, Vitelmo V. Bertero, and Raul Bertero. October 1999.
- PEER 1999/08** *Envelopes for Seismic Response Vectors.* Charles Menun and Armen Der Kiureghian. July 1999.
- PEER 1999/07** *Documentation of Strengths and Weaknesses of Current Computer Analysis Methods for Seismic Performance of Reinforced Concrete Members.* William F. Cofer. November 1999.
- PEER 1999/06** *Rocking Response and Overturning of Anchored Equipment under Seismic Excitations.* Nicos Makris and Jian Zhang. November 1999.
- PEER 1999/05** *Seismic Evaluation of 550 kV Porcelain Transformer Bushings.* Amir S. Gilani, Andrew S. Whittaker, Gregory L. Fenves, and Eric Fujisaki. October 1999.
- PEER 1999/04** *Adoption and Enforcement of Earthquake Risk-Reduction Measures.* Peter J. May, Raymond J. Burby, T. Jens Feeley, and Robert Wood.
- PEER 1999/03** *Task 3 Characterization of Site Response General Site Categories.* Adrian Rodriguez-Marek, Jonathan D. Bray, and Norman Abrahamson. February 1999.
- PEER 1999/02** *Capacity-Demand-Diagram Methods for Estimating Seismic Deformation of Inelastic Structures: SDF Systems.* Anil K. Chopra and Rakesh Goel. April 1999.

- PEER 1999/01** *Interaction in Interconnected Electrical Substation Equipment Subjected to Earthquake Ground Motions.* Armen Der Kiureghian, Jerome L. Sackman, and Kee-Jeung Hong. February 1999.
- PEER 1998/08** *Behavior and Failure Analysis of a Multiple-Frame Highway Bridge in the 1994 Northridge Earthquake.* Gregory L. Fenves and Michael Ellery. December 1998.
- PEER 1998/07** *Empirical Evaluation of Inertial Soil-Structure Interaction Effects.* Jonathan P. Stewart, Raymond B. Seed, and Gregory L. Fenves. November 1998.
- PEER 1998/06** *Effect of Damping Mechanisms on the Response of Seismic Isolated Structures.* Nicos Makris and Shih-Po Chang. November 1998.
- PEER 1998/05** *Rocking Response and Overturning of Equipment under Horizontal Pulse-Type Motions.* Nicos Makris and Yiannis Roussos. October 1998.
- PEER 1998/04** *Pacific Earthquake Engineering Research Invitational Workshop Proceedings, May 14–15, 1998: Defining the Links between Planning, Policy Analysis, Economics and Earthquake Engineering.* Mary Comerio and Peter Gordon. September 1998.
- PEER 1998/03** *Repair/Upgrade Procedures for Welded Beam to Column Connections.* James C. Anderson and Xiaojing Duan. May 1998.
- PEER 1998/02** *Seismic Evaluation of 196 kV Porcelain Transformer Bushings.* Amir S. Gilani, Juan W. Chavez, Gregory L. Fenves, and Andrew S. Whittaker. May 1998.
- PEER 1998/01** *Seismic Performance of Well-Confined Concrete Bridge Columns.* Dawn E. Lehman and Jack P. Moehle. December 2000.

ONLINE REPORTS

The following PEER reports are available by Internet only at http://peer.berkeley.edu/publications/peer_reports.html

- PEER 2011/103** *In-Situ Monitoring of the Force Output of Fluid Dampers: Experimental Investigation.* Dimitrios Konstantinidis, James M. Kelly, and Nicos Makris. April 2011.
- PEER 2011/102** *Ground-motion prediction equations 1964 - 2010.* John Douglas. April 2011.
- PEER 2011/101** *Report of the Eighth Planning Meeting of NEES/E-Defense Collaborative Research on Earthquake Engineering.* Convened by the Hyogo Earthquake Engineering Research Center (NIED), NEES Consortium, Inc. February 2011.
- PEER 2010/111** *Modeling and Acceptance Criteria for Seismic Design and Analysis of Tall Buildings.* Task 7 Report for the Tall Buildings Initiative - Published jointly by the Applied Technology Council. October 2010.
- PEER 2010/110** *Seismic Performance Assessment and Probabilistic Repair Cost Analysis of Precast Concrete Cladding Systems for Multistory Buildings.* Jeffrey P. Hunt and Božidar Stojadinovic. November 2010.
- PEER 2010/109** *Report of the Seventh Joint Planning Meeting of NEES/E-Defense Collaboration on Earthquake Engineering. Held at the E-Defense, Miki, and Shin-Kobe, Japan, September 18–19, 2009.* August 2010.
- PEER 2010/108** *Probabilistic Tsunami Hazard in California.* Hong Kie Thio, Paul Somerville, and Jascha Polet, preparers. October 2010.
- PEER 2010/107** *Performance and Reliability of Exposed Column Base Plate Connections for Steel Moment-Resisting Frames.* Ady Aviram, Božidar Stojadinovic, and Armen Der Kiureghian. August 2010.
- PEER 2010/106** *Verification of Probabilistic Seismic Hazard Analysis Computer Programs.* Patricia Thomas, Ivan Wong, and Norman Abrahamson. May 2010.
- PEER 2010/105** *Structural Engineering Reconnaissance of the April 6, 2009, Abruzzo, Italy, Earthquake, and Lessons Learned.* M. Selim Günay and Khalid M. Mosalam. April 2010.
- PEER 2010/104** *Simulating the Inelastic Seismic Behavior of Steel Braced Frames, Including the Effects of Low-Cycle Fatigue.* Yuli Huang and Stephen A. Mahin. April 2010.
- PEER 2010/103** *Post-Earthquake Traffic Capacity of Modern Bridges in California.* Vesna Terzic and Božidar Stojadinović. March 2010.
- PEER 2010/102** *Analysis of Cumulative Absolute Velocity (CAV) and JMA Instrumental Seismic Intensity (I_{JMA}) Using the PEER–NGA Strong Motion Database.* Kenneth W. Campbell and Yousef Bozorgnia. February 2010.
- PEER 2010/101** *Rocking Response of Bridges on Shallow Foundations.* Jose A. Ugalde, Bruce L. Kutter, and Boris Jeremic. April 2010.
- PEER 2009/109** *Simulation and Performance-Based Earthquake Engineering Assessment of Self-Centering Post-Tensioned Concrete Bridge Systems.* Won K. Lee and Sarah L. Billington. December 2009.
- PEER 2009/108** *PEER Lifelines Geotechnical Virtual Data Center.* J. Carl Stepp, Daniel J. Ponti, Loren L. Turner, Jennifer N. Swift, Sean Devlin, Yang Zhu, Jean Benoit, and John Bobbitt. September 2009.
- PEER 2009/107** *Experimental and Computational Evaluation of Current and Innovative In-Span Hinge Details in Reinforced Concrete Box-Girder Bridges: Part 2: Post-Test Analysis and Design Recommendations.* Matias A. Hube and Khalid M. Mosalam. December 2009.
- PEER 2009/106** *Shear Strength Models of Exterior Beam-Column Joints without Transverse Reinforcement.* Sangjoon Park and Khalid M. Mosalam. November 2009.
- PEER 2009/105** *Reduced Uncertainty of Ground Motion Prediction Equations through Bayesian Variance Analysis.* Robb Eric S. Moss. November 2009.
- PEER 2009/104** *Advanced Implementation of Hybrid Simulation.* Andreas H. Schellenberg, Stephen A. Mahin, Gregory L. Fenves. November 2009.
- PEER 2009/103** *Performance Evaluation of Innovative Steel Braced Frames.* T. Y. Yang, Jack P. Moehle, and Božidar Stojadinovic. August 2009.
- PEER 2009/102** *Reinvestigation of Liquefaction and Nonliquefaction Case Histories from the 1976 Tangshan Earthquake.* Robb Eric Moss, Robert E. Kayen, Liyuan Tong, Songyu Liu, Guojun Cai, and Jiaer Wu. August 2009.

- PEER 2009/101** *Report of the First Joint Planning Meeting for the Second Phase of NEES/E-Defense Collaborative Research on Earthquake Engineering.* Stephen A. Mahin et al. July 2009.
- PEER 2008/104** *Experimental and Analytical Study of the Seismic Performance of Retaining Structures.* Linda Al Atik and Nicholas Sitar. January 2009.
- PEER 2008/103** *Experimental and Computational Evaluation of Current and Innovative In-Span Hinge Details in Reinforced Concrete Box-Girder Bridges. Part 1: Experimental Findings and Pre-Test Analysis.* Matias A. Hube and Khalid M. Mosalam. January 2009.
- PEER 2008/102** *Modeling of Unreinforced Masonry Infill Walls Considering In-Plane and Out-of-Plane Interaction.* Stephen Kadysiewski and Khalid M. Mosalam. January 2009.
- PEER 2008/101** *Seismic Performance Objectives for Tall Buildings.* William T. Holmes, Charles Kircher, William Petak, and Nabih Youssef. August 2008.
- PEER 2007/101** *Generalized Hybrid Simulation Framework for Structural Systems Subjected to Seismic Loading.* Tarek Elkhoraibi and Khalid M. Mosalam. July 2007.
- PEER 2007/100** *Seismic Evaluation of Reinforced Concrete Buildings Including Effects of Masonry Infill Walls.* Alidad Hashemi and Khalid M. Mosalam. July 2007.

The Pacific Earthquake Engineering Research Center (PEER) is a multi-institutional research and education center with headquarters at the University of California, Berkeley. Investigators from over 20 universities, several consulting companies, and researchers at various state and federal government agencies contribute to research programs focused on performance-based earthquake engineering.

These research programs aim to identify and reduce the risks from major earthquakes to life safety and to the economy by including research in a wide variety of disciplines including structural and geotechnical engineering, geology/seismology, lifelines, transportation, architecture, economics, risk management, and public policy.

PEER is supported by federal, state, local, and regional agencies, together with industry partners.



PEER reports can be ordered at http://peer.berkeley.edu/publications/peer_reports.html or by contacting

Pacific Earthquake Engineering Research Center
University of California, Berkeley
325 Davis Hall, mail code 1792
Berkeley, CA 94720-1792
Tel: 510-642-3437
Fax: 510-642-1655
Email: peer_editor@berkeley.edu

ISSN 1547-0587X